Design, Synthesis, and Studies of Luminescent Organic Non-planar Push–pull Chromophores

Arif Hassan Dar

A thesis submitted for the partial fulfillment of
the degree of Doctor of Philosophy

Institute of Nano Science and Technology
Knowledge City, Sector-81, SAS Nagar, Manauli PO, Mohali 140306, Punjab, India

Indian Institute of Science Education and Research Mohali
Knowledge city, Sector 81, SAS Nagar, Manauli PO, Mohali 140306, Punjab, India.

February 2021

Dedication

Dedicated to my Parents

Declaration

I have carried out the work presented in this thesis under the guidance of Dr. Jayamurugan Govindasamy at the Institute of Nano Science and Technology, Mohali. This work has not been submitted in part or in full for a degree, a diploma, or a fellowship to any other university or institute. Whenever contributions of others are involved, every effort is made to indicate this clearly, with due acknowledgement of collaborative research and discussions. This thesis is a bonafide record of original work done by me, and all sources listed within have been detailed in the bibliography.

Arif Hassan Dar

In my capacity as the supervisor of the candidate's thesis work, I certify that the above statements by the candidate are true to the best of my knowledge.

Dr. Jayamurugan Govindasamy

Acknowledgments

The Ph.D. journey became a very memorable journey of my life with a lot of memories. There were always some people who stood by me in every situation, without whom my journey could have been incomplete. So before I discuss my Ph.D. journey, I would like to give my gratitude to them.

I would like to give my sincere thanks to my thesis supervisor **Dr. Jayamurugan Govindasamy** for his support, encouragement, and his priceless suggestions/teaching during my entire Ph.D. tenure. I can't forget the kind of inspirations and encouragements that he presented during the challenging moments of my journey in his lab. He always stood behind me in odd and even situations. The freedom he provided me to execute my research projects in the best possible way is worth remembering. I have learned a lot about research planning and execution during discussions with him, which have helped me get an enhanced interest in pursuing research. Apart from his research support, he stood and guided me during the tough times of my life. His qualities as a supervisor can't be stated in words, and I can simply say that this thesis could not have been completed without his guidance and unwavering support.

I would like to express my sincere gratitude to my research advisory committee (RAC), Dr. Prakash P. Neelakandan, and Dr. Asish Pal, for their valuable suggestions during the RAC meetings. Through their advice, it became possible for me to push my boundaries.

I would like to express my gratitude to Dr. Rehan Khan (INST-Mohali) and his student Mr. Anas for valuable discussions and support in making my results and thesis more effective from the experimental perspective in biosystems. I appreciate his kindness and helping nature. I am incredibly thankful to him for carrying out the experiments in cancer cell lines and photodynamic therapy.

I am also thankful to Dr. Md. Ehesan Ali (INST-Mohali) and his student Ms. Ashima Bajaj for carrying out the DFT simulation studies.

I thank Dr. A. Muthukrishnan (IISER-TVM) and his student Ms. Arya Gopal for electrochemical studies.

I thank Prof. H. N. Ghosh (INST-Mohali) for giving me access to TCSPC studies.

I thank Dr. P. S. Vijaya Kumar (INST-Mohali) for motivating me throughout my Ph.D. tenure.

I thank Dr. Dipankar Mandal (INST-Mohali) and his students for efficient collaboration, his student Mr. Varun has helped me carry out the electrospinning technique.

My sincere thanks to all my lab members Dr. J. Gowri, Dr. S. Kaur, A. Selim, K. M. Neethu, S. Sartaliya (for performing LC-MS studies), Dr. R. Mahajan, S. Jalwal, M. Nagpure, R. Sharma, and A. K. Solanki for maintaining a healthy and friendly environment in the lab. In particular, I would like to give my special gratitude to Dr. Gowri, who helped me during my whole Ph.D. tenure. It would have been impossible without her, and I always felt encouraged by her. The interactions we had helped me a lot in improving my research skills. She is an inspiration for me.

I thank Mr. Kamlesh Satpute and Dr. Nagaraja C. Mallaiah for access to the X-ray facility and single crystal data collection and refinement at IIT-Ropar. Also, Mr. Asif Ansari at IIT Bombay for help in refinement analysis.

I am also grateful to all the non-teaching staff, including Ms. Reena, Mr. Vikram, Mr. Deepak.

I am very thankful to my school friends, including Dr. Asif, Ubaid, Bilal, Amir, Sareer, Qaisar, Abid Bashir, Abid, Dr. Muneer, Shaista, and many others.

I am also thankful to my AMU friends, including Dr. Owies, Dr. Aadil, Dr. Ryhan, Dr. Akhtar, Dr. Bilal Masoodi, with whom I have spent great and memorable moments of my life.

I am also thankful to my INST-IISER friends, including Dr. Naimat, Anas, Khalid, Atikur, Mujeeb, Nadim, Riyaj, Rizaul, Naushad, Rohit, Zubair, Krishna, Venu, Jojo, Kashif.

Apart from friends at INST-IISER, I am very grateful to Dr. Javid and Nahida Hassan, who were always a source of encouragement throughout my Ph.D. tenure.

Acknowledgments

I am profoundly grateful to my parents (Mr. Ghulam Hassan and Mrs. Lateefa Bagum) for their unconditional love and support throughout my academic carrier. It is their unconditional trust and faith in me that has inspired me to reach this position. It is my great pleasure to acknowledge my late uncle (Mr. Mohd Assadullah), who has always pampered me in every corner of my life. In particular, I am very grateful to my brother (Mr. Muzamil Hassan) for his moral support, which helped me shape up my academic journey. I am also thankful to my sisters (Nusrat, Sumaira). I would like to thank my cousins, including Mr. Imran, Mr. Irshad, Mr. Muneer, Mr. Nazir, Mr. Tariq, Mr. Mubarak, Mr. Inam, Mr. Khalid, Mr. Umar.

I am thankful to Prof. A. K. Ganguli, Prof. H. N. Ghosh, and Prof. Amitava Patra, our founding, acting, and current directors of INST-Mohali, for creating outstanding infrastructure facilities an ideal research environment during my Ph.D. I also thank INST Mohali for providing my research fellowship. Finally, I would like to thank all those people whose names I missed here, despite their unconditional support to make my journey successful. To sum up, in a few words, it was a tremendous and incredible journey.

Contents Page No

TCBD	Tetracyano-1,3-butadiene
ICT	Intramolecular charge transfer
DMA	*N,N'*-Dimethylanilino
LC-MS	Liquid chromatography-mass spectrometry
UV/Vis	UV/Visible
FT-IR	Fourier-transform infrared
XRD	X-ray diffraction
TEM	Transmission electron microscopy
SEM	Scanning electron microscopy
DNA	Deoxyribonucleic Acid
AFM	Atomic force microscopy
TGA	Thermogravimetric analysis
NMR	Nuclear magnetic resonance
HPLC	High-performance liquid chromatography
NPs	Nanoparticles
λ	Wavelength (Lambda)
ε	Extinction coefficient
α	Alpha
σ	Sigma
γ	Gamma
δ	Delta
π	Pi
Å	Angstrom
^{o}C	Degree Celsius
nm	Nanometer
µm	Micrometer
cm	Centimeter

mL	Millilitre
µL	Microlitre
pM	Picomolar
µM	Micromolar
mM	Millimolar
θ	Theta
mW	Milliwatt
$CHCl_3$	Chloroform
$CDCl_3$	Deuterated chloroform
CH_3CN	Acetonitrile
CCDC	Cambridge Crystallographic Data Centre
d	Doublet
dd	Doublet of doublet
dt	Doublet of triplet
m	Multiplet
DMSO	Dimethylsulfoxide
CH_2Cl_2	Dichloromethane
DFT	Density functional theory
EtOH	Ethanol
Et_3N	Triethylamine
ESI	Electrospray ionization
Hz	Hertz
h	Hour
HPLC	High performance liquid chromatography
J	Coupling constant
KBr	Potassium bromide
KOH	Potassium hydroxide

K_2CO_3	Potassium carbonate
$LiClO_4$	Lithium perchlorate
MeOH	Methanol
MTT	3-(4,5-dimethylthiazol-2-yl)-2,5-diphenyl tetrazolium bromide
MD	Molecular dynamics
ORTEP	Oak ridge thermal ellipsoid plot
TCL	Thin layer chromatography
Ph	Phenyl
THF	Tetrahydrofuran
TFA	Trifluoroacetic acid
TOF	Time of flight

Chapter 1: Introduction to Organic Non-planar Push–pull Chromophores

The organic push–pull chromophores have been explored immensely for the past many decades and have found several applications in future generation soft organic materials especially in non-linear optical (NLO) devices. However, the use of organic push–pull chromophores remains limited owing to the type of EDG-substituents that in turn affect their light-emitting properties such as luminescence, etc. Though the generation of a new class of organic push–pull chromophores are continuously increasing concerning the strength of different donors [(*N*,*N'*-dialkylamino (typically *N*, *N*-dimethylamine), alkoxy groups (typically methoxy), electron-rich five-membered heteroaromatics (typically thiophene), or organometallic compounds (typically ferrocene)] and acceptors [tetracyanoethene (TCNE), tetracyanoquinodimethane (TCNQ)], still the existing reviews have not dealt with the comparison of reactivity profile in [2+2] CA–RE reaction vs electron-donating strengths (Field effect) and subsequent implication in the luminescent property. Hence, in this chapter, we have reviewed a short survey on the design, synthesis, and applications of organic non-planar push–pull chromophores exploiting formal [2+2] CA–RE between electron-rich alkynes and electron-deficient olefin (tetracyanoethene, TCNE) with a special focus on the reactivity profiles of EDG in terms of Hammett and Field effect constants (Figure 1). Further, the strategies available to generate fluorescent TCBDs were reviewed.

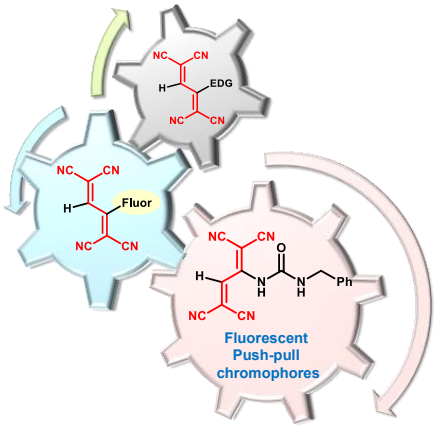

Figure 1. Reactivity profile of EDG in [2+2] CA–RE and method for fluorescent push–pull chromophores.

****

Chapter 2: Synthesis of TCBDs using TCNEO via [3+2] Cycloaddition-Ring Opening Reaction

In chapter 2, we explored tetracyanoethylene oxide (TCNEO) as new acceptor to obtain TCBDs instead of using conventional TCNE in [2+2] CA–RE reaction (Figure 2). Unlike the [3+2] cycloadduct of electron-donating group (EDG)-free alkynes with TCNEO, the EDG induced [3+2] cyclo-adduct underwent one-pot ring-opening and deoxygenation reactions to provide the established EDG-substituted non-planar 1,1,4,4-tetracyanobuta-1,3-dienes (TCBDs) push–pull chromophores. This is an alternate synthetic method that provides access to TCBDs other than the [2+2] cycloaddition–retroelectrocyclization reactions with TCNE.

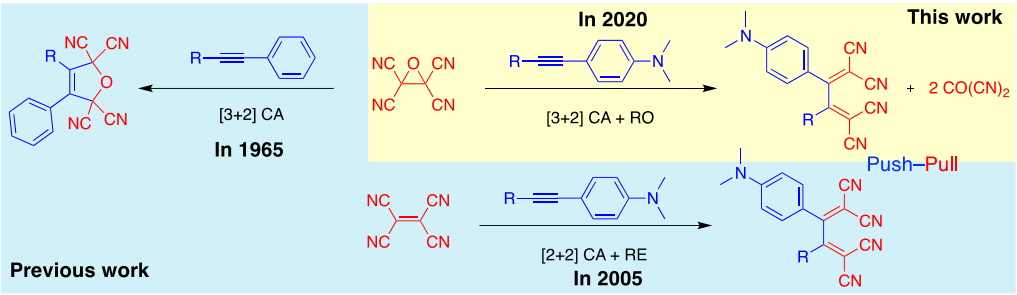

Figure 2. Synthesis of 1,1,4,4-tetracyano 1,3-butadiene (TCBD) based push–pull chromophore using TCNEO acceptor.

****

Chapter 3: Designing of Non-planar Push–pull Chromophores with Luminescent Properties

In general, TCBD type organic push–pull chromophores with strong ICT bands do not exhibit any fluorescence behavior. In chapter 3, we designed urea as a new electron-donating group to overcome photoinduced electron transfer (PET) due to the Field-effect (Figure 3). Urea-functionalized 4-ethynylbenzenes undergo facile formal [2+2] CA–RE with TCNE, yielding 1,1,4,4-tetracyanobuta-1,3-dienes (TCBDs) based push–pull chromophores. The unusual electron-donating ability of urea was ascribed to the Field-effect parameter rather Hammett constant. Unlike the *N*,*N*′-dialkylamino group, urea functionalization provides easy access to further functionalization on these chromophores. The resulting chromophores exhibit unexpected fluorescence properties apart from various inherent properties like the intramolecular charge-transfer band and redox behavior.

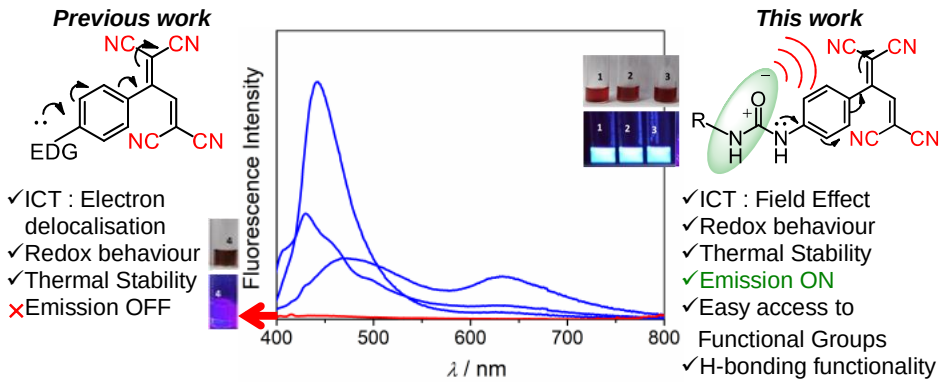

Figure 3. Synthesis of fluorescent push–pull chromophores using urea as EDG.

****

Chapter 4: Nanotechnology Assisted WLE from Single Chromophoric Organic Molecule

Chapter 4 deals with emission behavior governing parameters such as self-assembly, medium, and secondary interactions including solvent-dependent morphology in a selected example of urea-based push–pull chromophores. Urea-substituted TCBD with hexyl spacer was chosen as model TCBD (**Hexyl-TCBD**) to explore and understand its photophysical properties (White light emission, WLE) through supramolecular self-assembly phenomenon investigated by microscopic techniques and aggregation-induced emission (AIE) studies (Figure 4). Unlike in the solid-state of **Hexyl-TCBD**, we explored the containment of fluorescence in non-luminescent polystyrene fibers upon physical adsorption of **Hexyl-TCBD** using the electrospinning method. Further, we have studied the biocompatibility of urea-based push–pull chromophores in normal and cancer cell lines to validate the urea based push–pull chromophore as potential probes in the bio-imaging application.

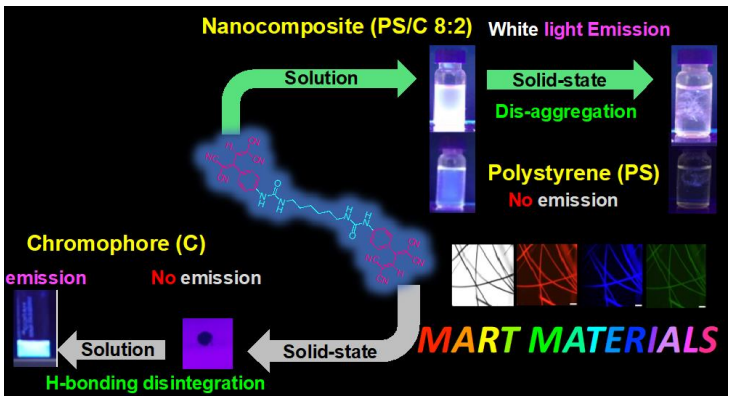

Figure 4. Nano-technology assisted solid-state luminescence of **Hexyl-TCBD** nanofibers in an aqueous medium.

****

Chapter 5: Push–pull Chromophore Encapsulated Nano-micelle as Active Nanoformulation for Bio-imaging and Photodynamic Therapy

In the course of our research work, the substituent on the C_3-position in 2,3-disubstituted TCBDs was found to play a crucial role in the efficiency of fluorescence. As the synthesized urea-substituted TCBDs are not soluble in the aqueous system and to apply them in biological applications and to further improve the emission in the NIR region (Stokes shift), we have adopted the AIE phenomenon in nano-micelle. Thus, in chapter 5, we attempted to enhance the fluorescence properties of urea-based push–pull chromophores and their solubility pattern *via* water-soluble, biocompatible nano-formulation of urea-functionalized 2,3-disubstituted TCBD (**phenyl-TCBD, 1**) (Figure 5). Spectroscopic studies including FT-IR have confirmed that the presence of encapsulation of aggregated **phenyl-TCBD** particles inside the non-luminescent tri-block copolymer (PF-127) based nano-micelle. Increasing water fraction experiment of **phenyl-TCBD** has indicated that the AIE phenomenon which in turn stimulated a remarkable Stokes shift (130 nm) and a 5-fold increase in fluorescence intensity along with the fluorescence quantum yield and lifetime. This red emission behavior of **phenyl-TCBD** was used as a photosensitizer in photodynamic therapy and bio-imaging applications.

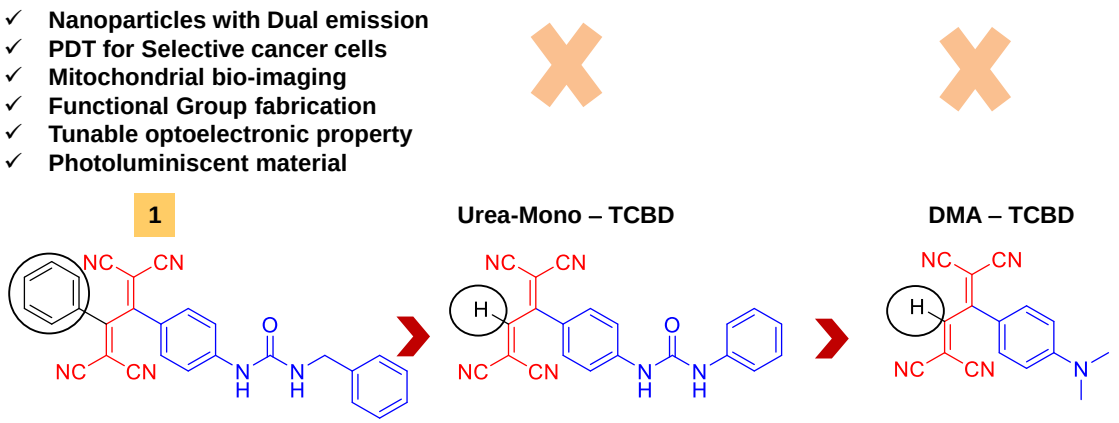

Figure 5. Schematic representation of the effect of the substituents in AIE of push–pull chromophore.

****

Chapter 1:

Introduction to Organic Non-planar Push–pull Chromophores

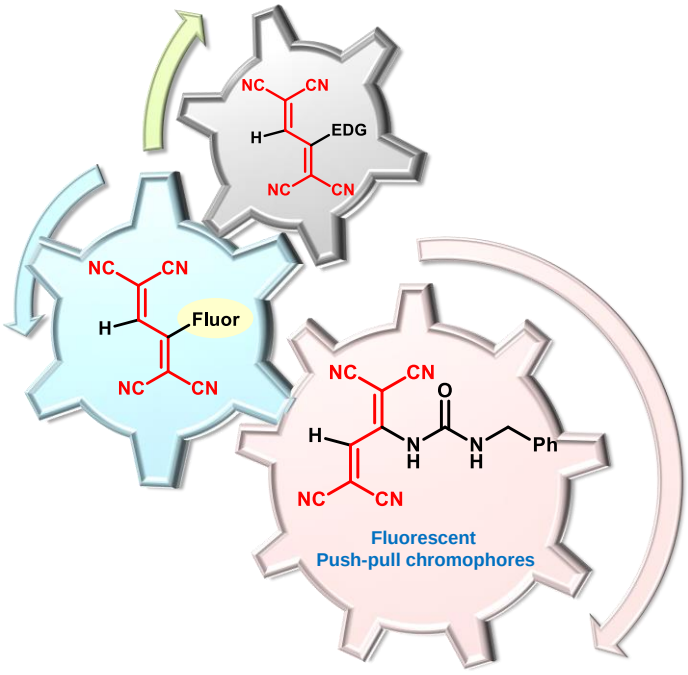

1.0 Organic push–pull chromophores:

Since the use of organic molecules for optical switching (rectifier) proposed by Aviram and Ratner (1974) has emerged as a potential material for soft electronic devices.[1] A thorough effort has been devoted to their synthetic and processing approach to enhance and define the structure-property relationships and generate functional molecules for next-generation electronic and optical applications (Figure 1.0). The organic conjugated system constitutes one of the promising systems in material organic chemistry. It has been found as an active layer in organic electronics (OE),[2] in particular semiconductors for organic thin-film (or field-effect) transistors (OTFTs or OFETs),[3] photovoltaic (or solar) cell (OPV or OSC),[4] light-emitting diodes (OLED) and non-linear optical (NLO)[5] applications. The donor-π-acceptor (D-π-A) chromophores featuring intense intramolecular charge-transfer interactions (ICT) have been found as active NLO materials[6–8] and have many other potential applications. For employment, in practical applications, the organic materials used in electronic and optoelectronic devices are generally in the form of thin films. Unfortunately, controlling their morphology is a vital issue for their sustainability. Easy crystallization leading to the spontaneous aggregate formation in the case of D-π-A molecules with low-molecular-weight compounds affect its optical properties.

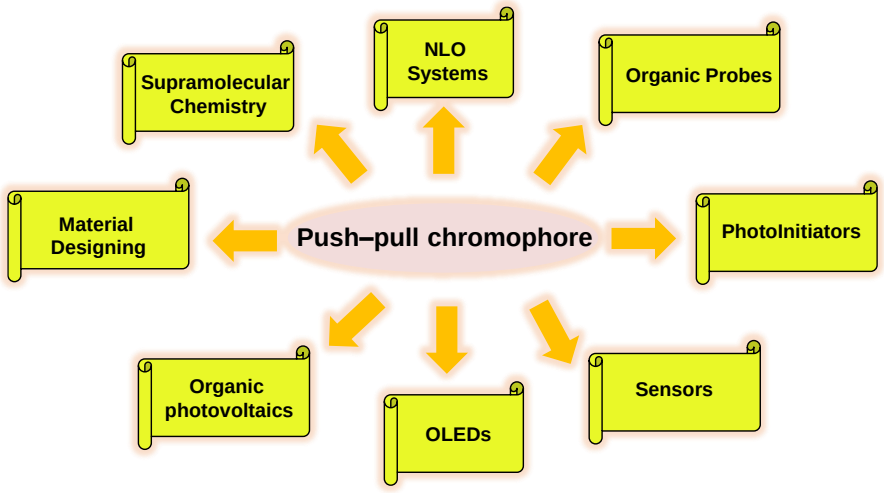

Figure 1.0. Applications of organic push–pull chromophores.

As the planar (D-π-A) push–pull chromophores have been extensively explored over many decades, variations in their donor and acceptor substituents enabled them to tune their HOMO–LUMO (H–L) gap.[3-8] However, in general, their material applications remain limited because their device fabrication and performance are un-accommodative

due to their inherent π–π stacking, which dramatically hinders properties like sublimation, solubility, and stability.

On the other hand, the non-planar or twisted push–pull chromophores, a subclass of chromophores with non-planarity in core structure containing electron-pushing donor (D) and -pulling acceptor (A) functionalities within a continuous conjugation of a molecule, can overcome these barriers. The conjugation over the donor and acceptor parts forms an essential aspect for designing organic push–pull chromophores. The positions of the D and A groups greatly influence the overall properties of the chromophores. Several different types of twisted push–pull chromophores have been reported by Marks and co-workers.[9,10] The following twisted non-planar chromophores have been reportedly found effective for all-optical switching applications (Figure 1.1).

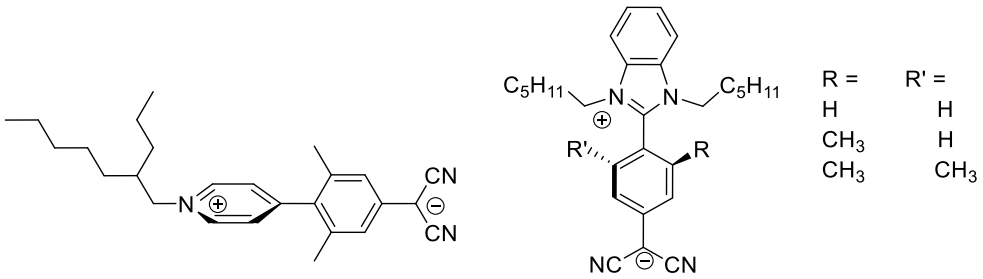

Figure 1.1. Selected examples of twisted non-planar organic push–pull chromophores

However, the class of non-planar push–pull chromophores synthesized under [2+2] CA–RE scheme has been categorized separately here. These non-planar (D-π-A)~(D/A/D-π-A) push–pull chromophores obtained through [2+2] cycloaddition (CA) followed by retroelectrocyclization (RE) reactions are quite interesting as they exhibit remarkable ICT leading to visible light absorption up to NIR region, amphoteric redox behavior, high melting point with good stability, more importantly, excellent solubility and sublimability owing to non-planarity. These features help achieve amorphous thin films, making them good candidates for potential use in optoelectronic devices because of their enhanced optical transparency, good processability, and homogeneous properties. Some systems were reported for polycyanohexa-1,3,5-trienes and polycyanoocta-1,3,5,7-tetraenes,[11] most of these chromophores generally contain tetracyanobuta-1,3-dienes with strong electron-withdrawing functional groups (FGs) (CN, COOR, CO) and electron-donating groups (metal ylides, thiophene, dialkylanilino, alkoxy, azulene, ynamide, triazine, pyrrole, phenothiazine, and recently urea). All these TCBDs exhibit salient features over the planar counterparts.

By employing a facile approach, the advanced properties of materials can also be enhanced and can tune the push–pull chromophores. The synthetic approaches and their NLO properties were always the core study for their evolution. While designing light-emitting diodes,[12,13] bio-imaging probes,[14] and other emitting devices, particularly in the visible region,[15] organic push–pull chromophores has been the first choice to consume for the cause. As most of the push–pull chromophores are not emissive, possessing strong ICT bands and the zwitterionic nature of the molecule. The non-emissive nature of push–pull chromophores significantly affect their future applications, such as in bioimaging probes, active NIR probes for deep imaging, etc. However, various strategies have been employed to achieve efficient full-color emitting materials, which are based on underlying mechanisms, including strong ICT,[16] twisted intramolecular charge-transfer (TICT),[17] excimer,[18] excited-state proton transfer (ESIPT),[19] and photo-induced electron transfer (PET).[20]

1.1. Non [2+2] CA–RE based selected luminescent Push–pull chromophores:

The synthesis of push-pull systems/dyes employing non [2+2] CA–RE reactions has been found to generate an exceptionally new chromophore class such as merocyanine dyes[21] and squaraine[22] type dyes. In merocyanine dyes, the assimilation of the π-conjugation between heterocyclic donor (D) and acceptor (A) groups via a polymethine chain enhances its dipole moment upto 10 D (**Merocyanine 1,2**). These dipole moments have been found to direct their self-assembly into different dimer aggregates.[23] Surprisingly, the generated self-assembled structures were efficient and far beyond those observed for other π-scaffolds whose self-assembly is driven primarily by dispersion forces. The inherent directional nature of these merocyanine dyes can be utilized to construct sophisticated supramolecular architectures of predictable geometry. Along with merocyanine dyes, squaraine dyes also establish themselves as active material in solar cells. Nithyanandan[24] and co-workers have developed a class of non-symmetrical squaraine **(SQS dye)** type dyes[25] with multiple polarities using alkyl groups for controlled aggregation, and efficient power conversion processes are needed to exploit the use of organic dyes in solar cells (Figure 1.2).

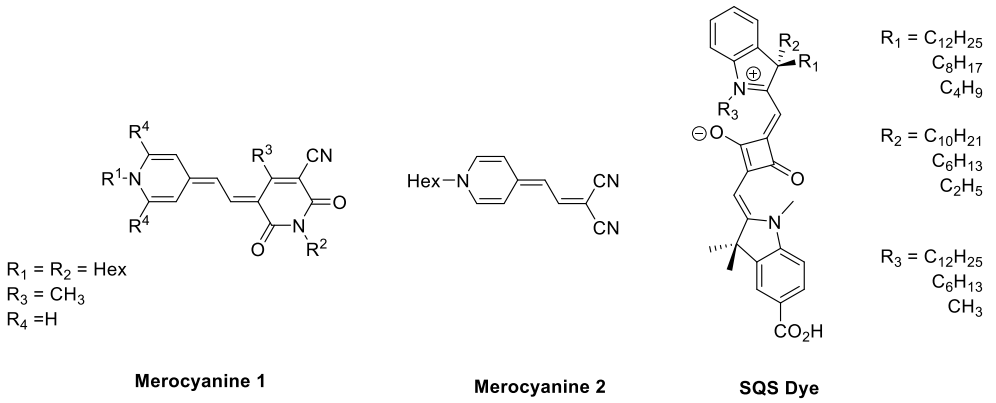

Figure 1.2. Representation of merocyanine and squaraine type push–pull dyes

The synthesis of two functionalized acrylonitriles (**Acrylonitrile-TPA** and **Acrylonitrile-CF$_3$**) with functional donor and acceptor embedded has been investigated.[26] The synthesized acrylonitrile's shows aggregation-induced emission (AIE) characteristics with promising applications in two-photon biomedical imaging. Efficient and straightforward protocols have been utilized to synthesize, mixing the two reactants using facile and transition metal-free synthetic methods. The two synthesized luminogens show a large stokes shift and two-photon absorption cross-section with bright red emission in the solid state.

Nanoformulation of synthesized luminogens has been utilized selectively to stain lysosome in live cells for live-cell imaging. Synthesized D–A chromophores show high biocompatibility and are successfully used in vivo long-term imaging of mouse tumors with a high signal-to-noise ratio (Figure 1.3).

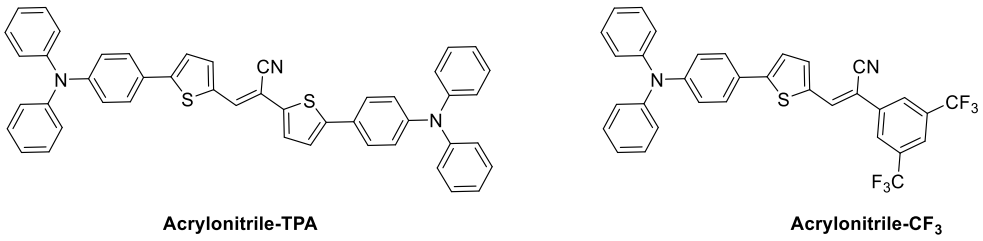

Figure 1.3. Representation of fluorescent Push–pull chromophores

However, two-photon fluorescence microscopy has become an indispensable technique for cellular imaging. Tremendous efforts have been made to further expand push–pull chromophores' structure for practical applications such as in two-photon fluorescent probes. Azulene has been reported as a new fluorophore for bioimaging. Azulene derivative acting as a chemodosimeter consists of a boronate ester receptor motif

conjugated to an appropriately substituted azulene to be an effective two-photon fluorescent probe for reactive oxygen species (Azufluor 483-Bpin).[27] The chemodosimeter shows an excellent cell penetration, high selectivity for peroxynitrite, no cytotoxicity, and excellent photostability (Figure 1.4).

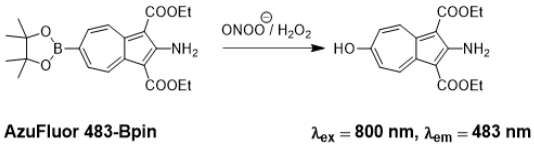

Figure 1.4. 2-Photon absorbing fluorescent class of push–pull chromophores in bio-imaging

The push–pull effect via ICT (directional change in dipole moment upon reaction with analyte) is the driving force for the behavior of azulene as chemo-dosimeter, which eventually has proven effective as the bio-imaging probe. Exploiting the inherent dipole moment of azulene of 1.08 D for an efficient ICT band change has been studied. We anticipate that azulene fluorophores, including the push–pull effect based on the design principles we have described here, will find many further applications in two-photon fluorescence imaging.

Why is organic non-planar (D-π-A)~(D/A/D-π-A) *push–pull chromophores (CA–RE products) so important?*

The (D-π-A)~(D/A/D-π-A) push–pull chromophores in molecular[28,29,] and polymeric systems[30,31,40] has been progressively studied since 1981. The impressive properties such as strong ICT bands, bathochromically shifted electronic absorptions, extending into the near-infrared (NIR) region,[32] high second and third-order optical nonlinearities,[6] and highly ordered crystal packings, and self-assemblies as a result of strong intra/intermolecular interactions are inevitable.[33] Their applications in optical data transmission and organic solar cell devices are increasing with time.[34] Their versatile approaches for the preparation of desirable entities are, however, relatively scarce. The optimization of the chromophores concerning the properties resembles the optimization process in drug discovery research.[35] The general model for the representation of non-planar push–pull chromophores synthesized by using formal [2+2] CA–RE reactions consists of "~" as a symbol for non-planarity between (D-π-A) parts (Figure 1.5).

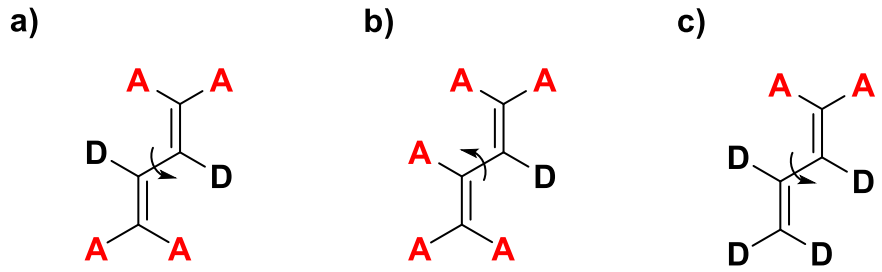

Figure 1.5. Representative model of available organic non-planar (D-π-A)~(D/A/D-π-A) push–pull chromophores using [2+2] CA–RE reactions a) (D-π-A)~(D-π-A) b) (D-π-A)~(A) c) (D-π-A)~(D).

As the synthesis of push–pull chromophores has been started by Bruce and co-workers in 1981.[36.] The exploration and investigation of their properties are still in process because of their dynamic nature. The property of (D-π-A)~(D/A/D-π-A) push–pull chromophores depend on many factors along with the nature of donor-acceptor moieties such as conjugation, location, strength, and self-assembling nature of donors and acceptors. This chapter mainly focuses on the evolution of new donors and acceptors followed by the synthesis and exploration of their luminescent push–pull chromophores for possible future applications. Since various categories of push–pull chromophores have been synthesized. However, interestingly both Planar (D-π-A) and non-planar (D-π-A)~(D/A/D-π-A) push–pull chromophores (D-π-A)~(D/A/D-π-A) got more attention. Along with ICT, through-space charge-transfer (CT) interactions has also been established by Staab and Rebafka[37] and Misumi and Otsubo,[38] and further explored by others.[39,40]All these push–pull chromophores synthesis exploit formal [2+2] cycloaddition-retroelectrocyclization (CA–RE) between electron-rich alkynes and electron-deficient alkenes, such as tetracyanoethene (TCNE) or 7,7,8,8-tetracyano-*p*-quinodimethane (TCNQ) and has been known as a convenient and robust method for preparing D-π-A~A/D/D-π-A chromophores. Since various approaches have been designed and reported for their synthesis, such as typical multistep reactions, one-pot [2+2] CA–RE,[40] [3+2] cycloaddition-ring opening (CA–RO) reactions.[41] However, among them [2+2] CA–RE got more attention because of robust reaction features. The thermal [2+2] CA of the strong electron acceptor TCNE with alkynes containing the electron-donating group Dar (EDGs), followed by RE yields EDG-substituted push–pull chromophores. Although the donors reported a decade ago have been quite effective from synthetic and application points, the breakthrough in designing push–pull chromophores was in 2005. In 2005, Diederich and co-workers' seminal work showed that metal-free

strong EDG-based *N,N'*-dialkyanilino (DMA) group could undergo clean transformation at ambient temperature with acceptor TCNE.[42] The products obtained are highly non-planar with an unprecedented NLO application.[43] This strategy was greatly expanded to synthesize various molecular structures like dendritic and dendralene systems involving cascade CA−RE reactions.[44] Following a continuous path, number of donors, come into play viz, azulene,[45] anisole, and thiophene,[46] *N,N'*-diphenyl aniline,[47] "electronically confused alkyne" having an EDG and an electron-withdrawing group such as –CN,[48] metal ylides,[49] carbazoles,[50] porphyrins,[51] ynamides[52] and very recently urea[53] have been explored. All these donors were observed as medium-weak or close with respect to *N, N'* dimethyl substituted alkynes. In general, these donors require more forcing conditions to carry [2+2] CA–RE. The reactivity of all these EDG-substituted alkynes with acceptors usually obey Hammett constant values, along with Hammett constant values field-effect values has been observed to show considerable contribution in determining the reactivity of alkynes.

1.2. Synthesis of organic non-planar push–pull chromophores:

- ***Role of donors and acceptors in* (D-π-A)~(D/A/D-π-A) *push–pull chromophores***

Push–pull chromophores would have been impossible without the expenditure of strong, medium, and weak donors and acceptors. Donors are usually designated as entities or molecular groups containing electronic clouds ready for donation, while acceptors are typically electron deficient moieties responsible for accepting electrons. The number of donors (metal ylides,[49] *N,N'*-alkyl derivatives,[54] ynamides,[52] urea,[53] BODIPY-derivatives,[55] thiophene,[46] TTF-derivatives,[56] O-alkyl derivatives,[57] anthracene-dithiole,[58] phenothiazine,[59] dinaphthyl-azepine,[60] carbazole-derivatives,[50] diisopropyltriazene,[61] ferrocene,[56] azulene[50]) (Figure 1.6) have been reported along with acceptors (**1**,[42] **2**,[55] **3**, [62] **4**,[63] **5**,[64] **6**,[65] **7**,[66] **8**,[66,67] **9**,[68] **10**,[69] **11**,[70] **12**,[71] **13**[72]) (Figure 1.7) so far.

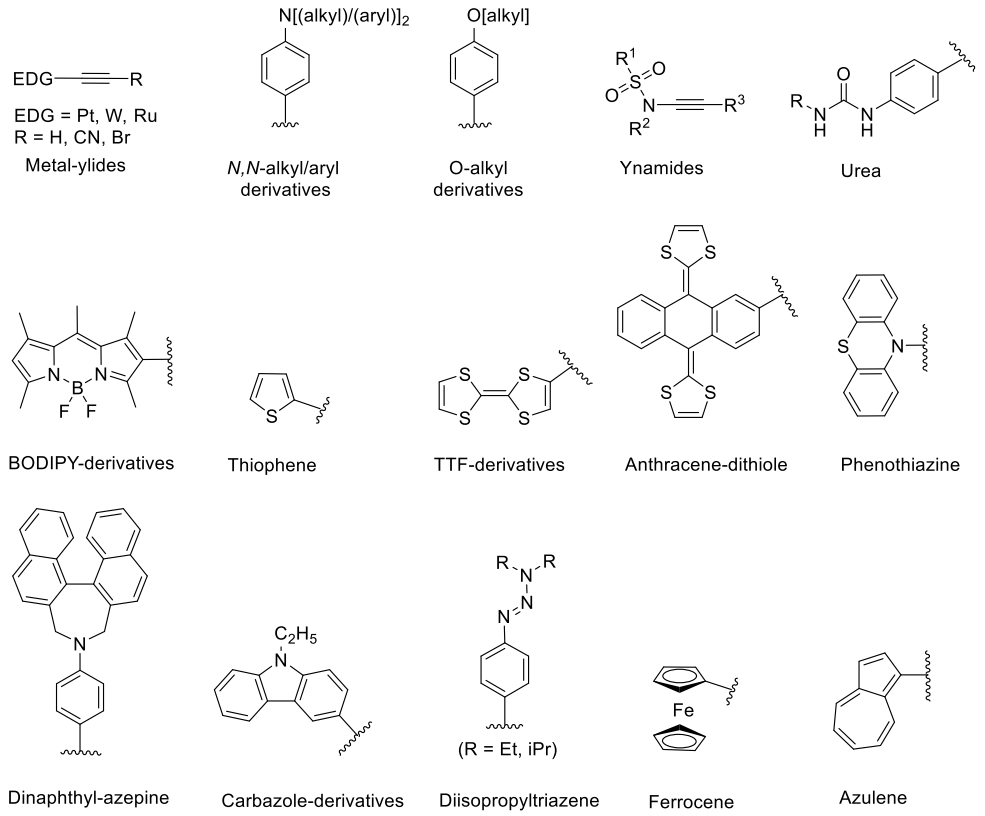

Figure 1.6. Selected examples of organic donor alkynes reported for [2+2] CA–RE.

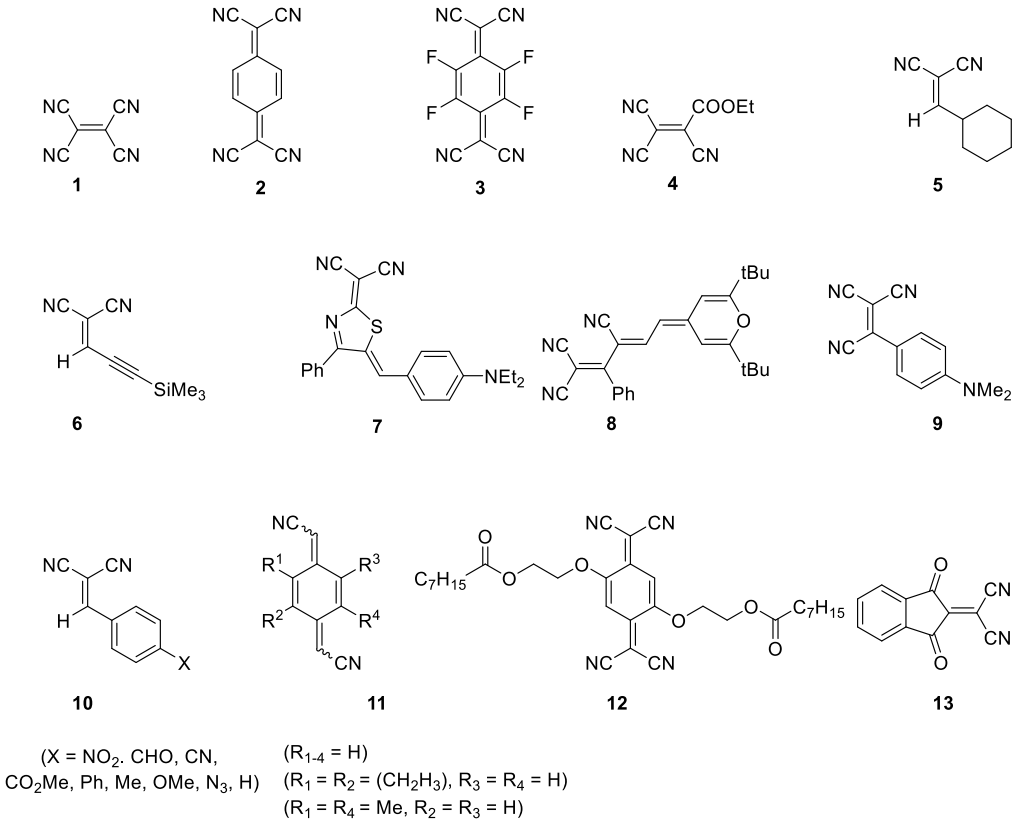

Figure 1.7. Selected examples of organic acceptors olefins reported for [2+2] CA–RE.

As the thermal [2+2] cycloaddition (CA) of the strong electron acceptor TCNE with alkynes containing the electron-donating groups (EDGs), followed by retroelectrocyclization (RE) yields EDG-substituted push–pull chromophores. Many research groups elucidated the scope of alkyne substitution in the formation of TCBD derivatives.[40] The essentiality of being considered an excellent organic donor towards CA–RE is the free electron for delocalization towards alkyne. The more electron-delocalization nature of the substituents, the faster is CA–RE reaction and better would be TCBD yields. Apart from the purely organic systems, a representative organometallic substance, ferrocene, has often been employed as a donor substituent. Interestingly, organometallic alkyne substituents Mochida and co-workers optimized the conditions and reported a CA–RE reaction of ethynyl ferrocene with TCNE yields up to 99% TCBD.[73] Since it has been observed that alkyne substituted directly with nitrogen shows good reactivity towards alkene acceptors. Fortunately, the interest for DMA as a strong donor arises because it results in the formation of purely organic push–pull chromophores. A thorough comparison of acyclic and cyclic, strained donor-substituted alkynes was carried out for [2+2] CA–RE reactions. It has been observed that the thermal [2+2] CA–RE reactions of TCNE with strained, electron-rich cyclooctyne lead to the formation of TCBDs. Accordingly, reaction rates of cycloaddition for cyclic, donor-substituted alkynes were found up to 5500 times greater than those of reactions which use corresponding acyclic alkynes. After observing the relative reactivity of different donors with acceptors, DMA has been established as one of the most influential donors to undergo [2+2] CA–RE reactions. The acceptors, especially TCNE, TCNQ have been found to undergo smooth [2+2] CA–RE to form TCBDs. Indeed, these transformations occur with exclusive involvement of exocyclic double bond, and only one of these bonds reacts and undergo [2+2] CA–RE. The reactivity towards electron-rich alkynes slightly decreased when substituents were introduced into the TCNQ moiety. Another strong acceptor 2,3,5,6-tetrafluoro–TCNQ (F_4-TCNQ) has been found to form the push–pull product in 65% yield at 20 ^{o}C.[48] However, the F_4-TCNQ adducts gradually decomposed upon contact with glass surfaces to form green, insoluble products. To avoid this decomposition, the glassware was deactivated by silylation with dimethyldichlorosilane (DMDCS). The nuclear magnetic resonance (^{1}H-NMR) spectra of the F_4-TCNQ adducts could not be recorded because of the presence of radical contaminations, as revealed by electron paramagnetic resonance (EPR) spectroscopy. Substitution of acceptor TCNQ by

2,5-dialkoxy-group featured lowered reactivity, and mild heating was necessary to initiate the reaction, but clean transformation into the corresponding push–pull chromophore was also demonstrated. Along with TCNE and TCNQ, dicyanovinyl moiety (DCV) was shown to be the minimal structural unit required for the CA–RE reactions. The reactivity of a series of other DCV derivatives has been reported and investigated under different conditions.[40]

- ***Synthesis of organic* (D-π-A)~(D/A/D-π-A) *push–pull chromophores using TCNE***

With the initial report on TCBDs by Bruce and co-workers on organometallic in 1981, several other TCBD derivatives were synthesized by [2+2] CA–RE of TCNE as strong A with D-substituted alkynes. Starting from 2005, Diederich and other research groups have conducted a comprehensive study on push–pull chromophores and systematically explored chromophores. Scheme **1** shows the general representation of the CA–RE reactions between TCNE and electron-rich alkynes. The CA–RE cascade starts with initial formal [2+2] cycloaddition (CA) between the electron-poor alkene **1** and activated alkyne **14** yielding cyclobutene intermediate **15**, which then undergoes retroelectrocyclization (RE) to afford donor-substituted tetracyanobuta1,3-diene (TCBD) **16** *(Scheme 1)*. Diederich and co-workers have tremendously expanded the chemical structure space or organic push–pull chromophores. Here are selected examples **17**, **18**, and **19** of donor-substituted TCBDs (Figure 1.8).[42]

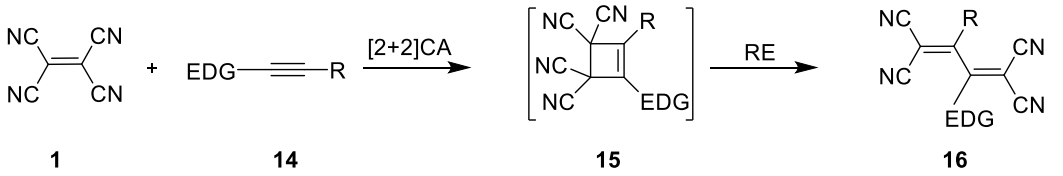

Scheme 1. Selected example of CA–RE reaction between TCNE and electron-rich alkynes.

As the number of exciting properties of push–pull chromophores such as thermal stability, solubility, large third-order optical nonlinearities (γ-rot), and gram-scale synthesis make donor-substituted TCBDs good candidates device construction. Recently, cyanoethnylethenes based push–pull chromophores have found applications in optical silicon-organic hybrid slot waveguides for all-optical high-speed signal processing with extraordinary performance.[43]

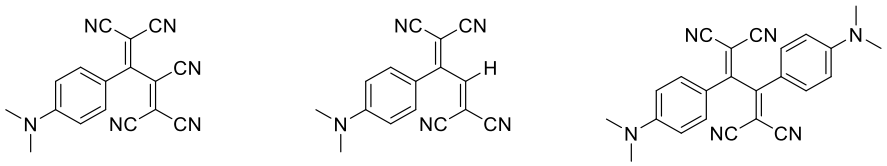

17

λ_{max} = 570 nm
E_{red}, 1 = –0.69 V
E_{ox}, 1 = +0.86 V

18

λ_{max} = 450, 643 nm
E_{red}, 1 = –0.30 V
E_{ox}, 1 = +1.00 V

19

λ_{max} = 450, 643 nm
E_{red}, 1 = –0.30 V
E_{ox}, 1 = +1.00 V

Figure 1.8. Donor-substituted TCBDs and their optoelectronic properties, CV data in CH_2Cl_2 (+0.1 M nBu_4NPF_6 vs. Fc^+/Fc).

The role of push–pull chromophores, including donors, acceptors, and spacer length on nonlinearity in third-order NLO applications, was also well studied by the Diederich group.[6,35] Interestingly, after the synthesis of many compounds inspired by the DDMEBT (**20**) structure (Figure 1.9), it has been observed that the third-order NLO properties of the chromophores **21** got tremendously impacted with the increasing spacer length, being reflected in γ_{rot} values.

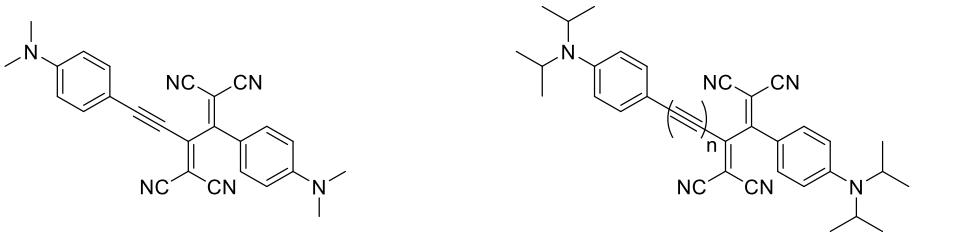

20

λ_{max} = 526 nm
γ_{rot} = (12±2) x 10^{-48} m^5 V^{-2}

21 (n = 0-5)

λ_{max} = 482 - 629 nm
γ_{rot} = (2±1) to (80±30) x 10^{-48} m^5 V^{-2}

Figure 1.9. Influence of spacer length on third-order NLO properties

1.3. Donor reactivity profile for TCBD formation using TCNE via [2+2] CA–RE:

To describe the reactivity pattern of organic substrates. The Hammett constant values have revealed the reactivity of different organic functional groups (FGs), derived from Hammett equations (and their extended forms). It has been one of the most widely used tools for studying and interpreting organic reaction reactivities and their mechanisms. However, along with its impact on physical organic chemistry, it has always been

criticized for its practical applicability for substrate reactivity, as some of the organic substrates do not follow the same Hammett constant values.

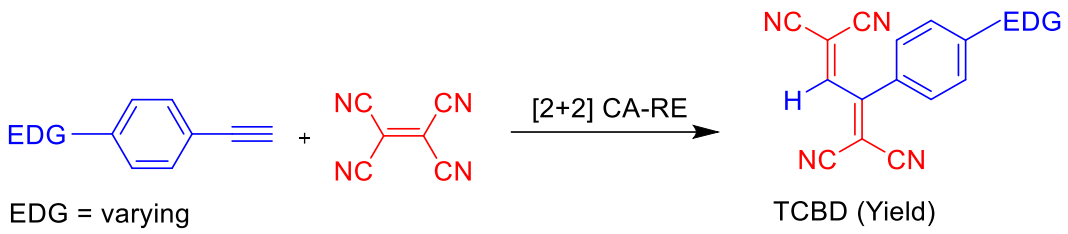

Scheme 2. Reactivity of electron-donating groups towards [2+2] CA–RE reaction.

The Field-effect (*F*) values introduced by Taft[74] have also been found to affect the reactivity pattern of organic substrates in addition to Hammett constant values. It combines electronic (electrostatic), steric, hydrophobic, hydrophilic, and hydrogen-bonding parameters. However, the contribution of the Field effect along with Hammett constant values in determining the reactivity of different donor alkynes under [2+2] CA–RE (Scheme 2) for TCBD formation has not been explored as Hammett constant values consider only mesomeric effects of FGs. While as the combination of electronic, steric, hydrophobic, hydrophilic, and hydrogen-bonding parameters has also been used to derive quantitative structure-activity relationships (QSAR) for a detailed study of interactions of organic compounds. Also, the influence of inductive/mesomeric effects of the chemical moieties in response to bond breaking and bond formation has been elucidated by a new reactivity influencing parameter called the Field-effect (*F*). So we suggest that while designing push–pull chromophores, we should take into account both Hammett and *F* effect values, as we observed in a recently published report on urea-based push–pull chromophores.

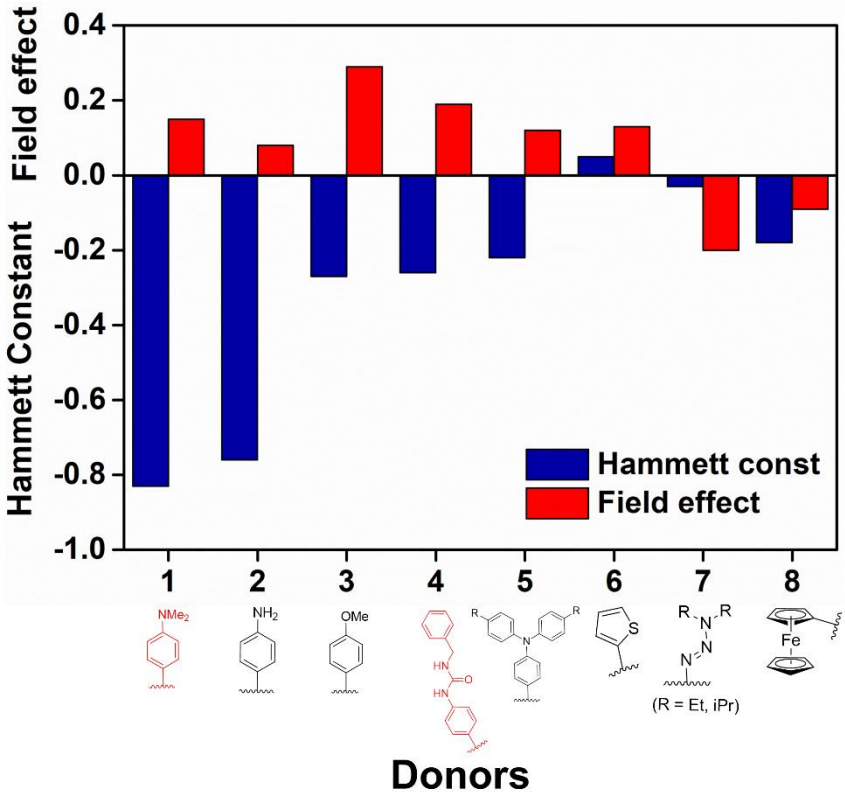

Figure 1.10. Electron donating profile for different donors (table 1) based on Hammett constant σ_p and Field-effect (*F)* values.

A comparative plot of the *F* effect and Hammett (σ_p) constant values for selected donor alkynes (Figure 1.10) will give us a broad insight in designing a selected push–pull chromophore by considering *F* values. As we have observed, in urea, reactivity towards TCBD formation is quite similar to DMA, irrespective of having a considerable margin in its Hammett constant values. It might be because of the Field effect values since the Field effect value of urea (0.19) coincides with that of a DMA (0.15). We observed a regular trend in the reactivity of selected donors towards TCBD formation with the few exceptions, as these exceptions may be because while considering Field effect values, we simultaneously include other electronic parameters.

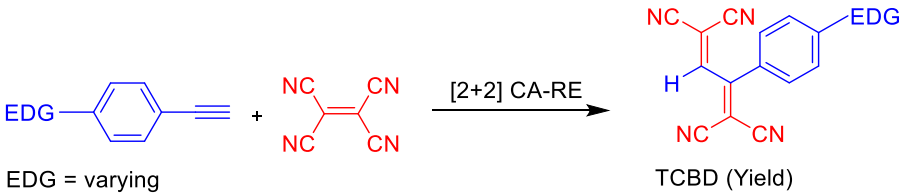

Scheme 3. Reactivity of electron-donating groups towards [2+2] CA–RE reactions.

Table 1: Field effect (F) and Hammett constant (σ_p) values of different donors.

S No	Donor (R)	Hamett constant (σ_p)	Field Effect (F)	Reaction condition	Yield (%)	References
1	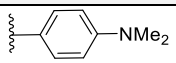	–0.83	0.15	THF/C_6H_6	97	42
2	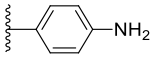	–0.76	0.08	CH_3CN, 25 °C	62	56
3	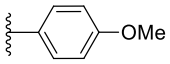	–0.27	0.29	Toluene, 110 °C	42	57
4	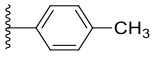	–0.17	–0.01	-		-
5	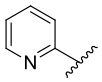	–0.33	0.40	-		-
6	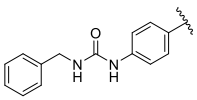	–0.26	0.19	DMF, 0 °C	60-70	53
7	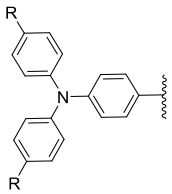	–0.22	0.12	CH_2Cl_2, 25 °C	85	75,76
8		0.05	0.13	$CHCl_3$, 25 °C	90	77
9	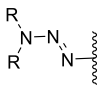 (R = Et, iPr	0.03	–0.02	CH_2Cl_2, 20 °C	40-64	61
10		–0.18	–0.09	$CHCl_3$, 20 °C	60-99	73

The reactivity of different donor substituted alkynes with TCNE and the respected TCBDs yields have been devised based on Hammett constant values (Figure 1.11).

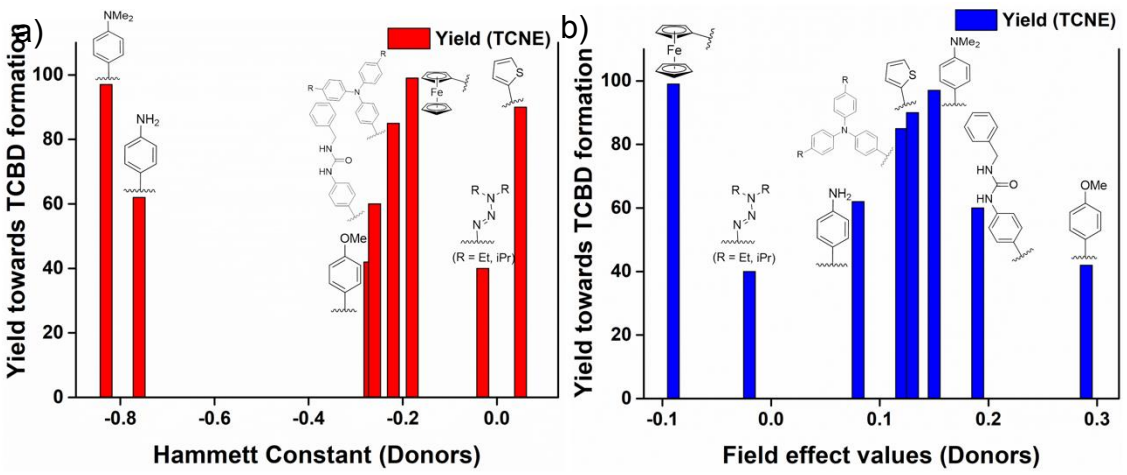

Figure 1.11. Reactivity profile for different donors (Table 1) based on a) Hammett constant (σ_p). b) Field-effect values (*F*) and % yield of TCBD formation.

We observed that the *F* effect is actively influencing the reactivity of different donors and alters the corresponding electronic properties of the organic moiety. The contribution of *F* effect values for specific donors significantly affects its reaction with TCNE. It shows an opposite trend in reactivity as observed for the Hammett constant values for TCNE (Table 1). It would be interesting to identify different donors with the same *F* effect values and same Hammett constant values and investigate their CA reaction with TCNE. Since the yield for the TCBD formation increases with the more negative value of Hammett constant (Figure 1.11), surprisingly, we did not observe a regular trend in reactivity pattern towards [2+2] CA–RE for TCBD formation the in case of urea. From the table 1 the designing and synthesis of a particular push–pull chromophores with desirable applications can be achieved by choosing an appropriate donor.

1.4. Designing of luminescent organic (D-π-A)~(D/A/D-π-A) push–pull chromophores:

Designing and synthesizing future generation push–pull chromophores mainly involves further expansion with existing donors and acceptor derivatives. Push–pull chromophores can be exploited tremendously in devices with active organic material or bioelectronics as it indeed allows alteration of the core structure or a molecule. The desired properties may be achieved by the multiple choices available in the form of donor, acceptor, conjugation part, and location within the molecules, which was found to have a massive impact on push–pull chromophores' properties.

The applications and synthetic protocols of push–pull chromophores are unique, simple click-type reactions leading to the formation of non-planar chromophores. However, there has always been a restriction to employ them for multiple photophysical-related applications. As the already available push–pull chromophore applications always remain limited due to the non-emissive nature of TCBDs. The non-emissive nature of TCBDs primarily is because of the existence of a twisted intramolecular charge transfer (TICT) along with a proximate conical intersection (CI) state. The luminescence in TCBD-based compounds is scarcely reported. There are reports on luminescence in TCBDs due to CT processes.

1.5 Recent shift towards luminescent organic (D-π-A)~(D/A/D-π-A) Push–Pull Chromophores:

The shift in expanding the scope of push–pull chromophores has been achieved very recently. Several fluorescent push–pull chromophores have been synthesized and explored for future applications. Interestingly, several possible opportunities to translate emission-less TCBD type push–pull chromophores to emissive chromophores (Figure 1.12). Nevertheless, two new approaches for the generation of luminescence in TCBDs are given below. I) Luminescence in TCBD-based push–pull chromophores by the introduction of the fluorophore. (ii) Luminescence in TCBD-based push–pull chromophores by the introduction of urea as a luminophore.

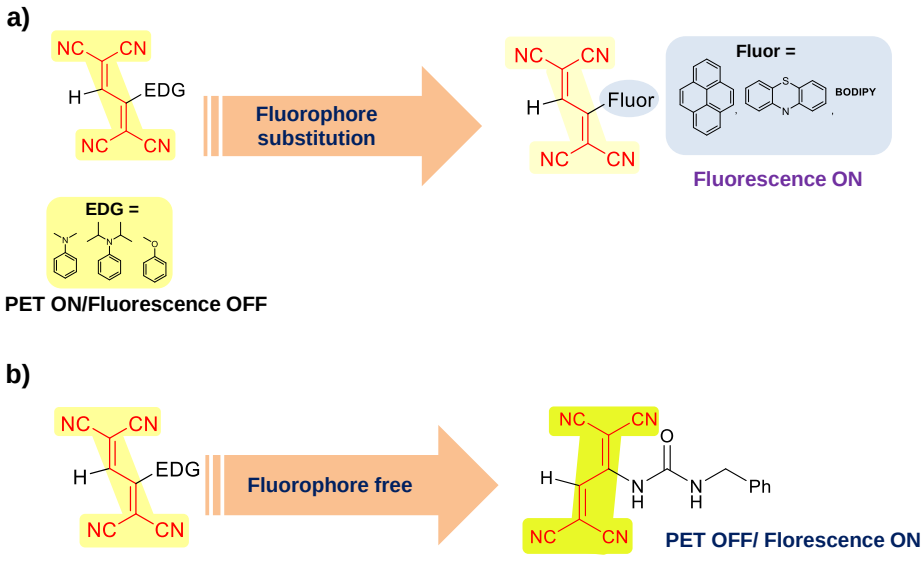

Figure 1.12. Schematic representation of approaches for obtaining fluorescent push–pull chromophores from non-fluorescent a). Introduction of fluorophore b). Fluorophore fee TCBDs by introducing urea as a donor

a). ***Luminescence in TCBD-based push–pull chromophores by the introduction of fluorophore:***

To implement the inherent properties of push–pull chromophores to further extents, it is imperative to add luminescence in them. One plausible method is the substitution of the fluorophore as a core moiety inside the push–pull system, which will eventually lead to luminescence. Before the luminescence from chromophore, the synthesis of alkyne with a fluorophore attached is a primary necessity. There are several reports on the synthesis of fluorophore-substituted TCBD-based push–pull chromophores. Recently, Trolez and co-workers (Scheme 4) introduced ynamide alkyne[52] with the fluorophore-substituted TCBD as NIR-imaging probes **22**, **23**[78]

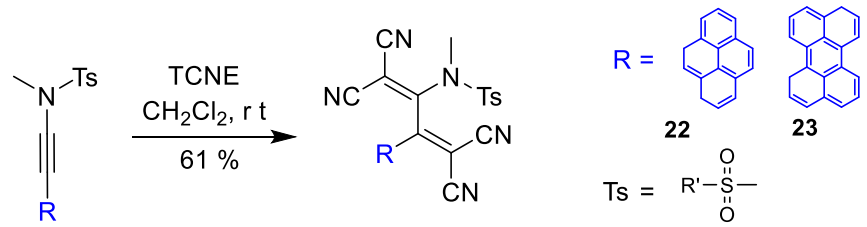

Scheme 4. Synthesis of luminescent TCBDs using fluorophores[78]

Mishra and co-workers (Scheme 5) introduced phenothiazine, triphenyl-amine **24, 25** as fluorophore-substituted luminescent TCBDs.[75,79] Furthermore, the AIE for the luminescence from TCBD-based push–pull chromophores is also possible. By following a *J*-aggregates of a bis-TCBD compound shows self-assembled vesicles or nanotubes shaped emissive structures.[80] It has been observed by Diederich and Amarolli that the increase in the viscosity of the matrix would restore the fluorescence by slowing down the rotational motions.[81] Radiative relaxation would operate by back transfer of electrons through the TICT state, which finally comes to the ground state (GS) and lead to emission. Also, different emissive peaks for a molecule may correspond to the difference in rotation rigidity for its conformers.

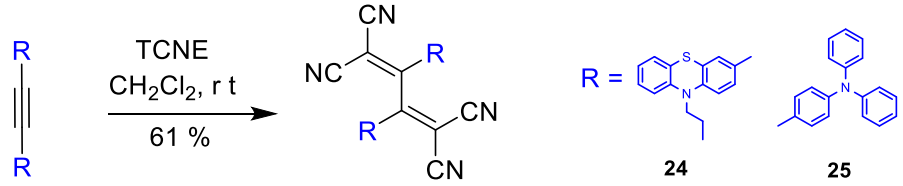

Scheme 5. Synthesis of luminescent TCBDs using fluorophores[79]

However, the critical planar push–pull chromophores are mostly less stable, and their consumption at the device level needs them to be stable enough. There are several approaches available to enhance the lifetime of these chromophores further. The supramolecular self-assembly of various functional π–systems has been extensively investigated in recent decades with improved suggestive properties.

b). ***Luminescence in TCBD-based push–pull chromophores by the introduction of Urea as luminophore:***

Along with the synthesis of push–pull chromophores, precise control over the spatial organization/arrangement mode is a progressive approach for designing future electronic materials ranging from biology to material sciences. Non-planar systems mainly possess stable chemical nature, as being observed in advanced material applications.[3,9,43] The synthesis of non-planar luminescent push–pull chromophores without fluorophore is a new approach for expanding luminescent non-planar push–pull chromophores. Recently our group has introduced urea-based luminescent non-planar push–pull chromophores **26** and **27** (Figure 1.13). The presence of luminescence in these chromophores are mainly due to TICT/PET off processes. Furthermore, these chromophores have been found effective for fluoride ion (F^-) sensing,[82] white light emission, bioimaging probes, etc.

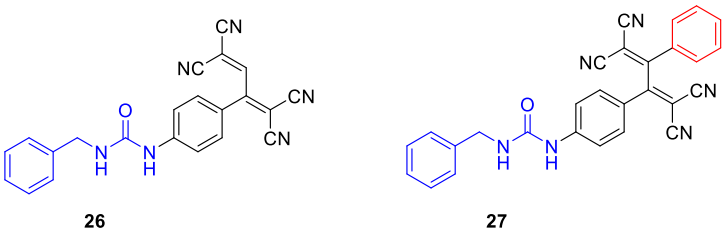

Figure 1.13. Selected TCBD-based luminescent push–pull chromophores without containing fluorophores.[82]

The non-covalent interactions, especially H–bonding interactions, have played a pivotal role in generating desired supramolecular nanostructures from suitably designed small molecular building blocks. Surprisingly, not much is known regarding the utility of simple fluorescent push–pull chromophores as self-complementary H–bonding functionalities. With the internal quest, we tried to elaborate and investigate the supramolecular self-assembly processes, mainly H–bonding architecture of these urea-based pushes–pull chromophores in chapters 4 and 5 of this thesis.

1.6. Scope of Research:

While the core concept of exploiting [2+2] CA–RE to synthesize (D-π-A)~(D/A/D-π-A) push–pull chromophores is overwhelming. However, their applications remain limited due to the lack of emissive properties. We expect in the coming years a further increase in the use of the CA–RE reactions for the production of bulk materials, including active electronic polymeric products, MOFs,[83] COFs, etc is evident from the recent reports on the luminescent TCBDs. We elucidate the use of CA–RE in the post functionalization process would lead the network of organic frameworks by TCNE or any other strong acceptor and found applications in conductive and magnetic materials and their inherent NLO applications. Along with the increase in usage of [2+2] CA–RE, we infer to highlight that the plots showing the reactive nature and TCBD formation yield by considering both Hammett constant and Field effect values for different donors are an eye-opener. The ongoing study on the synthesis of urea-based push–pull chromophores considering its Field effect values also suggests a bright prospect for the generation of tailor-made push–pull chromophores.

1.7. Conclusion:

The CA–RE reactions constitute a promising method for obtaining a new generation of functional organic molecules. The recent synthesis of fluorescent push–pull chromophores may increase their future applications and stimulate researchers to expand the window of existing chromophores.

The compiled reactivity profile of selected donors for [2+2] CA–RE has been explained with some exceptional donors. The influence of the Field (*F*) effect and Hammett constant on [2+2] CA–RE reactions and the approaches for the generation of luminescence in push–pull chromophores have been discussed.

1.8. References:

1. Aviram, A.; Ratner, M. A. *Chem. Phys. Lett*. **1974**, *29*, 277–283.
2. Vallaitis, T.; Bogatscher, S.; Alloatti, L.; Dumon, P.; Baets, R.; Scimeca, M. L.; Biaggio, I.; Diederich, F.; Koos, C.; Freude, W.; Leuthold, J. *Opt. Express*. **2009**, *17*, 17357–17368.

3. Senanayak, S. P.; Sangwan, V. K.; McMorrow, J. J.; Everaerts, K.; Chen, Z.; Facchetti, A.; Hersam, M. C.; Marks, T. J.; Narayan, K. S. *ACS Appl. Mater. Interfaces*. **2018**, *10*, 21492–21498.
4. Griesbeck, S.; Michail, E.; Wang, C.; Ogasawara, H.; Lorenzen, S.; Gerstner, L.; Zang, T.; Nitsch, J.; Sato, Y.; Bertermann, R.; Taki, M.; Lambert, C.; Yamaguchi, S.; B. Marder, T. *Chem. Sci.* **2019**, *10*, 5405–5422.
5. Pintre, C. I.; Serrano, J. L.; Ros, M. B.; Martínez-Perdiguero, J.; Alonso, I.; Ortega, J.; Folcia, C. L.; Etxebarria, J.; Alicantee, R.; Villacampae, B. *J. Mater. Chem*. **2010**, *20*, 2965–2971.
6. Tykwinski, R. R.; Gubler, U.; Martin, R. E.; Diederich, F.; Bosshard, C.; Günter, P. *J. Phys. Chem. B.* **1998**, *102*, 4451–4465.
7. Margulies, E. A.; Kerisit, N.; Gawel, P.; Mauck, C. M.; Ma, L.; Miller, C. E.; Young, R. M.; Trapp, N.; Wu, Y.-L.; Diederich, F.; Wasielewski, M. R. *J. Phys. Chem*. *C* **2017**, *121*, 21262–21271.
8. Maslak, P. *Adv. Mater.* **1994**, *6*, 405–407.
9. Lou, A. J.-T.; Righetto, S.; Barger, C.; Zuccaccia, C.; Cariati, E.; Macchioni, A.; Marks, T. J. *J. Am. Chem. Soc.* **2018,** *14*, 8746–8755.
10. Lou, A. J.-T.; Marks, T. J. *Acc. Chem. Res*. **2019**, *52*, 1428–1438.
11. Jayamurugan, G.; Finke, A. D.; Gisselbrecht, J.-P.; Boudon, C.; Schweizer, W. B.; Diederich, F. *J. Org. Chem*. **2014**, *79*, 426–431.
12. Hales, J. M.; Barlow, S.; Kim, H.; Mukhopadhyay, S.; Bredas,́ J.-L.; Perry, J. W.; Marder, S. R. *Chem. Mater*. **2014**, *26*, 549−560.
13. Luan, X.; Liu, J.; Pei, Q.; Bazan, G. C.; Li, H.; Bazan, G. C. *ACS Appl. Mater. Interfaces.* **2017**, *9*, 16750−16755.
14. Campagnola, P. *Anal. Chem*. **2011**, *83*, 3224−3231.
15. Feng, H.-T.; Zheng, X.; Gu, X.; Chen, M.; Lam, J. W. Y.; Huang, X.; Tang, B. Z. *Chem. Mater*. **2018**, *30*, 1285–1290.
16. Zhu, C. N.; Bai, T.; Wang, H.; Bai, W.; Ling, J.; Sun, J. Z.; Huang, F.; Wu, Z. L.; Zheng, Q. *ACS Appl. Mater. Interfaces.* **2018**, *10*, 39343–39352
17. Grabowski, Z. R.; Rotkiewicz, K.; Rettig, W. *Chem. Rev*. **2003**, *103*, 3899–4032.
18. Malliaris, A.; Le Moigne, Jacques.; Sturm, Jean.; Zana, R. *J. Phys. Chem*. **1985**, *89*, 2709–2713.
19. Dick, B. *Phys. Chem*. **1987**, *91*, 1205–1209.
20. Jin, Y.; Zhang, Q.; Zhang, Y.; Duan, C. *Chem. Soc. Rev*. **2020**, *49*, 5561–5600.

21. Würthner, F. *Acc. Chem. Res*. **2016**, *49*, 5, 868–876.
22. Bisht, R.; Kavungathodi, M. F. M.; Nithyanandhan, J. *Chem. Eur. J*. **2018**, *24*, 16368 –16378.
23. Würthner, F.; Yao, S.; Debaerdemaeker, T.; Wortmann, R. *J. Am. Chem. Soc*. **2002**, *124*, 9431–9447.
24. Singh, A K.; Maibam, A.; Javaregowda, B H.; Bisht, R.; Kudlu, A.; Krishnamurty, S.; Krishnamoorthy, K.; Nithyanandhan, *J. Phys. Chem. C*. **2020**, *124*, 18436–18451.
25. Singh, A K.; Mele, K. M F.; Nithyanandhan, J. *ACS Appl. Mater. Interfaces*. **2020**, *12*, 2555–2565.
26. Niu, G.; Zheng, X.; Zhao, Z.; Zhang, H.; Wang, J.; He, X.; Chen, Y.; Shi, X.; Ma, C.; Kwok, T. K. R.; Lam, W. Y. J..; Sung, H. Y. H.; Williams, D. I.; Wong, S. K.; Wang, P.; Tang, Z. B. *J. Am. Chem. Soc*. **2019**, *141*, 15111−15120.
27. Murfin, L. C.; Weber, M.; Jun, P. S.; Kim, W. T. Lopez-Alled C. M.; McMullin, C. L.; Pradaux-Caggiano, F.; Lyall, C. L.; Kociok-Köhn, G.; Wenk, J.; Bull, S. D.; Yoon, J.; Kim, H. M.; James, T; D.; Lewis, S. E. *J. Am. Chem. Soc.* **2019**, *141*, 19389–19396.
28. Kivala, M.; Diederich, F.; *Acc. Chem. Res*. **2009**, *42*, 235–248.
29. Levia, L.; Müller, J. J. T. *Chem. Soc. Rev*. **2016**, *45*, 2825–2846.
30. Washino, Y.; Murata, K.; Ashizawa, M.; Kawauchi, S.; Michinobu, T. *Polymers*. **2011**, *43*, 364–369.
31. Michinobu, T. *J Am. Chem. Soc*. **2008**, *130*, 14074–14075.
32. Fabian, J.; Nakazumi, H.; Matsuoka, M. *Chem. Rev*. **1992**, *92*, 1197–1226.
33. Chen, Z.; Lohr, A.; Saha-Möller, C. R.; Würthner, F. *Chem. Soc. Rev*. **2009**, *38*, 564–584.
34. Gendron, D.; Leclerc, M. *Environ. Sci*. **2011**, *4*, 1225–1237.
35. Murfin, L. C.; Weber, M.; Park, S. J.; Kim, W. T.; Lopez-Alled, C. M.; McMullin, C. L.; Pradaux-Caggiano, F.; Lyall, C. L.; Kociok-Köhn, G.; Wenk, J.; Bull, S. D.; Yoon, J.; Kim, H. M.; James, T. D.; Lewis, S. E. *J. Am. Chem. Soc*. **2019**, *141*, 19389–19396.
36. Bruce, M. I.; Rodgers, J. R.; Snow, M. R.; Swincer, A. G. *J. Chem. Soc, Chem. Commun*. **1981**, *6*, 271–272.
37. Rebafka, W.; Staab, H. A. *Angew. Chem. Int. Ed*. **1973**, *12*, 776–777.
32. Misumi, S.; Otsubo, T. *Acc. Chem. Res*. **1978**, *11*, 251–256.

39. Jayamurugan, G.; Gisselbrecht, J.-P.; Boudon, C.; Schoenebeck, F.; Schweizer, W. B.; Bernet, B.; Diederich, F. *Chem. Commun*. **2011**, *47*, 4520–4522.
40. For a review, see: Michinobu, T.; Diederich, F. *Angew. Chem. Int. Ed.* **2018**, *5*, 3552–3577.
41. Dar, A. H.; Gowri, V.; Neethu, K. M.; Jayamurugan, G. *ChemistrySelect.* **2020**, *5*, 12437–12441.
42. Michinobu, T.; May, J. C.; Lim, J. H.; Boudon, C.; Gisselbrecht, J.-P.; Seiler, P.; Gross, M.; Biaggio, I.; Diederich, F. *Chem. Commun*. **2005**, 737–739.
43. Koos, C.; Vorreau, P.; Vallaitis, T.; Dumon, P.; Bogaerts, W.; Baets, R.; Esembeson, B.; Biaggio, I.; Michinobu, T.; Diederich, F.; Freude, W.; Leuthold, J. *Nat. Photonics.* **2009**, *3*, 216–219.
44. Kivala, M.; Boudon, C.; Gisselbrecht, J.-P.; Seiler, P.; Gross, M.; Diederich, F. *Angew. Chem. Int. Ed*. **2007**, *46*, 6357–6360.
45. Shoji, T.; Ito, S.; Toyota, K.; Yasunami, M.; Morita, N. *Chem. Eur. J.* **2008**, *14*, 8398–8408.
46. Kim, H.-G.; Lee, J.-K.; Lee, J.-T.; Lee, C.-S. *Bull. Korean Chem. Soc*. **2000**, *21*, 345–347.
47. Tang, X.; Liu, W.; Wu, J.; Lee, C.-S.; You, J.; Wang, P. *J. Org. Chem*. **2010**, *75*, 7273–7278.
48. Reutenauer, P.; Kivala, M.; Jarowski, P. D.; Boudon, C.; Gisselbrecht, J.-P.; Gross, M.; Diederich, F. *Chem. Commun*. **2007**, *46*, 4898–4900.
49. Onuma, K.-i.; Kai, Y.; Yasuoka, N.; Kasai, N. *Bull. Chem. Soc. Jpn*. **1975**, *48*, 1696–1700.
50. Kato, S.; Noguchi, H.; Jin, S.; Nakamura, Y. *Asian J Org Chem*. **2016**, *5*, 246–256.
51. Koszelewski, D.; Nowak- Król, A.; Gryko, D. T. *Chem. Asian J.* **2012**, *7*, 1887–1894.
52. Betou, M.; Kerisit, N.; Meledje, E.; Leroux, Y. R.; Katan, C.; Halet, J.-F.; Guillemin, J.-C.; Trolez, Y. *Chem. Eur. J.* **2014**, *20*, 9553–9557.
53. Dar, A. H.; Gowri, V.; Gopal, A.; Muthukrishnan, A.; Bajaj, A.; Sartaliya, S.; Selim, A.; Ali, Md. E.; Jayamurugan, G. *J. Org. Chem*. **2019**, *84*, 8941–8947.
54. Michinobu, T.; Boudon, C.; Gisselbrecht, J.-P.; Seiler, P.; Frank, B.; Moonen, N. N. P.; Gross, M.; Diederich, F. *Chem. Eur. J.* **2006**, *12*, 1889–1905.

55. Niu, S.; Ulrich, G.; Retailleau, P.; Ziessel, R. *Org. Lett*. **2011**, *13*, 4996–4999.
56. Kato, S.-i.; Kivala, M.; Schweizer, W. B.; Boudon, C.; Gisselbrecht, J.-P.; Diederich, F. *Chem. Eur. J*. **2009**, *15*, 8687–8691.
57. Zhang, W.; Kraft, S.; Moore, J. S. *J. Am. Chem. Soc.* **2004**, *126*, 329–335.
58. Garcia, R.; Herranz, M. A.; Torres, M. R.; Bouit, P.-A.; Delgado, J. L.; Calbo, J.; Viruela, P. M.; Orti, E.; Martin, N. *J. Org. Chem*. **2012**, *77*, 10707–10717.
59. Okuno, T.; Iwahashi, H. *Acta Crystallogr. Sect. E* **2013**, *69*, 665.
60. Frank, B. B.; Blanco, B. C.; Jakob, S.; Ferroni, F.; Pieraccini, S.; Ferrarini, A.; Boudon, C.; Gisselbrecht, J.-P.; Seiler, P.; Spada, G. P.; Diederich, F. *Chem. Eur. J*. **2009**, *15*, 9005–9016.
61. Perrin, F. G.; Kiefer, G.; Jeanbourquin, L.; Racine, S.; Perrotta, D.; Waser, J.; Scopelliti, R.; Severin, K. *Angew. Chem. Int. Ed*. **2015**, *54*, 13393–13396.
62. Kivala, M.; Boudon, C.; Gisselbrecht, J.-P.; Enko, B.; Seiler, P.; I. Mller, B.; Langer, N.; Jarowski, P. D.; Gescheidt, G.; Diederich, F. *Chem. Eur. J*. **2009**, *15*, 4111.
63. Reekie, T. A.; Donckele, E. J.; Ruhlmann, L.; Boudon, C.; Trapp, N.; Diederich, F. *Eur. J. Org. Chem.* **2015**, *33*, 7264–7275.
64. Jarowski, P. D.; Wu, Y.-L.; Boudon, C.; Gisselbrecht, J.-P.; Gross, M.; Schweizer, W. B.; Diederich, F. *Org. Biomol. Chem.* **2009**, *7*, 1312–1322.
65. Wu, Y.-L.; Jarowski, P. D.; Schweizer, W. B.; Diederich, F. *Chem. Eur. J.* **2010**, *16*, 202–211.
66. Galan, E.; Andreu, R.; Garin, J.; Orduna, J.; Villacampa, B.; Diosdado, B. E. *Org. Biomol. Chem*. **2012**, *10*, 8684–8691.
67. Moreno-Yruela, C.; Garín, J.; Orduna,´ J.; Franco, S.; Quintero, E.; Navarrete,´ J. T. L.; Diosdado, B. E.; Villacampa, B.; Casado, J.; Andreu, R. *J. Org. Chem.* **2015**, *80*, 12115–12128.
68. Rijkers, D. T. S.; Lopez, F. de P.; Liskamp, R. M. J.; Diederich, F. *Tetrahedron Lett*. **2011**, *52*, 6963–6967.
69. Fabio; S.; Markus; J.; Kara; H.; Milan; K.; Pablo; Rivera-F.; Corinne; B.; Jean-Paul G.; Bernd; S. W.; Paul; S.; Melanie; C. *Chem. Eur. J*. **2011**, *17*, 6088–6097.
70. Chiu, M.; Jaun, B.; Beels, M. T. R.; Biaggio, I.; Gisselbrecht, J.-P.; Boudon, C.; Schweizer, W. B.; Kivala, M.; Diederich, F. *Org. Lett*. **2012**, *14*, 54–57.

71. Yusuke; W.; Kimie; M.; Minoru; A.; Susumu; K.; Tsuyoshi, M. *Polym. J*. **2011**, *43*, 364–369.

72. Donckele, E. J.; Finke, A. D.; Ruhlmann, L.; Boudon, C.; Trapp, N.; Diederich, F. *Org. Lett*. **2015**, *17*, 3506–3509.

73. Mochida, T.; Yamazaki, S. *J. Chem. Soc, Dalton Trans*. **2002**, *18*, 3559–3564.

74. Hansch, C.; Leo, A.; Taft, R. W. *Chem. Rev.* **1991**, *91*, 165–195.

75. Gautam, P.; Misra, R.; Thomas, M. B.; D'Souza, F. *Chem. Eur. J.* **2017**, *23*, 9192–9200.

76. Michinobu, T.; Satoh, N.; Cai, J.; Li, Y.; Han, L. *J. Mater. Chem. C* **2014**, *2*, 3367–3372.

77. Leliege, A.; Blanchard, P.; Roousseau, T.; Roncali, J. *Org. Lett*. **2011**, *13*, 3098–3101.

78. Bui, A. T.; Philippe, C.; Beau, M.; Richy, N.; Cordier, M.; Roisnel, T.; Lemiègre, L.; Mongin, O.; Paul, F.; Trolez, Y. *Chem. Commun*. **2020**, *56*, 3571–3574.

79. Rout, Y.; Gautam, P.; Misra, R. *J. Org. Chem*. **2017**, *82*, 6840–6845.

80. Xu, J.; Liu, X.; Lv, J.; Zhu, M.; Huang, C.; Zhou, W.; Yin, X.; Liu, H.; Li, Y.; Ye, J. *Langmuir*. **2008**, *24*, 4231–4237.

81. Monti, F.; Venturini, A.; Nenov, A.; Tancini, F.; Finke, A. D.; Diederich, F.; Armaroli, N. *J. Phys. Chem. A*. **2015**, *119*, 10677–10683.

82. Gowri, V.; Jalwal, S.; Dar A. H.; Gopal, A.; Muthukrishnan, A.; Bajaj, A.; Ali, E, Md.; Jayamurugan G. *J. Photochem. Photobiol. A* **2021**, *410*, 113613 (1)-113613 (9).

83. Cheng, S.; Li, K.; Hu, J.; He, J.; Zeller, M.; Xu, Z. *ACS Appl. Mater. Interfaces.* **2020**, *12*, 19201–19209.

Chapter 2

Synthesis of TCBDs using TCNEO via [3+2] Cycloaddition-ring Opening Reaction

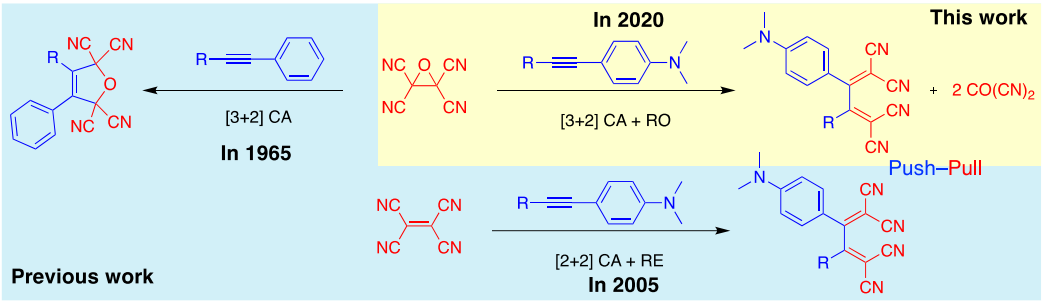

2.0. Introduction:

Push–pull chromophores with well-studied structural property relations were always fascinating to the scientific community.[1–4] The structural variation in acceptor and donor parts of push–pull chromophores was an active protocol to complete the transformation of the properties of the molecules. Undoubtedly, the exciting features of all the chromophores arise because of their encounter with the UV/Vis/NIR-radiations.[5–7] However, push–pull chromophores have an immense influence on the soft industries as well. Because of their vast applications in material fabrications, soft molecular device-optoelectronics designing, as fluorescence sensors,[8–12] in bio-imaging,[13] dye-sensitized solar cells,[14–17] photorefractive organic materials,[18] etc. The design of the donor and acceptor groups helps in tuning the interaction between the organic push–pull chromophores. This occurs primarily because of the control by the donor and acceptor groups over the intramolecular charge transfer (ICT) process. The methodology to explore new acceptors and donors is simple, thanks to the formal [2+2] cycloaddition−retroelectrocyclization (CA−RE) reaction between electron-rich alkynes and electron-deficient olefins yielding EDG-substituted 1,1,4,4-tetracyanobuta-1,3-dienes (TCBDs) is a versatile, well-studied transformation[19,20] so far. It can be regarded as a "click"-type reaction that is high yielding, atom-economic, requires no catalyst, and proceeds under mild conditions with excellent chemo and regioselectivity. The [2+2] CA–RE is a robust method for preparation of non-planar, π-conjugated, donor-acceptor (D–A) chromophores that exhibit intense, low-energy, intramolecular charge-transfer (CT) bands.[21–24] Some of them have found application in devices and has also shown remarkable third-order non-linear optical (NLO) properties.[6] Though many donors and acceptors has been reported so far based on CA–RE reactions, interestingly, all the works that deal with the synthesis of push–pull chromophore have changed mainly the donor substitution or donor group, such as metal ylides,[25] thiophenes,[26] amines,[27] ferrocene and TTF,[24] azulenes,[28] porphyrin,[29] carbazoles,[30] ynamides,[31] and ureas[32] from our group. In the case of acceptors, mainly the CN derivatives were used. TCNE, TCNQ have been used as benchmarks for acceptor substituted parts. Though the carboxylic ester group has also been used as an acceptor, it shows less reactivity, thus act as a mild accepting unit.[33] To expand the chemical space for TCBD based push–pull chromophores, it is essential to look for more acceptors to synthesize TCBDs apart from using the conventional [2+2] CA–RE reaction as the only choice.

The expansion of exploring new acceptors was started in late 1965 by Linn and Benson.[34] They introduced tetracyanoethylene oxide (TCNEO) as a new electron-deficient derivative to synthesize tetracyanodihydrofuran (TCDHF) type compounds using deactivated alkynes as donors.[35,36] Recently, graphene-TCNEO chemistry has been found to manipulate the electronic properties of graphene.[37,38] However, the reaction occurs at elevated temperatures. TCNEO being commercially available and accessible by lab synthesis, maybe a good candidate to compare with the benchmark acceptors. Since TCNEO has an epoxide ring containing lone pairs on oxygen atom acts as a 1,3-dipolar ion. Also, TCNEO has an inherent ability to undergo CA reactions with the potential alkynes.

Chapter 2 explored [3+2] cycloaddition-ring opening (CA–RO) reaction of TCNEO with activated alkynes under ambient conditions to synthesize efficient TCBD type push–pull chromophores in pretty good yield. However, while observing the reaction in different polarity solvents, such as in acetonitrile (CH_3CN) under suitable conditions, we end up with other products.

a) 1,1,4,4-tetracyanobuta-1,3-dienes (TCBD) via [2+2] CA-RE reactions between EDG-alkynes and TCNE by Diederich & co-workers[21]

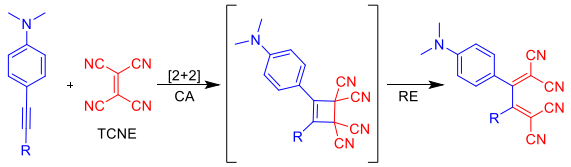

High yielding
Simpler condition

b) Tetracyanodihydrofuran adducts via [2+2] CA reactions between EDG-free alkyne and TCNEO by Linn & Benson[34]

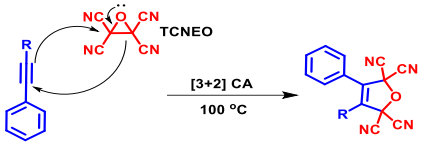

Moderate yield
Harsher condition

c) This work: TCBDs via [2+2] CA-RO reactions between EDG-alkynes and TCNEO

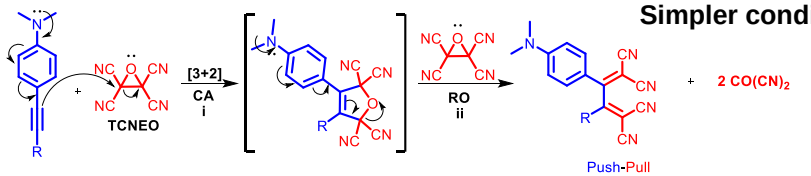

High yielding
Simpler condition

Figure 2.0. a) Push–pull TCBDs synthesis from EDG-alkynes and TCNE using formal "click"-type [2+2] CA–RE reaction.[21] b) [3+2] CA reaction between EDG-free alkynes and TCNEO providing stable tetracyanodihydrofurans.[34] c) Push–pull TCBDs synthesis from EDG-alkyne and TCNEO via [3+2] CA–RO reaction.

2.1. Results and Discussion:

The acceptor TCNE undergoes reaction with activated alkynes and results in the formation of TCBDs (Figure 2.0a). The TCNEO acts as a 1,3-dipolar species at above 100 ^{o}C. Thus the generated carbonyl ylide was found to undergo [3+2] CA reaction with EDG-free alkyne to give a stable TCDHF product (Figure 2.0b). We tried to use activated alkynes for ring-opening of TCDHF under the influence of delocalized electrons from the donor-substituent (Figure 2.0c). The TCBDs formation by EDG-alkynes 3 and 5 proceeds under ambient conditions, respectively, indicating that the first step is initiated by the nucleophilic attack from EDG-activated alkyne, assisted by the electron delocalization from the donor *N,N* dimethyl group towards alkyne. Herein we explored TCNEO as a new class of organic acceptor to undergo [3+2] cycloaddition with electron-rich alkynes. Initially, we tried to synthesize **2** using TCNEO (scheme 1). After several optimized conditions, we end up with complex reaction mixtures (Table 1). The [3+2] cycloaddition reaction between EDG-substituted alkyne and TCNEO is followed by forming a five-membered furan type ring containing significant influence from four cyanide atoms. The furan ring undergoes repeatable rearrangements initiated by ring-opening through electronic delocalization of super donor DMA unit. This combined effect of electronic delocalization from DMA and ring-opening of tetracyanodihydrofuran ring adduct results in a complex reaction mixture and trace amounts of **2.**

Further, the use of additive such as $LiClO_4$ has been found to assists similar reactions like [3+2] cycloaddition–rearrangement and sometimes altering different reactivity.[39,40] Unfortunately, the use of $LiClO_4$ does not show significant results in product yields. The unexpected high reactivity of TCNEO with activated mono-alkynes instigates us to investigate the role of solvents in determining the pathways for TCBD formation. The various attempts to improve the yield of TCBD were failed, including changing the strong EDG (–NMe_2) into weaker EDG (–OMe) group such as 4-ethynyl anisole. We infer that the high reactivity could be because of the presence of active hydrogen atom at

the unsubstituted dicyanovinyl group in the 2-substituted 1,1,4,4-tetracyanobuta-1,3-dienes. We predicted that the TCNEO represents a potential candidate to expand the space push further–pull chromophores. We investigated the role of TCNEO with DMA-acetylene and explored its synthetic paths using different conditions (scheme 1). The screening of various alkynes was carried out for the best results. Regardless of TCNEO equivalents (equiv), no [3+2] cycloadduct of tetracyanodihydrofuran was observed by TLC, and instead, only the TCBD products were noticed TLC. Also, after careful observation, we found that 2 equiv of TCNEO was the optimum amount for the formation of TCBD product; increasing more equiv of TCNEO did not significantly improve the yield.

2.2. Optimization Table:

Since all the TCBD products were already known through the [2+2] CA–RE reaction, the identity of the compounds was cross-checked against the authentic sample of respective product formed in the reaction mixture using silica TLC.

Scheme 1: *Synthesis of 2-(4-(dimethylamino)phenyl)buta-1,3-diene-1,1,4,4-tetracarbonitrile using TCNEO*

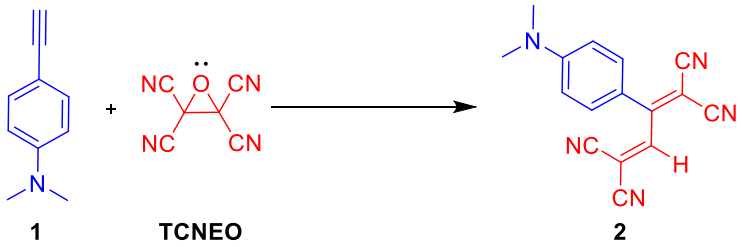

Table 1. Optimization table for the synthesis of compound **2**.[a]

entry	TCNEO equiv	Temp (°C)	Solvent	Additive	TCBD 2 Yield (%)[b]
1	1	25	CH_2Cl_2	none	Trace
2	2	25	CH_2Cl_2	none	10
3	2	0	CH_2Cl_2	None	5
4	2	25	CH_3CN	None	3

5	1	60	CH_3CN	None	2
6	2	25	CH_2Cl_2	$LiClO_4$	Complex
7	2	0	CH_3CN	$LiClO_4$	Complex
8	2	60	CH_3CN	$LiClO_4$	Complex

[a] Reactions were carried out on a 0.1 mmol scale.

[b] Isolated yield.

2.3. Synthesis of TCBDs using TCNEO as an Acceptor:

After following the reaction conditions of TCNEO with EDG-substituted mono-alkynes (Table 1), we synthesized bis-substituted alkynes of amine **3** and **5** to investigate their reactivity's with TCNEO and respective TCBD formations. We isolated the best yield for **4** and a slightly lower yield for **6** (85% yield) while using chlorinated solvent CH_2Cl_2. Whereas, in relatively more polar solvents such as CH_3CN and *N,N'*-dimethylformamide, we end up with a better yield of 95% for **6**. Though the reaction can be performed without the inert atmosphere, the presence of air leads to a ~20% decrease in the TCBD yield.

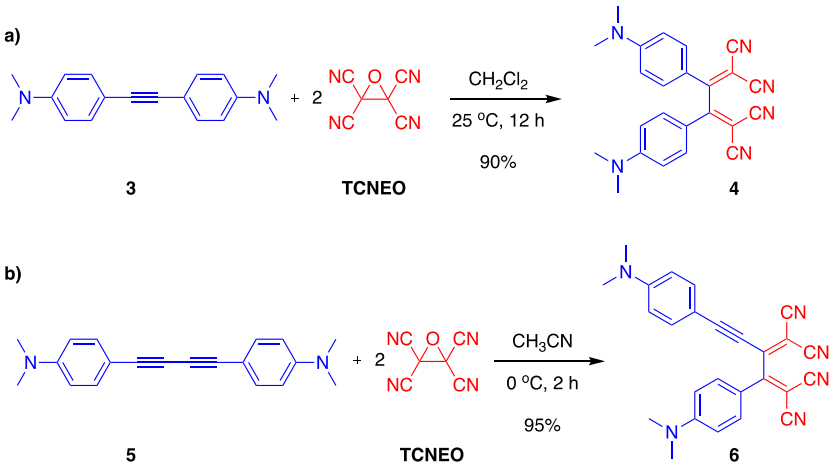

Scheme 2: *Synthesis of 2, 3-disubstituted TCBDs using TCNEO and bis-substituted alkynes via [3+2] CA followed by RO reactions.*

It was known that alkyne attached with TCBD tends to undergo a second CA–RE reaction at high temperature to provide the octacyano[4]dendralenes as a new class of cyano-rich non-planar organic acceptor.[41] Compound **6** was subjected to further reaction

with TCNEO to test whether the **6** having similar features would undergo additional [3+2] CA–RO reaction and provide the corresponding octacyano[4]dendralene, i.e., 3,4-Bis(dicyanomethylidene)-2,5-bis[4(dimethylamino)phenyl]hexa-1,5-diene-1,1,6,6-tetracarbonitrile. However, both TLC and LC-MS have confirmed that such octacyano[4]dendralene did not form (Figure 2.13). Nevertheless, a new blue-colored compound formed as a primary compound, and its structural identity with different chemistry needs to be established with greater detail.

2.4. Mechanism using TCNEO as Acceptor:

After successfully synthesizing TCBDs using TCNEO, a plausible mechanism has been devised to validate the TCBD formations. As the electrophilic character of the oxygen atom bonded between two $–C(CN)_2$ has been proven before for the reaction between the TCNEO and anthracene. The first step of reaction between TCNEO and bis-alkyne generates zwitterionic intermediate I (Figure 2.1). The cationic charge is favorably stabilized as an iminium ion, and such step occurrence has postulated to form in the first step of the CA–RE reaction.[42] This, upon cyclization by the dicyanomethide anion, generates the [3+2] cycloadduct intermediate, *i.e.*, TCDHF derivative II (Figure 2.1b). Unlike the isolable furan adduct formed in the non-activated alkyne,[34] the facile furan ring-opening and generation of oxide ion III are facilitated by electron delocalization from the EDG and the stabilization by the generation of donor-substituted dicyanovinyl (D–A) moiety. The removal of an oxygen atom (deoxygenation) from this derivative is a prerequisite for the formation of TCBD. This is achieved without any extra reagent but with an additional TCNEO molecule, which acts as reducing agent and undergoes nucleophilic attack by the oxide anion at the electrophilic carbon atom generating the new oxide anion intermediate IV. There are two possible mechanistic pathways that can be envisioned for the generation of push–pull TCBDs. In pathway *a* the generated unstable dioxetane may further decompose into two molecules of carbonyl cyanide ($CO(CN)_2$) via retro-electrocyclization. On the other hand, in pathway *b* the elimination of two $CO(CN)_2$ and push–pull TCBD molecules may occur in a single step.

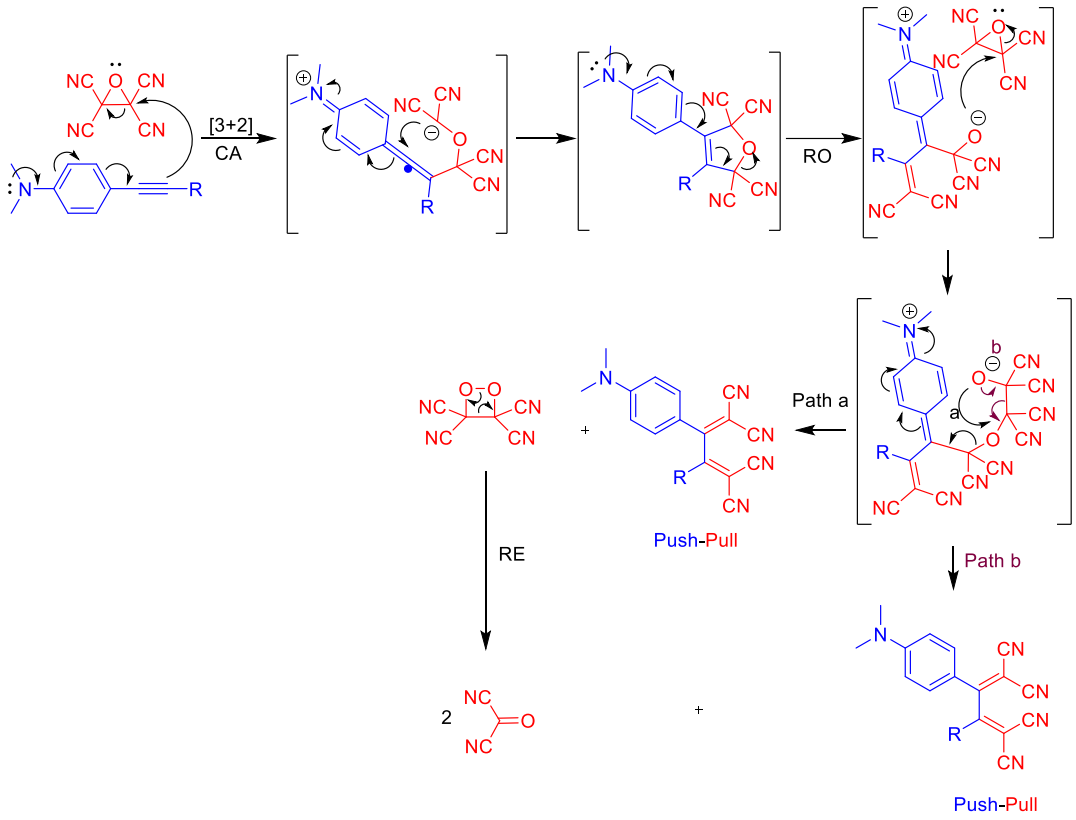

Figure 2.1. a) Proposed mechanism for [3+2] CA–RO reaction for EDG-alkyne.

2.5. Mechanistic studies:

We tested and analyzed the in-situ reaction mixture using LC-MS and ATR FT–IR studies to gain insights on which pathway is being governed in this reaction. To see whether the characteristic peaks corresponding to the dioxetane and $CO(CN)_2$ are present. The ATR FT–IR spectrum of the crude reaction mixture has shown the characteristic peak corresponding to the dioxetane ring O—O the stretching frequency at 670 cm^{-1}, which is absent in both TCBD and TCNEO.[43]

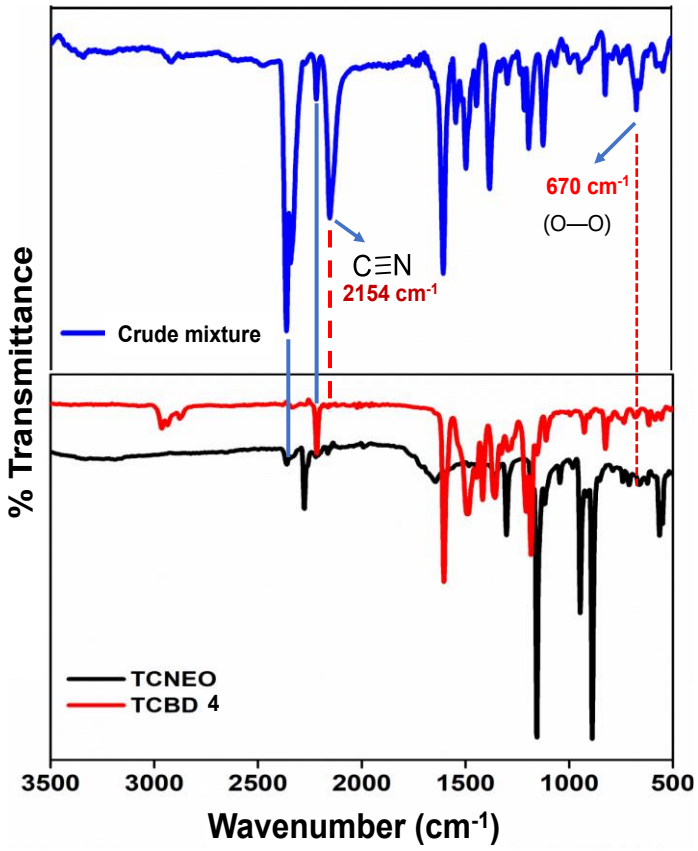

Figure 2.2. FT-IR (ATR) spectra of the crude reaction mixture, TCNEO, and TCBD **4**.

2.6. General Methods of Synthesis and Materials:

All reagents and solvents were obtained from commercial suppliers (Aldrich and TCI-India) and used without further purification. CH_3CN, CH_2Cl_2 was freshly distilled from CaH_2 under the nitrogen (N_2) atmosphere. Column chromatography (CC) was carried out with neutral silica gel. Thin-layer chromatography (TLC) was performed on precoated plastic sheets of silica gel G/UV-254 of 0.2 mm thickness (MachereyNagel, Germany) using appropriate solvents and visualized with UV light (λ = 254 nm). Melting points (M.p.) were measured in open capillaries with a Stuart (automatic melting point SMP50) apparatus and are uncorrected. "Decomp" refers to decomposition. ^{1}H NMR spectra were measured on Bruker Avance II 400 MHz instrument at 25 °C in $CDCl_3$ or DMSO-d_6. Residual solvent signals in the ^{1}H NMR spectra were used as an internal reference. Chemical shifts (δ) are reported in ppm downfield from $SiMe_4$, with the residual solvent signal. Coupling constants (J) are given in Hz. The apparent resonance multiplicity is described as s (singlet), d (doublet), t (triplet), and m (multiplet). Transmission Spectra were measured using ATR FT-IR Bruker Vertex 70; signal designations; s (strong), m (medium), and w (weak). Single-crystal X-ray diffraction data were collected using a

Rigaku XtaLABmini X-ray diffractometer equipped with a Mercury charge-coupled device detector with graphite monochromatic Mo Kα radiation (λ = 0.71073 Å) at 100.0 (2) K using ω scans. The data were reduced using CrysAlisPro 1.171.38.46, and the space group determination was done using Olex2.37. The crystal structures were solved by using ShelXT38 and refined using ShelXL39 through the Olex2 suite. All of the hydrogen atoms were geometrically fixed and refined using the riding model. Absorption correction was done by a multiscan method. All of the packing and interaction diagrams have been generated using Mercury. Liquid chromatography (LC) was performed on a Waters ACQUITY UPLC M-Class LC instrument using a Zorbax Eclipse Plus C18 column (250 × 4.6 mm; 5 μm pore size) from Agilent.

***Synthesis and characterization of push–pull chromophore 4 using TCNEO*:** A solution of TCNEO (20 mg, 0.14 mmol) in anhydrous degassed CH_2Cl_2 (10 mL) was treated dropwise 4,4'-(ethyne-1,2-diyl)bis(*N,N'*-dimethylaniline) **3** (18 mg, 0.07 mmol) at 25 °C in degassed CH_2Cl_2 solvent (10 mL) stirred at the same temperature for 12 h. The solution color changes occur approximately after 3 h. The reaction mixture saturated NaCl solution was poured and extracted with CH_2Cl_2 (3 × 10 mL). The combined organic layers were washed with brine, dried over anhydrous Na_2SO_4, and evaporated. The crude product was columned using silica (hexane/CH_2Cl_2 7:3) and recrystallized by slow diffusion of hexane into CH_2Cl_2 to afford the pure product **4** (49 mg, 90 % yield). R_f = 0.3 (SiO_2; hexane/CH_2Cl_2 7:3) Reddish metallic solid, M.p. 274–275 ^oC (Decomp); ^1H NMR (400 MHz; 298 K, $CDCl_3$) δ = 3.14 (s, 12 H), 6.70 (d, J = 9.0 Hz, 4 H), 7.79 ppm (d, J = 9.0 Hz, 4 H).

***Synthesis and characterization of push–pull Chromophore 6* using TCNEO**: A solution of TCNEO (20 mg, 0.14 mmol) in anhydrous degassed CH_3CN (10 mL) was cooled at 0 °C, treated dropwise *4,4'*-(buta-1,3-diyne-1,4-diyl)bis(*N,N'*-dimethylaniline) **5** (20 mg, 0.07 mmol), in degassed CH_3CN (10 mL) stirred at the same temperature for 2 h. After completion of the reaction, acetonitrile was vacuum evaporated. The residue was dissolved in CH_2Cl_2, mixed with water, and extracted with CH_2Cl_2 (3 × 10 mL). The combined organic layers were washed with brine, dried over anhydrous Na_2SO_4, and evaporated. The crude product was columned using silica (hexane/CH_2Cl_2 7:3) and recrystallized by slow diffusion of hexane into CH_2Cl_2 to afford the pure product **6**[21] (55 mg, 95 % yield). R_f = 0.3 (SiO_2; hexane/CH_2Cl_2 8:2) Black colored solid, M.p. 190–193 ^oC (Decomp); ^1H NMR (400 MHz, 298 K; $CDCl_3$) δ = 3.04 (s, 6 H), 3.14 (s, 6 H), 6.62

(d, *J* = 8.0 Hz, 2 H), 6.70 (d, *J* = 8.0 Hz, 2 H), 7.47 (d, *J* = 8.0 Hz, 2 H), 7.78 ppm (d, *J* = 8.0 Hz, 2 H).

2.7. X-ray studies:

X-ray Data for Compound 6:

The identity of the compounds was checked against the authentic sample of respective product formation in the reaction mixture using silica TLC prepared using TCNE since all the TCBD products were already known through the [2+2] CA–RE reaction. Further, the successful formation of TCBDs **4** and **6** was characterized by melting point, ^{1}H-NMR, and unambiguous proof for the TCBD constitution was obtained from the single-crystal study. While compound **4** provided the same structure as previously reported CCDC deposition number 256339,[21] in the case of TCBD **6**, the obtained crystal structure (CCDC deposition number 2009612) is a new polymorphism (II) with monoclinic unit cell and P 21/c (14) space group (Figure 2, for details), unlike the previously reported polymorphism (I) showing triclinic lattice with $P1^{-}$ space group (CCDC deposition number 256338).[21] The comparison table of these two polymorphs is provided in Table 2.

The crystal structure obtained in the previous study using TCNE is called here ***polymorph I,*** *and in this study using TCNEO is called* ***polymorph II***.

Table 2. Crystal structure data and experimental details of **polymorph-I**[21] and **-II** of **6**.

	Polymorph I	**Polymorph II**
Crystal data		
CCDC deposition number	256338	2009612
Chemical formula	$C_{26}H_{20}N_6$•2(CH_2Cl_2)	$C_{26}H_{20}N_6$
M_r (g mol^{-1})	586.33	416.48
Crystal system, space group	Triclinic, $P\bar{1}$ (no.2)	Monoclinic, $P2_1/c$ (no.14)
Temperature (*K*)	263	293
a, b, c (Å)	7.3661(1), 9.5653(2), 20.8690(4)	17.2509(19), 17.0756(17), 8.2275(9)
β (°)	95.014(7)	94.912(4)
V (Å^3)	1462.03(5)	2414.7(4)

Z	2	4
Radiation type	Mo K_α	Mo K_α
μ (mm^{-1})		0.071
Crystal size (mm)		0.10 x 0.31 x 0.34
Data collection		
Diffractometer	Bruker-Nonius Kappa-CCD	Bruker D8 Venture PHOTON 100
Absorption correction		Multi-scan
T_{min}, T_{max}		0.592, 0.745
Number of measured,	11122, 6573, and 5258	24495, 4907 and 3253
Independent and observed [$I > 2\sigma(I)$] reflections		
R_{int}	0.03	0.0568
R_{sigma}		0.0569
(sin $\theta/\lambda)_{max}$ ($Å^{-1}$)	0.7107	0.71073
Refinement		
$R[F^2 > 2\sigma(F^2)]$, w$R(F^2)$, S		0.0963 (3253), 0.2434 (4907), 1.03
Number of reflections	2223	4907
Number of parameters	348	289

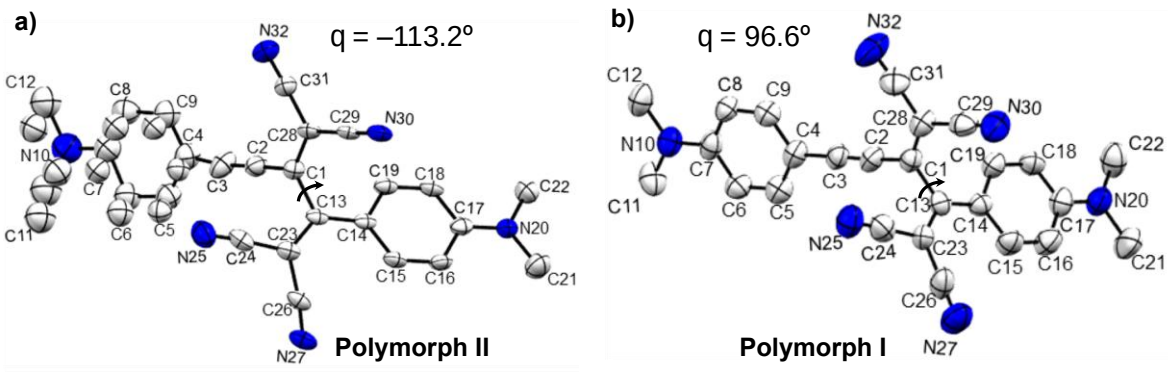

Figure 2.4. ORTEP plots of a) 6 polymorph II, b) 6 polymorph I[21] (arbitrary numbering, H-atoms are omitted for clarity).

a) ORTEP plot of 6 polymorph II. Atomic displacement parameters are drawn at a 50% probability level. Selected bond lengths [Å], angles [°], and torsional angles [°]: C1–C2 1.387(12), C1–C13 1.499(11), C2–C3 1.211(11), C3–C4 1.410(12), C4–C5 1.393(12), C4–C9 1.342(12), C5–C6 1.391(11), C6–C7 1.482(11), C7–N10 1.415(10), C7–C8 1.269(11), C8–C9 1.460(10), C13–C14 1.434(10), C14–C15 1.411(11), C14–C19 1.408(10), C15–C16 1.363(11), C16–C17 1.426(11), C17–N20 1.347(10), C17–C18 1.406(11), C18–C19 1.364(10), C28–C1–C13 120.60(7), C3–C2–C1 177.53(8), C2–C3–C4 170.59(8), C23–C13–C1 114.47(6), C24–C23–C26 111.55(7), C31–C28–C29 116.41(8), C14–C13–C1–C28: 67.24 (8), C15–C14–C13–C23: 15.08(8), C28–C1–C13–C23: –113.22(8), C31–C28–C1–C2: –2.11(8).

b) ORTEP plot of 6•2CH$_2$Cl$_2$ polymorph I.[21] (arbitrary numbering, H-atoms are omitted for clarity). Atomic displacement parameters are drawn at a 50% probability level. Selected bond lengths [Å], angles [°], and torsional angles [°]: C1–C2 1.397(12), C1–C13 1.515(11), C2–C3 1.179(11), C3–C4 1.430(12), C4–C5 1.392(12), C4–C9 1.417(12), C5–C6 1.358(11), C6–C7 1.410(11), C7–N10 1.370(10), C7–C8 1.421(11), C8–C9 1.348(10), C13–C14 1.431(10), C14–C15 1.394(11), C14–C19 1.408(10), C15–C16 1.346(11), C16–C17 1.400(11), C17–N20 1.336(10), C17–C18 1.394(11), C18–C19 1.364(10), C28–C1–C13 120.45(7), C3–C2–C1 175.25(8), C2–C3–C4 178.77(8), C23–C13–C1 113.32(6), C24–C23–C26 114.03(7), C31–C28–C29 116.67(8), C15–C14–C13–C23: 0.49 (8), C28–C1–C13–C23: 96.64(8), C31–C28–C1–C2: –0.10(8).

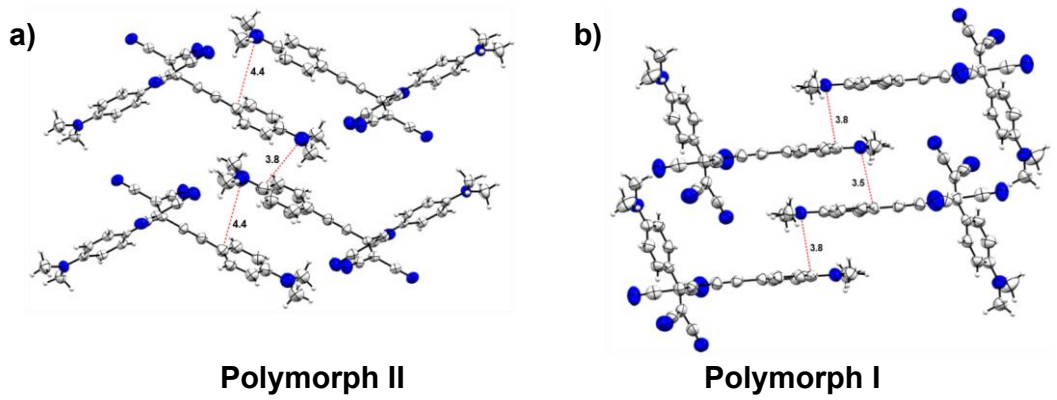

Figure 2.5. Arrangement of neighboring molecules in the crystal packing of a) 6 in polymorph II, b) 6•2(CH_2Cl_2)$_2$ in polymorph I.

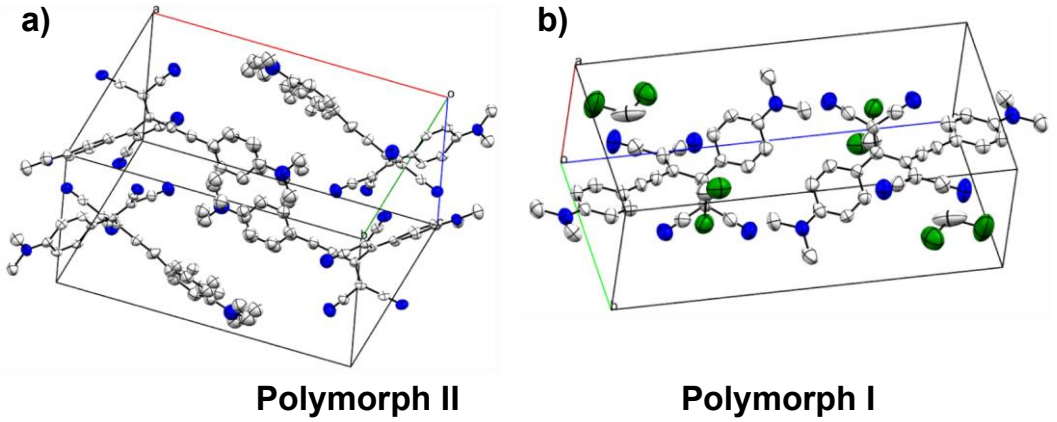

Figure 2.6. Unit cell lattice showing the number of molecules of a) 6 in polymorph II, b) 6•2CH2Cl22 in polymorph I.

2.8. NMR Spectra:

*^{1}H-NMR spectra of TCBDs **4** and **6**.*

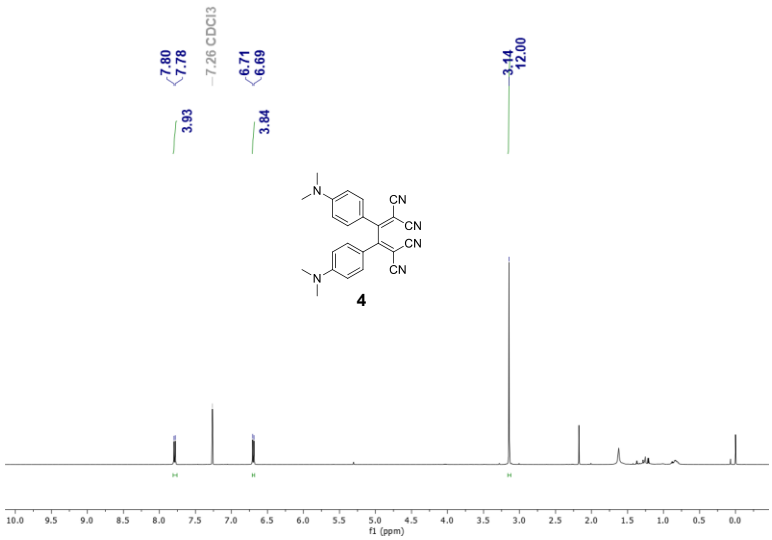

Figure 2.7. 400 MHz ^{1}H NMR spectrum of **4** recorded at 298 K in $CDCl_3$.

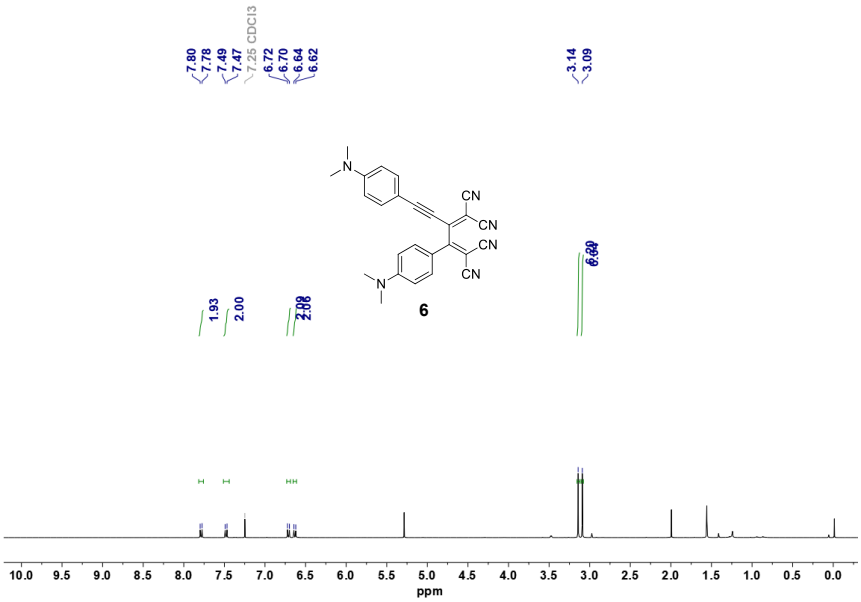

Figure 2.8. 400 MHz ^{1}H NMR spectrum of **6** recorded at 298 K in $CDCl_3$.

2.9. LC-MS Data:

To approve the plausible pathway for the mechanism, we performed LC-MS spectroscopy for the crude reaction mixture. After injecting the sample carefully, we observed the molecular ion (*m/z* 160.06 Daltons) peak corresponds to the 3,3,4,4-tetracyano-1,2-dioxetane in the LC-MS spectrum of the crude reaction mixture. Since

both the pathways hypothesized for the synthesis of TCBDs using TCNEO eventually lead to the formation of $CO(CN)_2$, the evidence for the presence of 3,3,4,4-tetracyano-1,2-dioxetane (intermediate), in particular, suggests that pathway *a* is operated in the reaction.

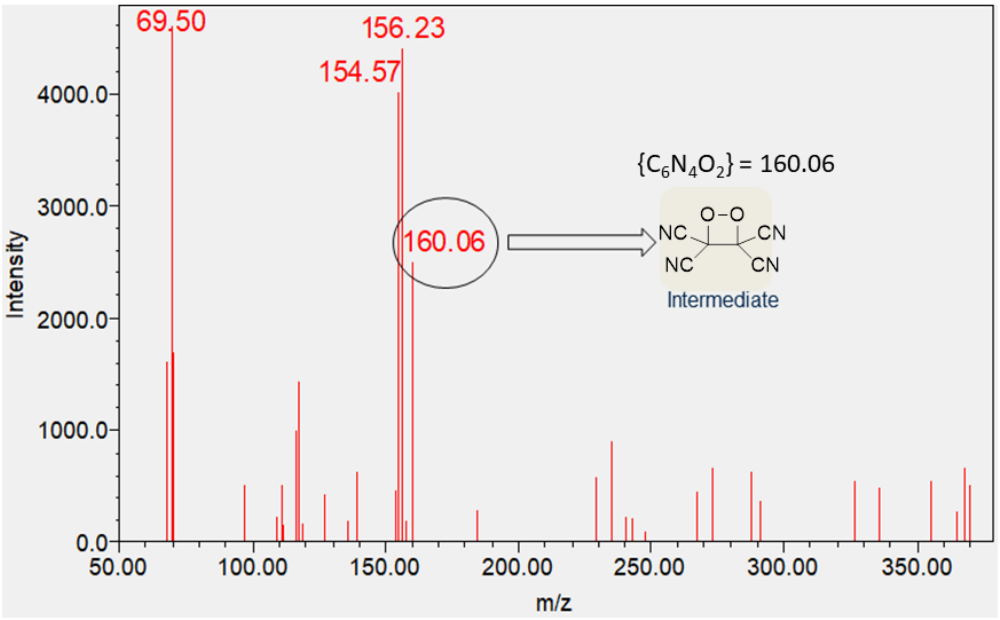

Figure 2.9. LC-MS spectrum of the crude reaction mixture for the **3** and TCNEO (MS-ESI) m/z Calcd for {C6N4O2}: 160.00, found 160.06.

Liquid chromatography-mass spectrometry (LC-MS): All the analysis performed on reactive intermediates using LC-MS is carried out using a reverse-phase HPLC system from waters equipped with a photodiode array detector (Waters 2998).

2.10. Monitoring of Reaction of Alkynes with TCNEO by TLC and LC:

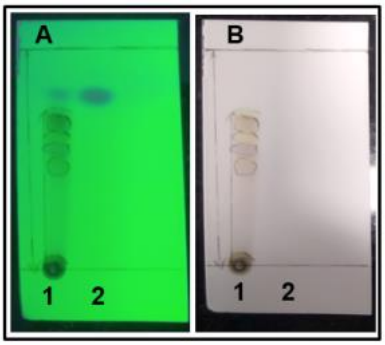

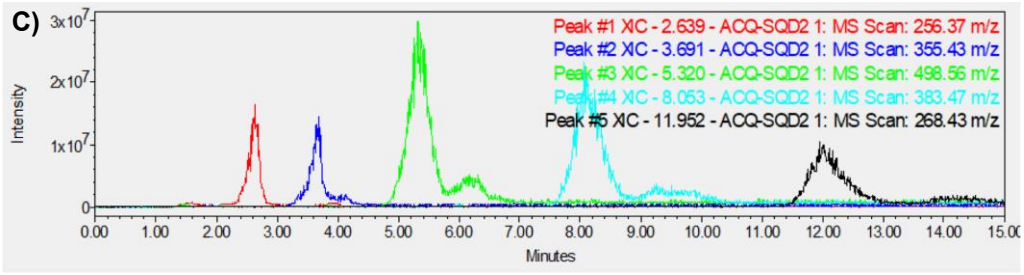

Figure 2.10. TLC of 4-ethynyl-*N,N'*-dimethylaniline **1** with one equivalent (equiv) of TCNEO in CH_2Cl_2 (TLC eluent: EtOAc/hexane 25:75) visualized in the A) presence and B) absence of UV light (280 nm). Spot 1 indicates the reaction mixture, and spot 2 is starting material **1**. Note: some spots are visible with the naked eye than in the photo due to less intensity. C) LC-MS profile for entry 1 in Table 1.

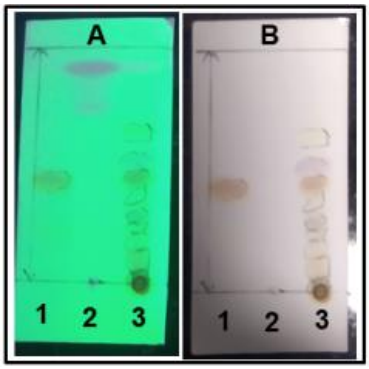

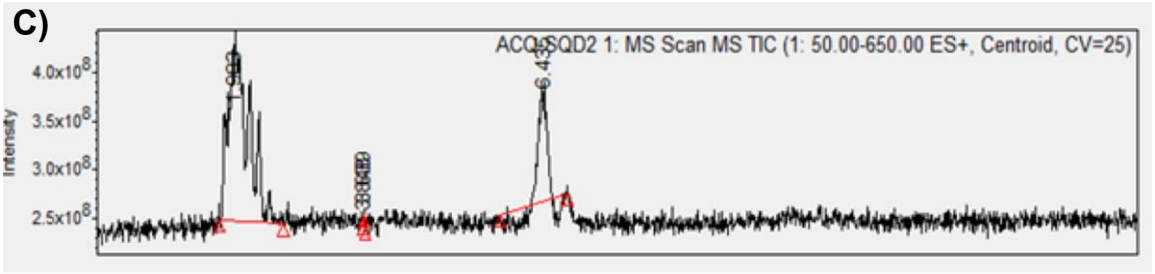

Figure 2.11. TLC of 4-ethynyl-*N,N'*-dimethylaniline **1** with 1 equiv of TCNEO in CH_3CN (TLC eluent: EtOAc/hexane 25:75) visualized in the A) presence and B) absence of UV light (280 nm). Spot 1 indicates the authentic compound **2**, spot 2 corresponds to the starting material **1**, and spot 3 is the reaction mixture. C) LC-MS profile for entry 2 in Table 1.

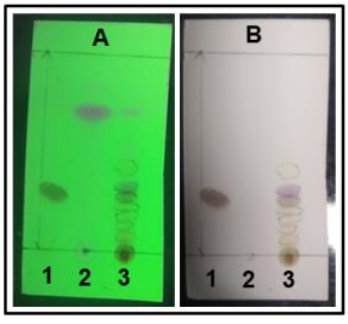

Figure 2.12. TLC of 4-ethynyl-*N,N'*-dimethylaniline **1** with 2 equiv of TCNEO in CH_2Cl_2 at 25 C (TLC eluent: EtOAc/hexane 20:80) visualized in the A) presence and B) absence of UV light (280 nm). Spot 1 indicates the authentic compound **2**, spot 2 corresponds to the starting material **1**, and spot 3 is the reaction mixture for entry 4 in Table 1.

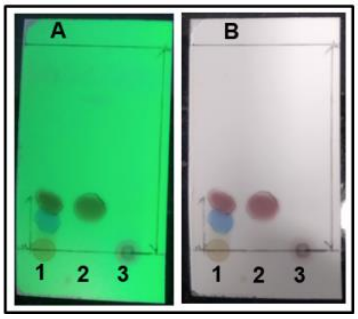

Figure 2.13. TLC of chromophore **6** with 1 equiv of TCNEO in $ClCH_2CH_2Cl$ at 110 °C, 24 h (TLC eluent: EtOAc/hexane 15:85) visualized in the A) presence and B) absence of UV light (280 nm). Spot 1 is reaction mixture, spot 2 correspond to the starting material **6**, spot 3 correspond to the authentic compound octacyano[4]dendralene i.e., 3,4-Bis(dicyanomethylidene)-2,5-bis[4-(dimethylamino)phenyl]hexa-1,5-diene- 1,1,6,6-tetracarbonitrile synthesized as per literature.

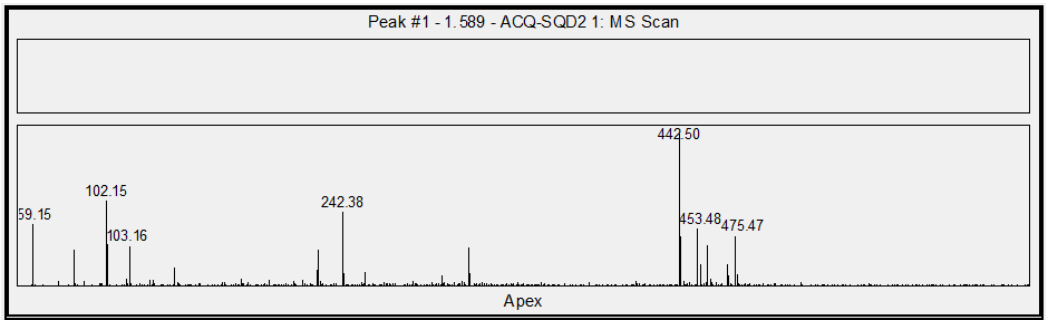

Figure 2.14. LC-MS profile of the reaction indicating the newly formed blue spot, which surprisingly does not correspond to the octacyano[4]dendralene, i.e., 3,4-Bis(dicyanomethylidene)-2,5-bis[4-(dimethylamino)phenyl]hexa-1,5-diene- 1,1,6,6-tetracarbonitrile whose calculated mass is {$C_{32}N_{20}N_{10}$}: 544.18.

2.11. Conclusion:

The synthesis of non-planar push–pull chromophores require strong organic acceptors and donors to undergo [2+2] CA-RE reactions. Unfortunately, the acceptor part is very scarce, and there is always a window to look for more acceptors to expand the availability of acceptor synthons for the synthesis of TCBDs. Here, we demonstrated that the EDG-substituted TCBDs could be synthesized from an unconventional method using TCNEO

as the precursor for the first time instead of TCNE *via* [3+2] CA–RO reactions. Though the low yields of TCBDs have been observed during the reaction of TCNEO with EDG-substituted mono-alkynes, which may be due to the high reactivity of unsubstituted TCBDs leading to further reaction pathways. In contrast, disubstituted EDG-alkynes underwent smooth conversion to TCBDs under specific conditions with TCNEO. Overall, the procedure is much simpler, additive-free, and a valuable method for synthesizing TCBDs in just a single step with excellent yields. The key for the synthesis of TCBDs is EDG in the alkyne, which facilitated the RO reaction following the first step [3+2] CA reaction step. A mechanism involves the deoxygenation from the tetracyanodihydrofuran derivative, which is driven by the nucleophilic addition of another molecule of TCNEO, leading to the formation of 3,3,4,4-tetracyano-1,2-dioxetane that may decompose to carbonyl cyanide. FT-IR and LC-MS studies confirm the formation of TCBDs as the essential products. Though some shortcomings exist with the present methodology to synthesize TCBDs, such as mono-substituted alkynes, do not yield clean outcomes, not being atom-economical, but on the other side offers advantages, for instance, an alternative way to make TCBDs with excellent yields for disubstituted alkynes. Lastly, the synthesis of TCBDs using TCNEO via ring-opening under the influence of electron delocalization from the donor opens up a new window to explore different reactivity products and expand the chemical space for push–pull chromophores.

2.12. References:

1. Ostroverkhova, O. *Chem. Rev*. **2016**, *116*, 13279−13412. (b) Mayor, M. *Chimia*. **2010**, *64*, 348–420.
2. Vallaitis, T.; Bogatscher, S.; Alloatti, L.; Dumon, P.; Baets, R.; Scimeca, M. L.; Biaggio, I.; Diederich, F.; Koos, C.; Freude, W.; Leuthold, J. *Opt. Express*. **2009**, *17*, 17357–17368.
3. Dou, L.; Liu, Y.; Hong, Z.; Li, G.; Yang, Y. *Chem. Rev*. **2015**, *115*, 12633–12665.
4. Senanayak, S. P.; Sangwan, V. K.; McMorrow, J. J.; Everaerts, K.; Chen, Z.; Facchetti, A.; Hersam, M. C.; Marks, T. J.; Narayan, K. S. *ACS Appl. Mater. Interfaces*. **2018**, *10*, 21492–21498.
5. Klikar, M.; Kityk, I. V.; Kulwas, D.; Mikysek, T.; Pytelaa, O.; Bures, F. *New J. Chem*. **2017**, *41*, 1459–1472.

6. Koos, C.; Vorreau, P.; Vallaitis, T.; Dumon, P.; Bogaerts, W.; Baets, R.; Esembeson, B.; Biaggio, I.; Michinobu, T.; Diederich, F.; Freude, W.; Leuthold, J. *Nat. Photonics.* **2009**, *3*, 216–219.
7. Bui, A. T.; Philippe, C.; Beau, M.; Richy, N.; Cordier, M.; Roisnel, T.; Lemiègre, L.; Mongin, O.; Paul, F.; Trolez, Y. *Chem. Commun*. **2020**, *56*, 3571–3574.
8. Gopalan, A.-I.; Komathi, S. S.; Muthuchamy, N.; Lee, K.-P.; Whitcombe, M. J.; Dhana, L.; Sai-Anand, G. *Prog. Polym. Sci*. **2019**, *88*, 1–129.
9. Chen, L.; Wu, D.; Yoon, J. *ACS Sens.* **2018**, *3*, 27–43.
10. Dey, N.; Kulhánek, J.; Bureš, F.; Bhattacharya, S. *J. Org. Chem*. **2019**, *84*, 1787–1796.
11. Pramanik, S.; Deol, H.; Bhalla, V.; Kumar, M. *ACS Appl. Mater. Interfaces* **2018**, *10*, 12112−12123.
12. Li, Y.; Ashizawa, M.; Uchida, S.; Michinobu, T. *Macromol. Rapid Commun*. **2011**, *32*, 1804−1808.
13. Campagnola, P. S. *Anal. Chem*. **2011**, *83*, 3224–3231.
14. Clifford, J. N.; Martınez-Ferrero, E.; Viterisi, A.; Palomares, E. *Chem. Soc. Rev*. **2011**, *40*, 1635–1646.
15. Liang, M.; Chen, J. *Chem. Soc. Rev*. **2013**, *42*, 3453–3488.
16. Chen, F.; Zhang, J.; Wan, X. *Chem. – Eur. J*. **2012**, *18*, 4558–4567.
17. Abbotto, A.; Beverina, L.; Bozio, R.; Bradamante, S.; Ferrante, C.; Pagani, G. A.; Signorini, R. *Adv. Mater*. **2000**, *12*, 1963–1967.
18. Wurthner, F.; Wortmann, R.; Meerholz, K. *Chem. Phys. Chem*. **2002**, *3*, 17–31.
19. Michinobu, T.; Diederich, F. *Angew. Chem. Int. Ed*. **2018**, *57*, 3552–3577.
20. Bures, F. *RSC Adv*. **2014**, *4*, 58826–58851.
21. Michinobu, T.; May, J. C.; Lim, J. H.; Boudon, C.; Gisselbrecht, J.-P.; Seiler, P.; Gross, M.; Biaggio, I.; Diederich, F. *Chem. Commun*. **2005**, 737–739.
22. Michinobu, T.; Boudon, C.; Gisselbrecht, J.-P.; Seiler, P.; Frank, B.; Moonen, N. N. P.; Gross, M.; Diederich, F. *Chem. – Eur. J*. **2006**, *12*, 1889–1905.
23. Michinobu, T.; Diederich, F. *Angew. Chem. Int. Ed*. **2018**, *57*, 3552–3577.
24. Kato, S.-i.; Diederich, F. *Chem. Commun*. **2010**, *46*, 1994–2006.
25. For a review, see Bruce, M. I. *Aust. J. Chem*. **2011**, *64*, 77−103.
26. Pappenfus, T. M.; Schneiderman, D. K.; Casado, J.; Navarrete, J. T. L.; Delgado, M. C. R.; Zotti, G.; Vercelli, B.; Lovander, M. D.; Hinkle, L. M.; Bohnsack, J. N.; Mann, K. R. *Chem. Mater*. **2011**, *23*, 823−831.

27. Kato, S.-i.; Kivala, M.; Schweizer, W. B.; Boudon, C.; Gisselbrecht, J.-P.; Diederich, F. *Chem. – Eur. J*. **2009**, *15*, 8687–8691.
28. Shoji, T.; Ito, S.; Toyota, K.; Yasunami, M.; Morita, N. *Chem. – Eur. J*. **2008**, *14*, 8398–8408.
29. Sasaki, S.; Mizutani, K.; Kunieda, M.; Tamiaki, H. *Tetrahedron* **2013**, *16*, 9772–9778.
30. Kato, S.-i.; Noguchi, H.; Jin, S.; Nakamura , Y. *Asian J. Org. Chem*. **2016**, *5*, 246–256.
31. Betou, M.; Durand, R. J.; Sallustrau, D. A.; Gousset, C.; Le Coz, E.; Leroux, Y. R.; Toupet, D. L.; Trzop, E.; Roisnel, T.; Trolez, Y. *Chem. Asian J*. **2017**, *12*, 1338–1346.
32. Dar, A. H.; Gowri, V.; Gopal, A.; Muthukrishnan, A.; Bajaj, A.; Sartaliya, S.; Selim, A.; Ali, M. E.; Jayamurugan, G. *J. Org. Chem*. **2019**, *84*, 8941−8947.
33. Reekie, T. A.; Donckele, E. J.; Ruhlmann. L.; Boudon, C.; Trapp, N.; Diederich, F. *Eur. J. Org. Chem*. **2015**, 7264–7275.
34. Linn, W. J.; Webster, O. W.; Benson, R. E *J. Am. Chem. Soc*. **1965**, *87*, 3651–3656.
35. Linn, W. J. Tetracyanoethylene oxide. *Org. Synth*. **1973**, 1007.
36. Brown, P. R.; Cookson, C. *Tetrahedron* **1968**, *24*, 2551–2566.
37. Frolova, L. V.; Magedov, I. V.; Harper, A.; Jha, S. K.; Ovezmyradov, M.; Chandler, G.; Garcia, J.; Bethke, D.; Shaner, E. A.; Vasiliev, I.; Kalugin, N. G. *Carbon* **2015**, *81*, 216–222.
38. Peng, X.; Li, Y.; Zhang, G.; Zhang, F.; Fan, X. *J. Nanomaterials*. **2013**, 841789.
39. Donckele, E. J.; Finke, A. D.; Ruhlmann, L.; Boudon, C.; Trapp, N.; Diederich, F. *Org. Lett*. **2015**, *17*, 3506−3509.
40. Donckele, E. J.; Reekie, T. A.; Trapp, N.; Diederich, F. *Eur. J. Org. Chem*. **2016**, 716–724.
41. Brieten, B.; Wu, Y.-L.; Jarowski, P. D.; Gisselbrecht, J.-P.; Boudon, C.; Griesser, M.; Onitsch, C.; Gescheidt, G.; Schweizer, W. B.; Langer N.; Lennartz, C.; Diederich, F. *Chem. Sci*. **2011**, *2*, 88–93.
42. Wu, Y.; Jarowski. P. D.; Schweizer, W. B.; Diederich, F. *Chem. – Eur. J*. **2010**, *16*, 202–211.
43. Kopecky, K. R.; Gomez, R. R. *Can J. Chem*. **1984**, *62*, 277−279.

Chapter 3:

Designing of Non-planar Push−pull Chromophores with Luminescent Properties

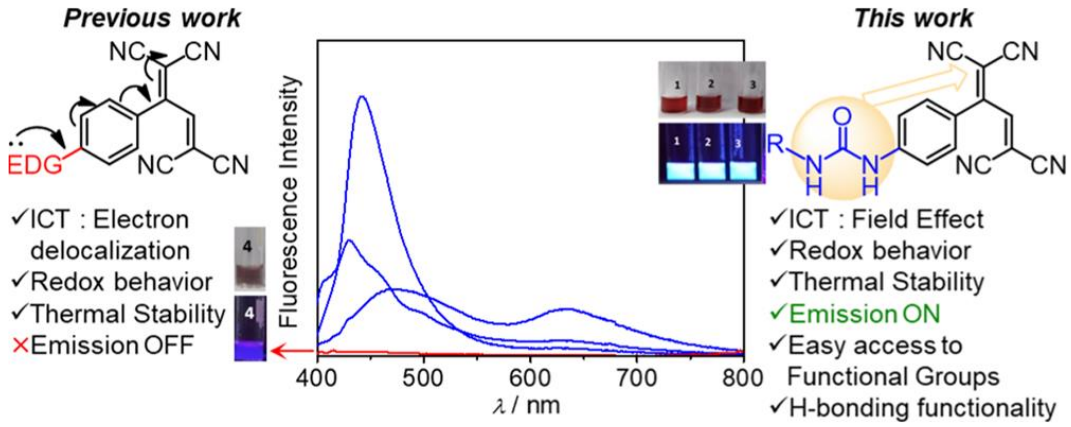

3.0 Introduction:

Organic conjugated systems constitute one of the promising systems in organic material chemistry. They have been active materials in organic electronics, optoelectronics,[1–4] fluorescence sensing,[5] bio-imaging[6] conductors, photovoltaics, and solar photon conversion devices (as an active layer in DSSCs), etc. New strong organic electron donors and acceptors are continuously being developed and conjugated into π-systems featuring low-energy charge-transfer (CT) bands and explore their future applications. The strong intermolecular D–A interactions are known to produce bimolecular CT complexes and salts, some of which exhibit high electric conductivity or interesting magnetic properties such as tatracyanoquinodimethane-tetrathiafulvalene (TCNQ-TTF) complexes. Furthermore, stable, strong organic acceptors attract interest as *p*-type dopants to improve the performance of organic light-emitting diodes (OLEDs) and organic solar cells. Organic push−pull chromophores can also be modified by manipulating their structural behavior using different spacers with different donors and acceptors. The respective properties of push−pull chromophore also get altered with a change in the spacer, donor, and acceptor parts.

As the planar and non-planar push–pull chromophores receive considerable attention because of their potential applications in optoelectronic devices. The vast majority of the compounds studied involve planar systems to retain linear π-conjugation. Although planar systems show extraordinary properties, there is a strong demand for their non-planar counterparts. Chromophores are generally utilized as thin films in devices, and the morphology of these films is crucial. Improved solubility and processability of the non-planar push–pull chromophores create essential advantages over their planar counterparts. Accordingly, these non-planar systems represent fundamental structures in advanced material science.

Along with the synthesis of push–pull chromophores, precise control over the mode of spatial organization is indeed a progressive approach for designing future electronic materials ranging from biology to material sciences. The supramolecular self-assembly of various functional π–systems has been investigated extensively in recent decades, which governs the photophysical properties of the resulting self-assembled material. The non-covalent interactions, especially H-bonding interactions, have played a pivotal role in generating desired supramolecular nanostructures from suitably designed small

molecular building blocks. Surprisingly not much is known regarding the utility of simple fluorescent push−pull chromophores as self-complementary hydrogen-bonding functionalities.

Here we focus on fundamental and application-related aspects of the already exploiting formal [2+2] cycloaddition-retroelectrocyclization (CA−RE) reactions between electron-rich triple bonds and electron-deficient alkenes. The reaction was remarkably efficient when strong donors were present on the alkyne moiety or highly electron-poor olefins were used. In the course of these studies, the scope of available push−pull chromophores was expanded by a wide variety of unprecedented chemical structures with remarkable optoelectronic, chiroptical, and electrochemical properties. A series of synthetic and mechanistic studies were performed by utilizing novel substrates with inherent, intrinsic properties and potential applications to understand better and enrich the library of push-pull chromophores.

This chapter will give a detailed study of exploring the urea functional group as a potential electron donor to synthesize fluorescent organic push−pull chromophores. Urea is an immensely exploited organic compound both as organic fertilizers and drug-related critical organic molecules. However, its versatile polar amide functional group finds many uses in suitable organic technologically oriented products, such as organic sensors for gases, anions, and cations.[7] Biologically applied organic molecules such as synthetic ion channels[8] also deploy urea-based modified functional organic molecules. In particular, several substituted urea have been recently shown to possess a marked inhibiting effect on HIV protease enzyme.[9] Due to the increasing importance of these compounds, during the last years, there has been considerable interest in developing new efficient, selective, and environmentally friendly protocols for their preparation as urea moiety imports its consumption in various forms, as mentioned above. We started expanding the structure space of urea-based compounds in material sciences by synthesizing highly fluorescent urea-based push−pull chromophores. We used amide of urea as donor moiety, which undergoes CA−RE with electron-deficient tetracyanoethylene (TCNE) at room temperature. Urea having two amide linkages is in continuous resonance with carbonyl oxygen. We exploited the idea of having one lone pair of amide free for making alkyne moiety electron-rich to undergo cycloaddition reaction with TCNE, resulting in the formation of 1,1,4,4-tetracyanobuta-1,3-dienes

(TCBD) functionalized urea push−pull chromophore. Push−pull chromophores are very much imported from the last decade for their eminent applications in organo-electronic materials, Organic photonics, fluorophores for tagging proteins, and biologically important organic molecules such as DNA.

Many electron-donating groups (EDG) have been investigated to synthesize EDG-substituted TCBDs push−pull chromophores exhibiting intense ICT band, redox behavior with high stability.[10] Those EDGs, have limitations, i.e., further functionalization on the D-A moiety is difficult or nearly impossible,[11,12] which typically involve multistep synthesis to obtain the precursor with lower yields, and in general, they do not exhibit any fluorophore behavior.[13,14] To overcome this and get a new push−pull chromophore class with new photophysical properties, we used urea as EDG for CA−RE reaction with TCNE. In 2005, Diederich and co-workers' seminal work showed that metal-free strong EDG based on *N,N'*-dialkyanilino-alkyne (DMA) group could undergo clean transformation at ambient temperature.[15-17] The products obtained are highly non-planar, and some of them showed a remarkable third-order nonlinear optical property. This strategy was greatly expanded to synthesize various molecular structures like dendritic and dendralene systems, including cascade CA−RE reactions.

Similarly, Shoji and co-workers have used azulene as EDG to obtain push−pull TCBDs.[11,12] Interestingly, not only strong EDG, weaker EDGs like anisole and thiophene,[18] *N,N'*-diphenyl aniline,[19–22] and "electronically confused alkyne" having an EDG and an electron-withdrawing group (EWG) such as -CN,[23,24] and very recently EWG-substituted ynamides[25] were known to undergo CA−RE reaction but in general require more forcing conditions. We show for the first time that urea not only acts as an efficient electron donor it also brings additional features like easy access with desired functional groups, as many of the isocyanates are commercially available, which eventually give different core structures to urea-based push−pull chromophores.

3.1. Origin of the proposal:

The synthesis of urea-based TCBDs has envisaged us to investigate the real reasons for the surprising high reactivity of urea-alkyne towards CA−RE reaction. After carefully observing the literature related to the reactivity parameters and pattern of different substituents. We found that the high reactivity of urea quite comparable to that of DMA-alkyne because both DMA and urea exhibit similar Field/inductive substituent

parameters (F = 0.15 for NMe_2 and F = 0.19 for $NHCONHCH_2CH_3$).[26,27] As the Hammett constant values for urea and DMA are pretty different, the structural reactivity elaboration of urea and DMA based on Hammett's constant values seems to show a nonlinear relationship. Hammett's constant values and Hammett's theory for reactivity pattern distribution have been utilized efficiently throughout most organic moieties' reactivity patterns. However, there are limitations, for e. g explain reactivity urea-alkyne towards CA−RE. We show for the first time that urea not only facilitated the CA–RE reaction (Figure 3.0), it also brings additional features like fluorescent TCBDs, easy access to desired functional groups, strong ICT driven by field-effect, redox behavior, thermal stability, H-bonding receptor. The Field effect results from combined effective interactions operating in a molecule involving electrostatic and electronic delocalization effects of inductive/ mesomeric/ resonance effects. Moreover, it offers easy access to functional groups (FGs), hydrogen bonding moiety, and unique electron-donating ability, which is expected to show new photophysical properties.

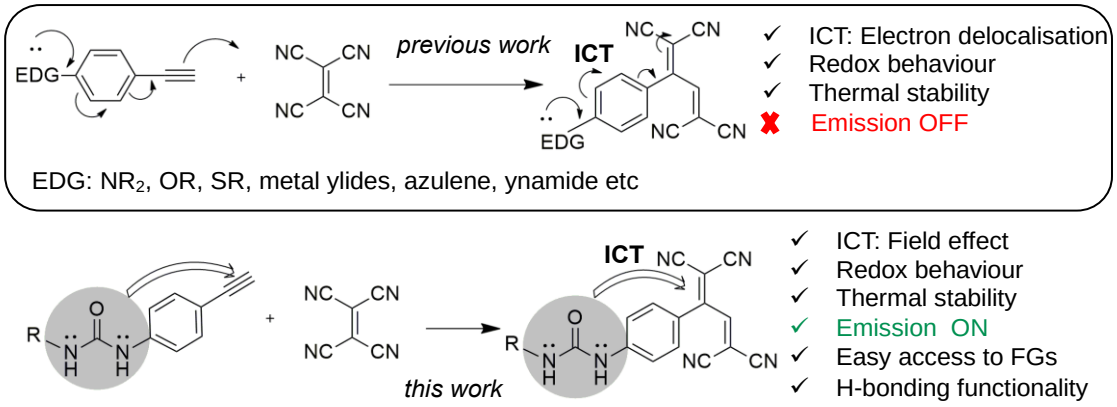

Figure 3.0. TCBDs synthesis from EDG-substituted alkyne and electron-acceptor alkene.

We then studied their photophysical properties after successfully synthesizing chromophores **1**, **2**, and **3** (Scheme 1). The urea functionalized chromophores are maroon in color and high melting solids (262–269 ^oC), which are slightly soluble in CH_3CN, whereas highly soluble in polar solvents acetone, DMF, and DMSO due to the presence of H-bonding facilitating urea group.

3.2. Results and discussions:

Scheme 3.0 shows the synthetic methodology adopted to synthesize urea-substituted phenyl-TCBDs **1**−**3** (urea-TCBDs) in two-step reactions. The alkyne precursors **8**, **9**, and

10 were synthesized starting from the commercially available different isocyanates **5**, **6**, and **7**, respectively, in reaction with 4-ethynylaniline (EA). Characterizations of the starting alkynes (**8**, **9**, and **10**) match well with NMR (^{1}H and ^{13}C), ESI-MS data.

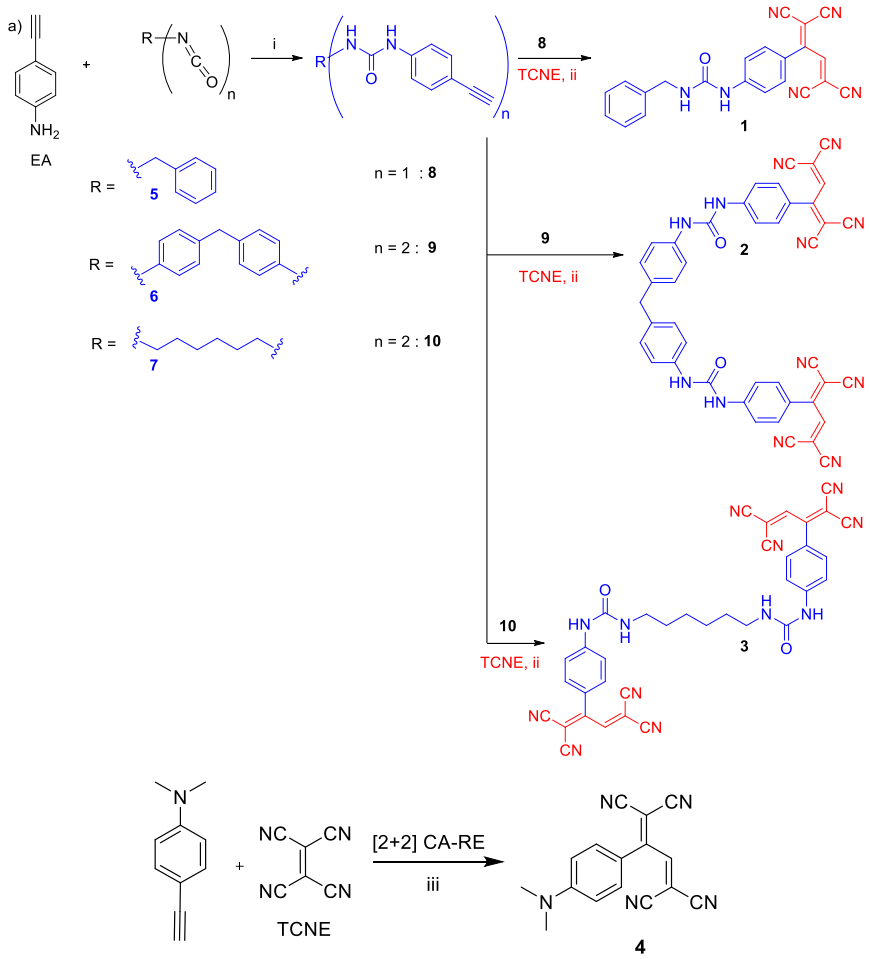

Scheme 3.0. **Synthesis of Urea-Functionalized TCBD Derivatives. Reagents conditions**:
(i) CH_2Cl_2, 25 °C, 90 (**8**), 93 (**9**), 92% (**10**); (ii) DMF, 0 °C; 60% (**1**), 25 °C; 72% (**2**),0°C; 70% (**3**), (iii) C_6H_6, 25°C, 97% (**4**)[16].

After synthesizing urea-alkynes from corresponding different isocyanates, we tested the versatility of their (**8**, **9,** and **10**) reaction with TCNE using the CA−RE reaction. The spacer R group was chosen with different electron-donating moieties along with special supramolecular self-assembly patterns. The donor ability of substituents like aryl and alkyl moieties are quite different and was investigated. The monoalkyne and dialkynes were used to study their reactivity towards the CA−RE reaction. Besides considering the effect of mono-and di-TCBD units, solvent DMF was chosen as a solvent because alkynes **8**, **9**, and **10** are not soluble in common organic solvents. It was found that alkyl spacers **8** and **10** afforded **1** (60%) and **3** (70%), respectively, in good yields even at low

temperatures (0 °C). Reaction performed at 25 °C yielded poor yield with a more complex reaction mixture due to urea-substituted alkynes' high reactivity. However, aryl-alkyne **9** afforded **2** in 72% isolated yield at 25 °C, indicating the aryl spacer is relatively less reactive than the alkyl spacer. Reactivity of EDG alkynes substituted with −OMe and $-NMe_2$ in CA−RE reaction with TCNE usually obey Hammett constant values, and the –OMe ($\sigma_p = -0.27$) group considered to be weak EDG in comparison with $-NMe_2$ ($NMe_2 = -0.82$).[18,26] Despite the Hammett constant for urea (NHCONHEt, $\sigma_p = -0.26$)[26,27] is close to the value of −OMe, the reactivity of the urea substituent is largely comparable with the NMe_2 group. The high reactivity of urea may not be surprising because of both NMe_2 and urea exhibit similar field/inductive substituent parameters (F = 0.15 for NMe_2 and F = 0.19 for NHCONHEt). Because out of three TCBDs (**1**, **2**, and **3**), **1** and **3** are attached with the alkyl (CH2) group hence, the *F* value for −NHCONHEt is more appropriate to compare than with −NHCONHPh. To the best of our knowledge, *F* values are not reported for aryl-substituted urea in the literature. However, the observed high reactivity for all three TCBDs (**1**, **2**, and **3**) implies that the F value of −NHCONHPh might be close enough with −NHCONHEt. The compound urea-TCBDs **1**, **2**, and **3** were fully characterized by IR and ESI-MS spectral data, whereas ^{1}H NMR of di-TCBDs **2** and **3** showed additional peaks, unlike mono-TCBD **1** in DMSO-d_6, even after several batches of samples showed similar behavior, thus ruling out the possibility of impurities. Furthermore, the ^{13}C NMR spectra of bis-TCBDs **2** and **3** showed a downfield shifted urea carbonyl peak at 198 ppm compared to mono-TCBD **1,** which showed a peak at 168 ppm, indicating intra-/inter-molecular H-bonded network in the former case.[28] To verify H-bonding interactions, compound **3** was examined by the concentration-dependent ^{1}H NMR studies in dimethyl sulfoxide (DMSO), and no significant change was observed. Hence, the H-bonding facilitating solvent such as acetone-d_6 was used to measure ^{1}H NMR and was found to be similar to DMSO, unlike mono- TCBD **1** and di-TCBDs **2** and **3** that showed more pronounced additional peaks corresponding to partially aggregated species. To further verify the presence of H-bond mediated partial aggregated species, D_2O titration experiments were performed to ascertain the effect of D_2O to disrupt the H-bonding in the acetone-d_6 solvent. This resulted in changes in ^{1}H NMR signals, indicating the disruption of H-bonding and the presence of additional species as the mixture.[29] However, an investigation of more detailed study about its self-assembly behavior and properties is explained in the next chapter of the thesis. The DMA-TCBD

4 was synthesized and characterized starting from 4-ethynyl-*N*,*N*′-dimethylaniline (EDA) to compare photophysical properties of urea-TCBDs with *N*,*N*′-dimethylamino-substituted phenyl substituted TCBDs.[16] It is well known that previously synthesized TCBDs with other organic donors such as $N(alkyl)_2$, $N(aryl)_2$, O(alkyl), thiophene, azulene, and ynamide does not exhibit luminescence due to quenching by photo-induced electron transfer (PET)/twisted intramolecular charge transfer (TICT) processes.[18,30] The UV/Vis studies of chromophores **1**, **2**, **3**, and **4** were carried out in CH_3CN (5×10^{-5} M) (Figure 3.1). The quantum yield was determined by the comparative method with quinine sulfate (ΦF = 0.54 in 0.1 M H_2SO_4)[30] as a standard. The estimated ΦF value for urea-TCBDs chromophores **1**, **2**, and **3** was found to be 0.034, 0.033, and 0.043, respectively at λ_{ex} = 375 nm (Figure 3.2). Although the fluorescence quantum yields of urea-TCBDs were found to be 3.3–4.3%, such emission from the DMA analogue **4** with significant fluorescence has not been observed, presumably due to the PET from EDG (NMe_2). Chromophores **1** and **3** with alkyl spacers exhibit absorption bands centered at ~262, 394, and 417 nm corresponding to π-π∗, and n-π∗ transitions. Whereas **2** with aryl spacer showed bathochromic shifted bands at 272 and 300 nm. Time-Dependent Density Functional Theory (TD-DFT)[31] calculations matches the assignment (vide supra). Importantly, all chromophores exhibit longer wavelengths absorption bands at 482, 550, and 591 nm due to intramolecular charge transfer (ICT). The acid-base titration experiments corroborated this. All ICT bands of **1**, **2**, and **3** have diminished upon the addition of trifluoroacetic acid, indicating the absence of ICT due to protonation on the urea moiety (Figure 3.3, 3.4, 3.5, 3.6).[32] The protonated state showed a hypsochromic shifted band at 460 nm, in addition to the n-π* bands at 394 and 417 nm. Interestingly, upon neutralization with Et_3N, it regained the ICT band due to regeneration of its original state prior to acidification.

3.3. General experimental details:

Compounds EA, EDA, **5**, **6**, **7,** and chemicals were purchased from Aldrich and TCI-India and used as received. Compound **4** synthesized according to literature procedure. Dimethylformamide (DMF), CH_3CN, CH_2Cl_2 were freshly distilled from CaH_2 under a nitrogen atmosphere. THF was dried in sodium. Column chromatography (CC) was carried out with neutral Al_2O_3 (particle size 60m-325m). TLC was performed on precoated plastic sheets of silica gel G/UV-254 of 0.2 mm thickness (MachereyNagel,

Germany) using appropriate solvents and visualized with UV light (λ = 254 nm). Melting points (M.p.) were measured in open capillaries with a Stuart (automatic melting point SMP50) apparatus and are uncorrected. "Decomp" refers to decomposition. ^{1}H NMR and ^{13}C NMR spectra were measured on Bruker Avance II 400 MHz instrument at 25 °C in CD3CN or DMSO-d_6. Residual solvent signals in the ^{1}H and ^{13}C NMR spectra were used as an internal reference. Chemical shifts (δ) are reported in ppm downfield from $SiMe_4$, with the residual solvent signal. Coupling constants (J) are given in Hz. The apparent resonance multiplicity is described as s (singlet), d (doublet), t (triplet), and m (multiplet). Fourier transform infrared (FT-IR) were recorded on a Cary Agilent 660 IR spectrophotometer; signal designations; s (strong), m (medium), and w (weak). Selected absorption bands are reported in wavenumbers (cm^{-1}). UV/Vis spectra were recorded on a Shimadzu UV/Vis spectrophotometer. The spectra were measured in a quartz cuvette of 1 cm at 298 K. The absorption maxima (λ_{max}) are reported in nm with the extinction coefficient (ε) in $dm^3\ mol^{-1}\ cm^{-1}$ in brackets. Shoulders are indicated as sh. Fluorescence spectra were measured on an Edinburgh FS5 spectrophotometer in a 1 cm quartz cuvette. ESI-MS spectra were measured on a Bruker maXis ESI-Q-TOF spectrometer. The most important signals are reported in m/z units with M+ as the molecular ion.

Quantum yields for **1**, **2**, and **3** were determined by comparing the integrated PL intensities (excited at 375 nm) and the absorbance values (at 375 nm) of the urea-chromophores using quinine sulphate (Φ_F = 0.54) as a reference.

3.4. Electrochemistry:

The redox properties were measured by cyclic voltammetry. *N*,*N*-dimethylformamide (DMF) (HPLC grade, spectrochem, India) was distilled over anhydrous calcium hydride protected by 4 Å molecular sieves under argon atmosphere before each experiment. Tetrabutylammonium perchlorate ([Bu_4NClO_4], TBAP) (Sigma-Aldrich, electrochemical grade) was used as a supporting electrolyte without further purifications. For all the studies, one mM solutions of the compounds in distilled DMF were used.

The voltammetric experiments were carried out in a single compartment electrochemical cell using the three-electrode potentiostat (CH Instruments 660A). The working electrode (Glassy Carbon (GC) electrode of 3 mm dia, CH Instruments, USA) was polished with 0.05-micron alumina slurry to mirror finish and sonicated to remove the abrasive particles before each experiment. The Ag/Ag^{+}(0.01M) electrode is used as a quasi-

reference electrode prepared from the same supporting electrolyte in acetonitrile (caution: preparation of the Ag/Ag^+ reference electrode in DMF/TBAP leads to the formation of Ag nanoparticles). Platinum wire was used as the counter electrode. Later, the potential scale is corrected with the ferrocene/ferrocenium-ion using the ferrocene as an internal standard. Cyclic voltammetry experiments were performed with a CH Instruments three-electrode potentiostat.

3.5. Synthesis of mono- and disubstituted urea alkynes from available isocyanates:

The precursors for the synthesis of urea-functionalized 4-ethynyl benzenes (**8**, **9**, and **10**) were obtained from using a commercial source such as 4-ethynylaniline (EA) and isocyanates bearing alkyl and aryl substituents (R) **5**, **6**, and **7**, respectively (schemes 3.1, 3.2, 3.3). For comparison, *N*,*N*'-dimethylamino-substituted phenyl TCBD (DMA-TCBD) **4** was synthesized starting from 4-ethynyl-*N*,*N'*-dimethylaniline (EDA) as per the reported procedure.[ref]

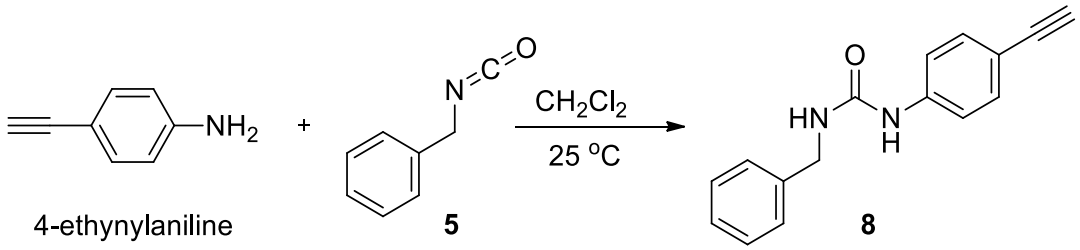

Scheme 3.1. Synthesis of monosubstituted urea alkyne (Benzyl Alkyne).

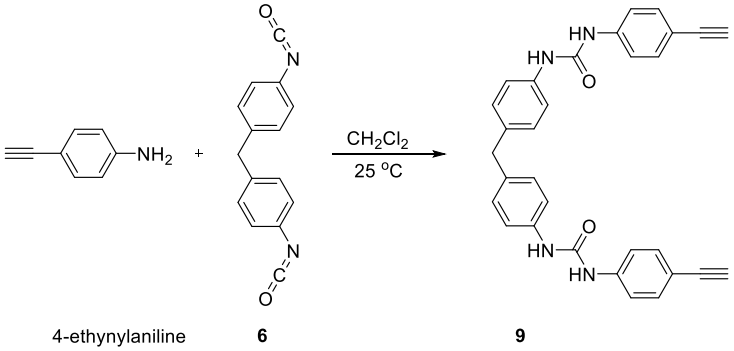

Scheme 3.2. Synthesis of disubstituted urea alkyne (Diphenyl Alkyne).

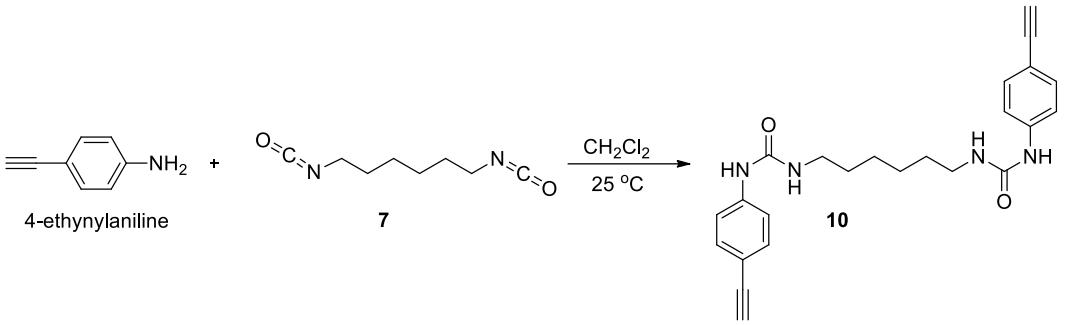

Scheme 3.3. Synthesis of disubstituted urea alkyne (Hexyl Alkyne).

3.6. Synthetic Procedures and characterization for urea functionalized push−pull chromophores:

Urea-substituted phenyl-TCBDs **1**–**3** (urea-TCBDs) were synthesized in a one-step click type reaction with TCNE in DMF (schemes 3.4, 3.5, 3.6). To test the versatility of urea-substituted alkynes **8**, **9**, and **10** reactivity towards CA−RE reaction with TCNE, the spacer R group was chosen with different electron-donating groups like aryl and alkyl moieties. DMF was selected as a solvent because the alkynes **8**, **9**, and **10** are not soluble in common organic solvents. It was found that alkyl spacers **8** and **10** afforded **1** (60%) and **3** (70%), respectively, in good yields even at low temperatures (0 ^{o}C). Reaction performed at 25 ^{o}C yielded poor yield with a more complex reaction mixture owing to its high reactivity. However, aryl-alkyne **9** afforded **2** (72%) in good yield at 25 ^{o}C, indicating aryl spacer is relatively less reactive than alkyl spacer. Characterizing the starting alkynes (**8**, **9**, and **10**) matches well with NMR (^{1}H and ^{13}C), ESI-MS data. Similarly, urea-TCBDs **1**, **2**, and **3** match well with IR, NMR, and ESI-MS. However, the ^{13}C-NMR spectra of bis-TCBDs **2** and **3** showed a downfield shifted urea carbonyl peak at 198 ppm compared to mono-TCBD **1,** which showed a peak at 168 ppm, indicating a robust H-bonded network in the former case. The presence of H-bonding was further corroborated by adding D_2O into the acetone-d_6 solvent.

1-benzyl-3-(4-(1,1,4,4-tetracyanobuta-1,3-dien-2-yl)phenyl)urea (1)

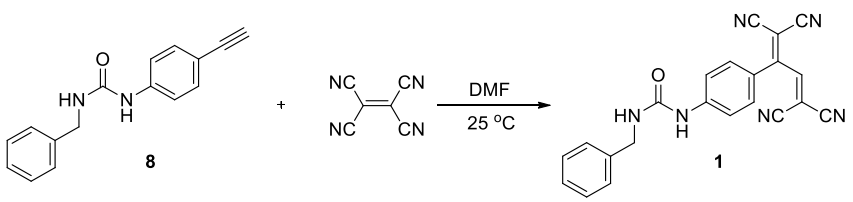

Scheme 3.4. Synthesis of Urea-TCBD based push−pull chromophore (Benzyl-TCBD).

Characterization data of 1:

The compound **1** (60%) obtained is well soluble in acetone, DMF, DMSO, MeOH and less soluble in MeCN, R_f = 0.3 (SiO_2; CH_2Cl_2/MeOH 90:10); mp 268–270 °C; (decomp.); ^{1}H NMR (400 MHz, DMSO–d_6, 298K) δ = 4.32 (d, J = 5.8 Hz, 2H), 6.87 (t, J = 6.2 Hz, 1H), 7.23 – 7.36 (m, 5H), 7.43 (d, J = 8.4 Hz, 2H), 7.55 (d, J = 8.5 Hz, 2H) 7.94 (s, 1H), 9.08 ppm (s, ^{1}H); ^{13}C NMR (100 MHz, CD_3CN, 298K); δ = 44.2, 114.1, 114.6, 114.8, 115.9, 116.3, 116.8, 117.5, 117.7, 118.6, 118.8, 123.0, 127.9, 128.1, 129.4, 131.1, 141.1, 144.0, 156.1, 161.4, 168.7, 173.1 ppm; IR (KBr) $\tilde{\nu}$ 3303 (m), 2873 (m), 2871 (s), 2356 (s), 2210 (s), 1627 (s), 1583 (m), 1401 cm^{-1} (m); LRMS (ESI): m/z (%) 441.36 (100, $[M+H+Na+K]^+$, calcd for $C22H15N6ONaK^+$:441.08), 379.38 (10, $[M+H]^+$, calcd for $C22H15N6O^+$:379.13).

1,1'-(methylenebis(4,1-phenylene))bis(3-(4-(1,1,4,4-tetracyanobuta-1,3-dien-2-yl)phenyl)urea)(2)

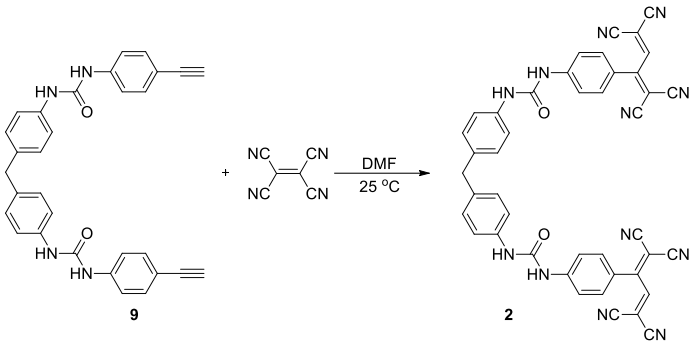

Scheme 3.5. Synthesis of Bis-Urea-TCBD based push−pull chromophore (Diphenyl-TCBD).

Characterization data of 2:

The compound **2** (72%) obtained is well soluble in $(CH_3)_2CO$, DMF, DMSO, CH_3OH and less soluble in CH_3CN. R_f = 0.25 (SiO_2; CH_2Cl_2/MeOH 90:10); mp: 269–271 °C (decomp.); ^{1}H NMR (400 MHz, DMSO–d_6) δ = 3.80 (s, 2H), 7.06 – 7.40 (m, 10H), 7.50 – 7.90 (m, 8H), 8.73 (s, 2H), 9.05 ppm (s, 2H); ^{13}C NMR (100 MHz, CD_3CN, 298 K) δ = 41.1, 118.6, 119.2, 120.6, 123.5, 130.1, 130.6, 131.1, 132.2, 137.5, 138.0, 143.4, 145.2, 153.4, 161.3, 168.7, 173.0, 197.7 ppm; IR (KBr) $\tilde{\nu}$ 3359 (w), 2925 (w), 2362 (w), 2215 (w), 1660 (m), 1589 (m), 1509 (m), 1411 cm^{-1} (w); HRMS (ESI, negative mode); *m/z* (%): calcd for $C_{43}H_{23}N_{12}O_2$ $[M-H]^-$: 739.2067, Found: 740.1595.

1,1'-(hexane-1,6-diyl)bis(3-(4-(1,1,4,4-tetracyanobuta-1,3-dien-2-yl)phenyl)urea)(3)

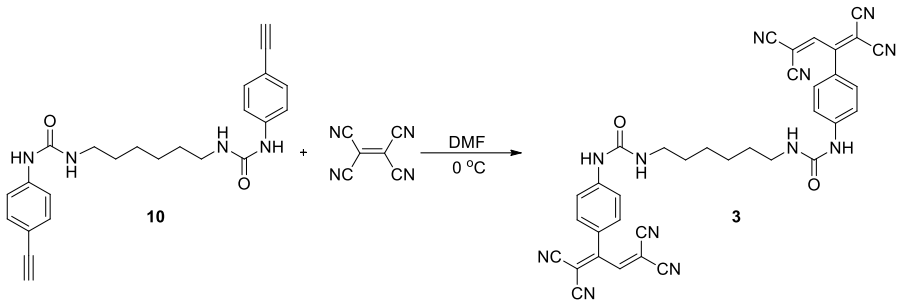

Scheme 3.6. Synthesis of Bis-Urea-TCBD based push−pull chromophore (Hexyl-TCBD).

Characterization data of 3:

The compound **3** (70 %) obtained is well soluble in $(CH_3)_2CO$, DMF, DMSO, CH_3OH and less soluble in CH_3CN. R_f = 0.3 (SiO_2; CH_2Cl_2/MeOH 90:10); mp 262–265 °C; (decomp.); ^{1}H NMR (400 MHz, DMSO–d_6) δ = 1.28 – 1.35 (m, 4H), 1.39 – 1.49 (m, 4H), 3.05 – 3.14 (m, 4H), 6.32 – 6.42 (m, 2H), 7.35 – 7.55 (m, 8H), 7.81 – 7.86 (m, 2H), 8.90 – 8.98 ppm (m, 2H); ^{13}C NMR (100 MHz, CD_3CN) δ = 27.0, 30.6, 40.4, 118.7, 119.0, 121.0, 122.8, 128.1, 130.6, 131.1, 133.6, 142.2, 144.2, 146.0, 156.0, 156.2, 161.4, 168.7, 173.1, 197.6 ppm; IR (KBr) $\tilde{\nu}$ 3359 (w), 2933 (w), 2852 (w), 2364 (m), 2206 (w), 1671 (m), 1590 (m), 1527 (m), 1410 cm^{-1} (w); HRMS (ESI); *m/z* (%): calcd for $C_{36}H_{27}N_{12}O_2^+$ $(M+H)^+$: 659.2380 Found: 659.2382

3.7. UV/Vis and Fluorescence Spectroscopies:

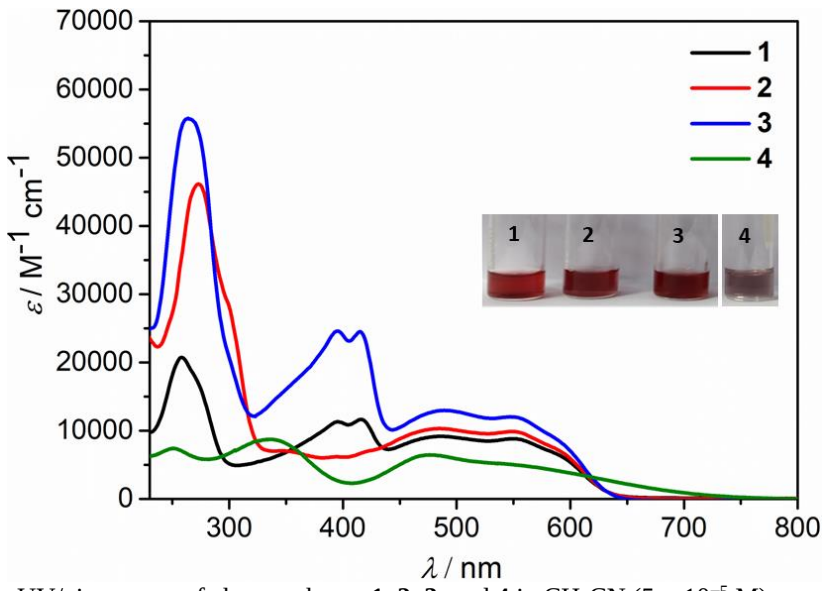

Figure 3.1. UV/vis spectra of chromophores **1**, **2**, **3**, and **4** in CH_3CN (5×10^{-5} M).

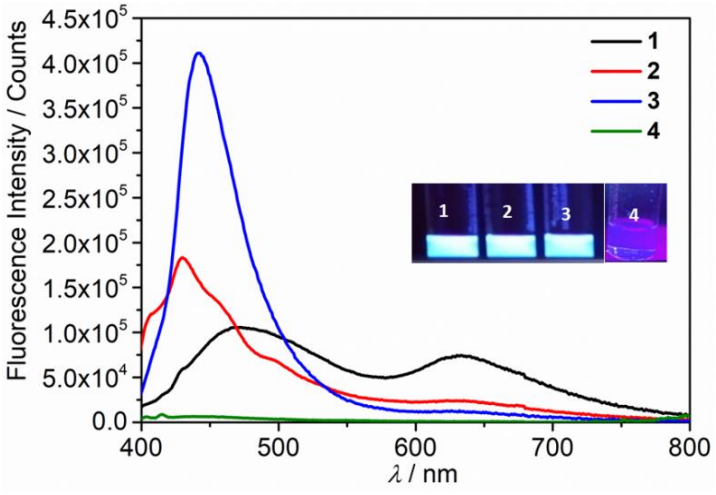

Figure 3.2. Fluorescence spectra of TCBDs based chromophores **1**, **2**, **3**, and **4** in CH_3CN (5×10^{-5} M). The inset shows the images of chromophores taken under the UV lamp (365 nm).

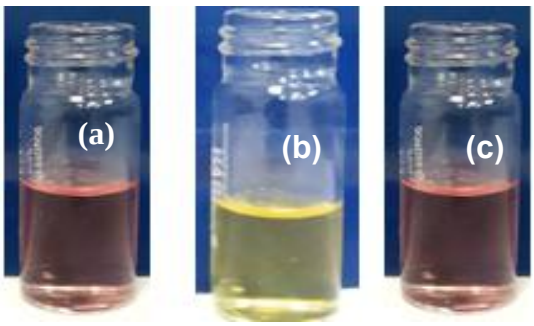

Figure 3.3. a) A solution of **1** in CH_3CN (5×10^{-5} M), b) upon addition of TFA, c) after re-neutralization with Et_3N.

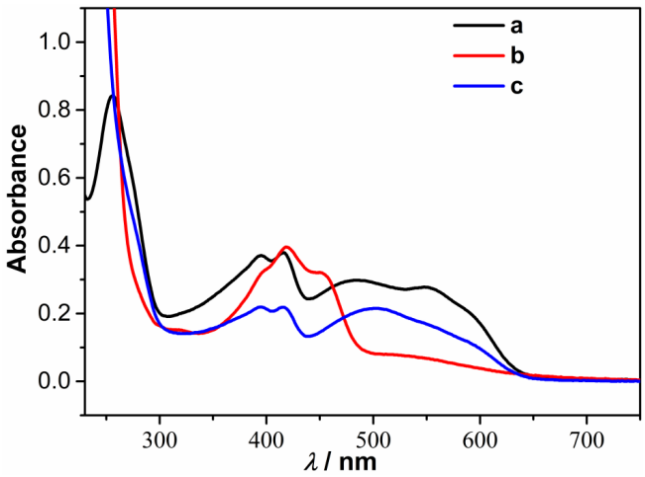

Figure 3.4. UV/Vis absorption spectra of **1** in CH_3CN (5×10^{-5} M) at 298 K recorded a) neat, b) after acidification with trifluoracetic acid (TFA), and c) neutralization with Et_3N.

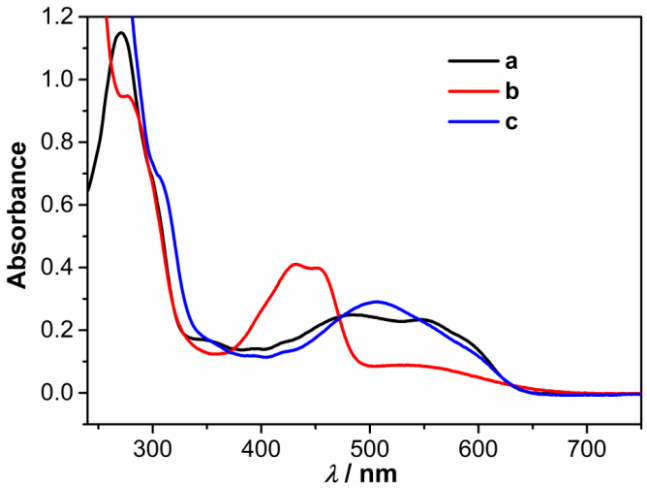

Figure 3.5. UV/Vis absorption spectra of **2** in CH_3CN (5×10^{-5} M) at 298 K recorded a) neat, b) after acidification with TFA, and c) neutralization with Et_3N.

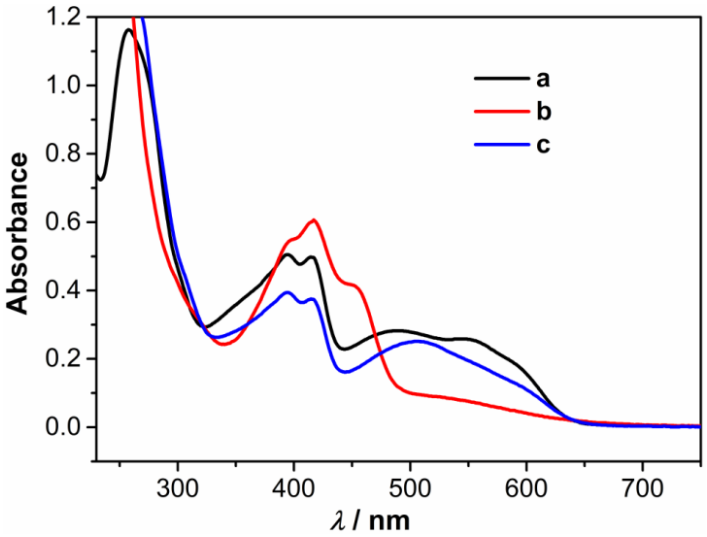

Figure 3.6. UV/Vis absorption spectra of **3** in CH_3CN (5×10^{-5} M) at 298 K recorded a) neat, b) after acidification with TFA, and c) neutralization with Et_3N.

3.8. Electrochemistry studies:

Table 1. Electrochemical data of **1**, **2**, **3**, and **4**[1] observed by cyclic voltammetry (CV) (Scan Rate v = 0.1 V s^{-1}) in DMF (in the presence of 0.1M Bu_4NClO_4).

Compound	Peak parameters				
	$E°$ [V][a]	ΔE_p [mV][b]	E_p [V][c]	DPV [V][d]	HOMO–LOMO (H–L) Gap [V][e]
			+0.643		
1 Benzyl-TCBD	–0.911	84		–0.932	1.549
	–1.78	90		–1.752	

2 Diphenyl-TCBD	–0.898	36	+0.863 +0.643	–0.858 –1.784	1.541
3 Hexyl-TCBD	–0.916 –1.760	46 83	+0.850	–0.913 –1.741	1.766
4[g] TCBD-DMA	–0.58 –1.199	80 83	+0.952 +0.863		1.443

[a]E^o = (E_{pc} + E_{pa})/2, where E_{pc} and E_{pa} correspond to the cathodic and anodic peak potentials, respectively; Values reported versus Fc/Fc^+. [b]$\Delta E_p = E_{pa} - E_{pc}$. [c]$E_p$ = Irreversible peak potential. [d]DPV: Differential pulse voltammetry. [e]H–L = $E_{red,1}$ + $E_{ox,1}$.

3.9. Computational Studies:

The density functional theory (DFT) calculations were performed to investigate the molecular and electronic structure properties to interpret observations in the optical and electrochemical studies. The molecular orbitals are obtained in DFT calculations adopting the B3LYP/def2-TZVP method.[33] The electronic spectra were computed applying time-dependent DFT16b calculations using the CAMB3LYP[34] functional. The highest occupied molecular orbital (HOMO) is delocalized over the spacer urea-phenyl except for the unsubstituted dicyanovinyl moiety, which is also an indication of facile electron delocalization that eventually leads to the ICT by the urea and spacers. The lowest unoccupied molecular orbital (LUMO) and LUMO + 1 are entirely localized on the TCBD moiety. The lowest energy electronic transitions for 1 and 4: H → L, for 2: H → L, H – 1 → L, H − 2 → L, H − 3 → L, and for 3: H → L, H − 1 → L correspond with the CT bands (Figure 3.7).

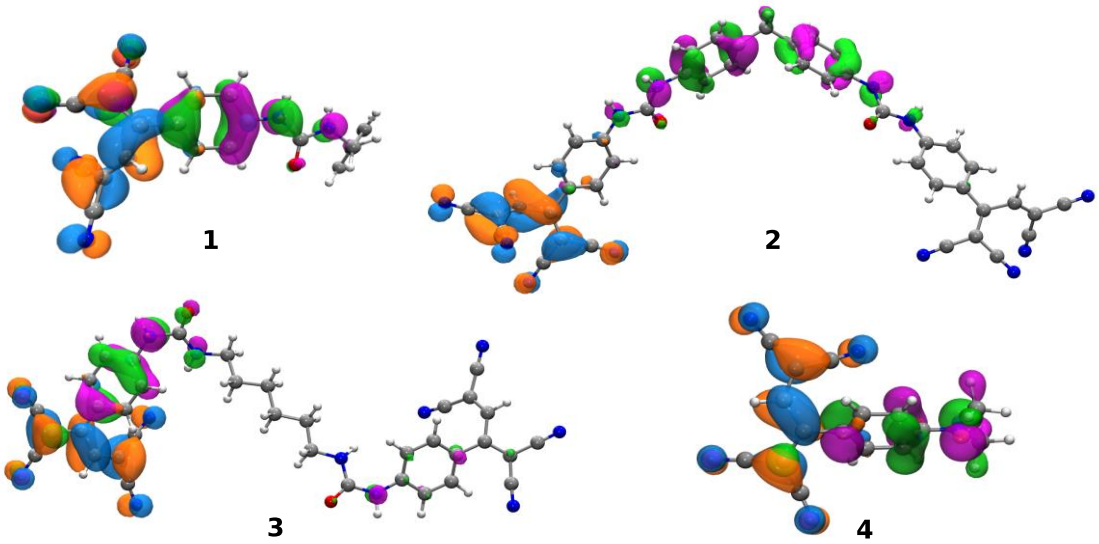

Figure 3.7. The combined HOMO (pink and green) and LUMO (orange and blue) as obtained from B3LYP/def2-TZVP method are plotted for compounds 1 to 4 with an isosurface value 0.04 a.u.

3.10. NMR Spectra:

Spectra of Newly Synthesized Compounds

NMR (^{1}H and ^{13}C) Spectra

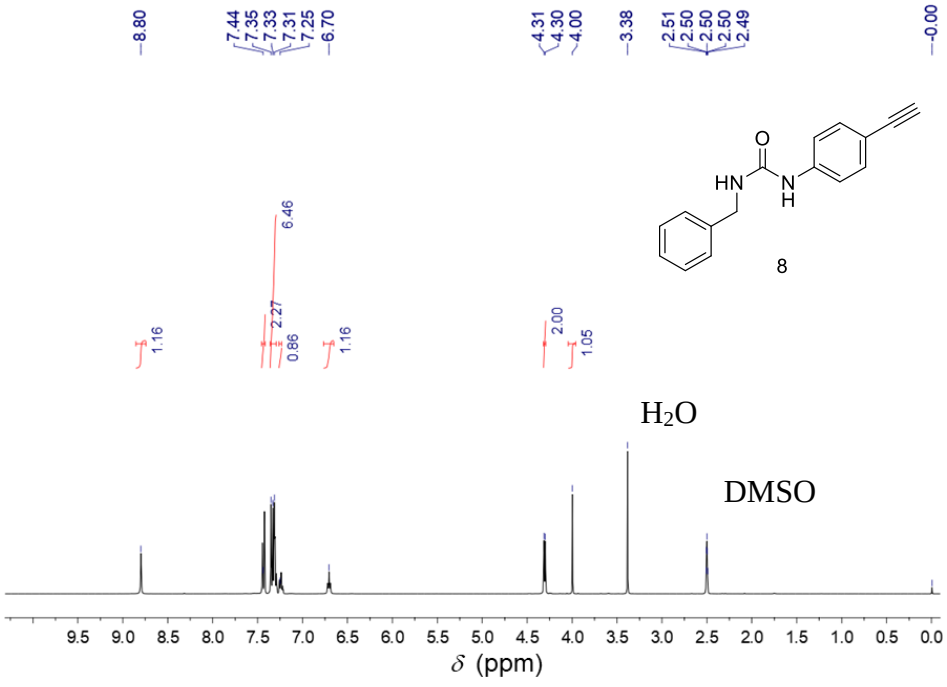

Figure 3.8. 400 MHz ^{1}H NMR spectrum of **8** recorded at 298 K in DMSO-d_6.

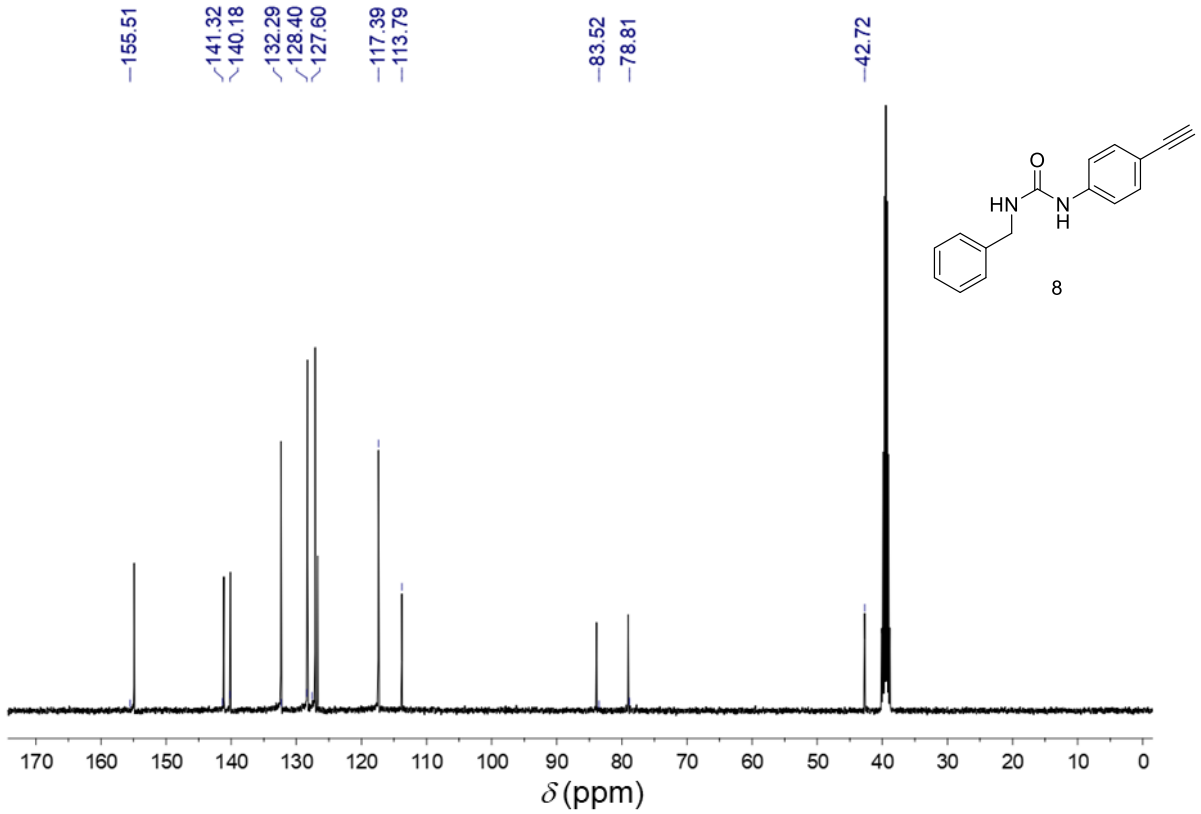

Figure 3.9. 100 MHz ^{13}C NMR spectrum of **8** recorded at 298 K in DMSO-d_6.

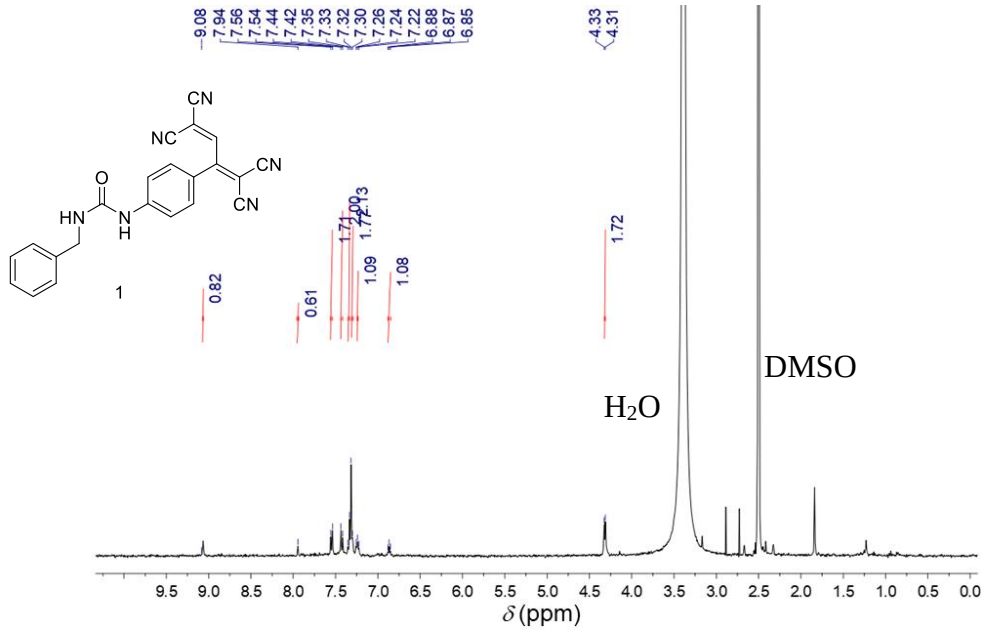

Figure 3.10. 400 MHz ^{1}H NMR spectrum of **1** recorded at 298 K in DMSO-d_6.

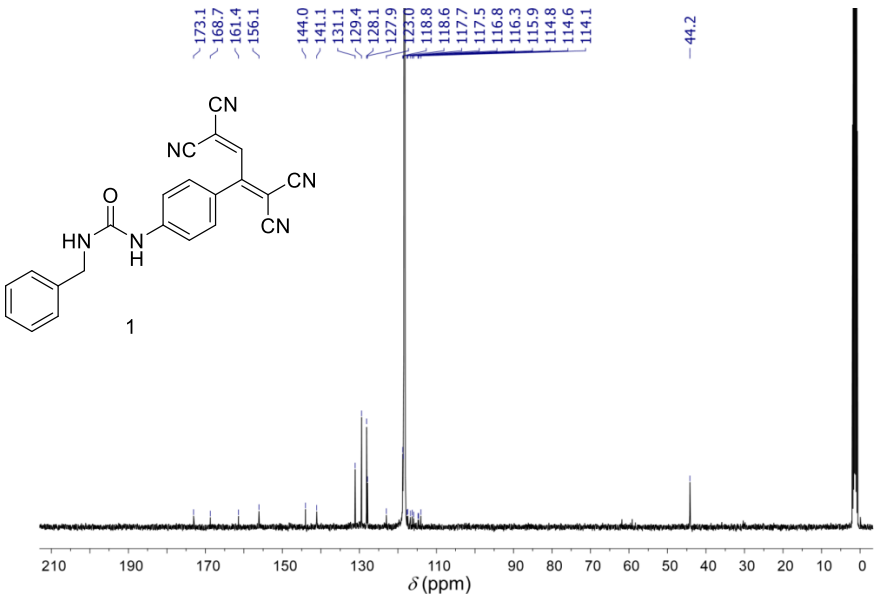

Figure 3.11. 100 MHz ^{13}C NMR spectrum of **1** recorded at 298 K in CD_3CN.

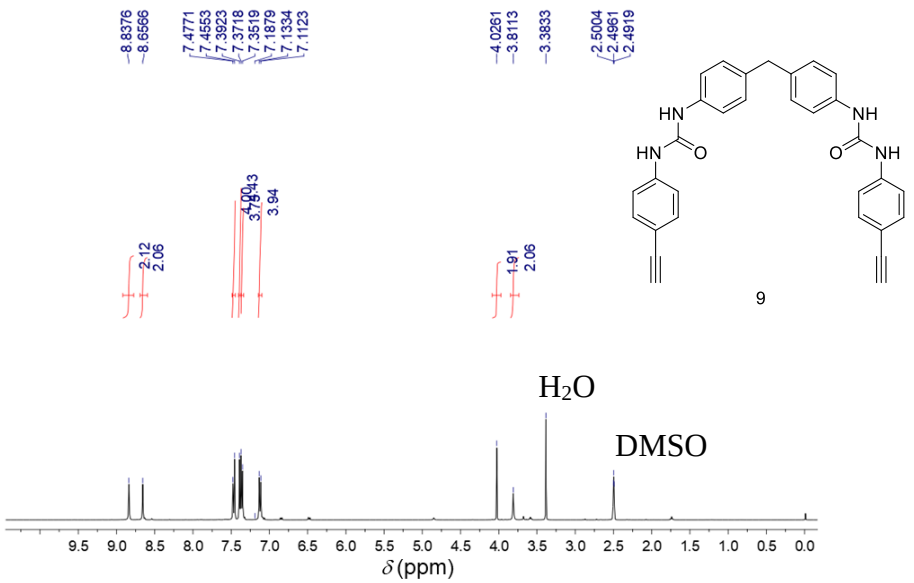

Figure 3.12. 400 MHz ^{1}H NMR spectrum of **9** recorded at 298 K in DMSO-d_6.

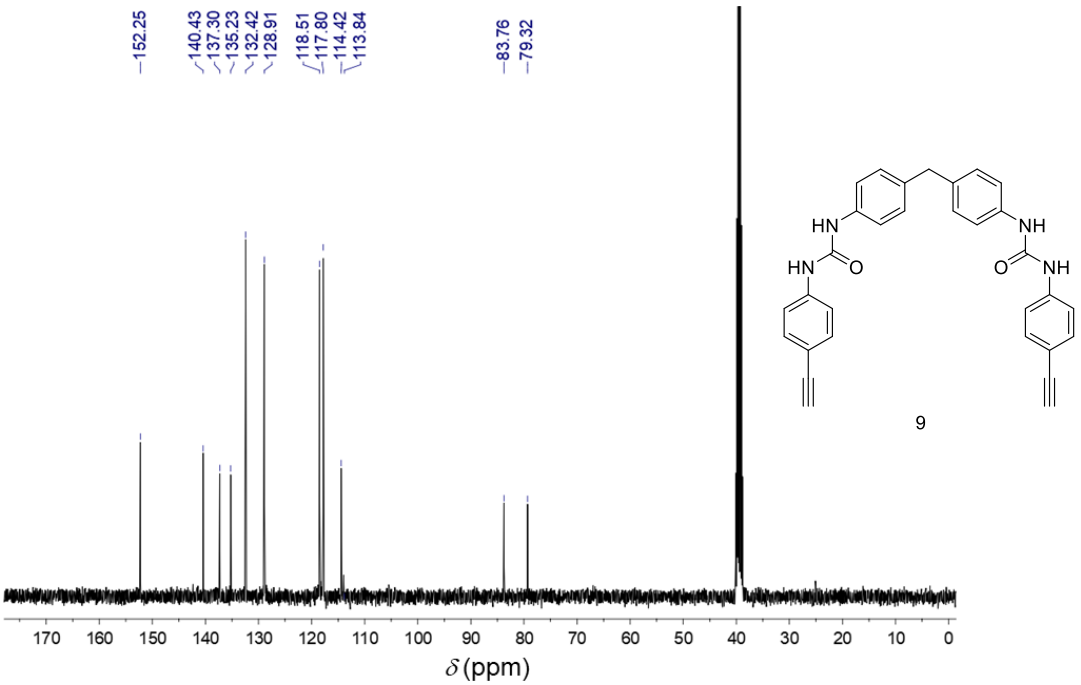

Figure 3.13. 100 MHz ^{13}C NMR spectrum of **9** recorded at 298 K in DMSO-d_6.

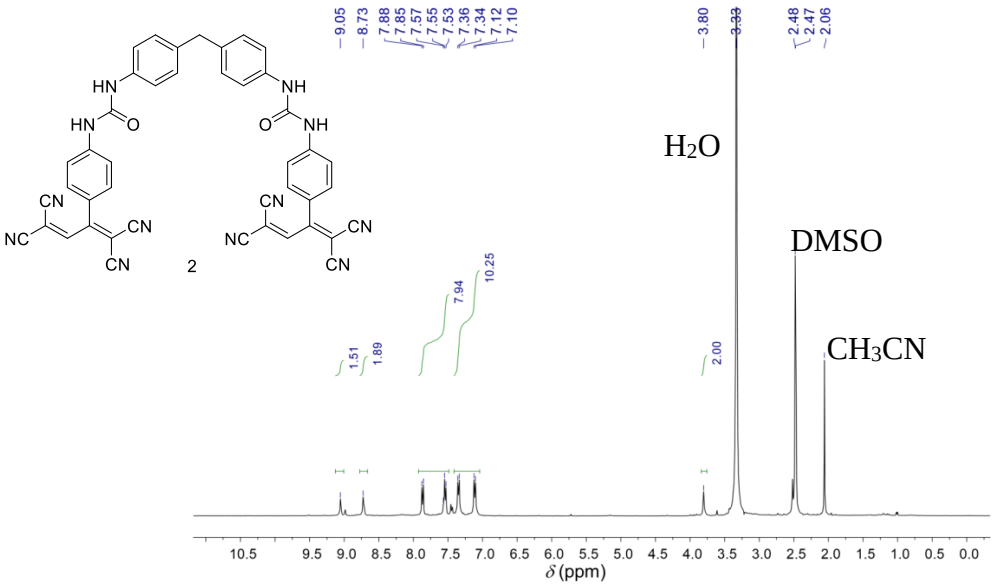

Figure 3.14. 400 MHz ^{1}H NMR spectrum of **2** recorded at 298 K in DMSO-d_6.

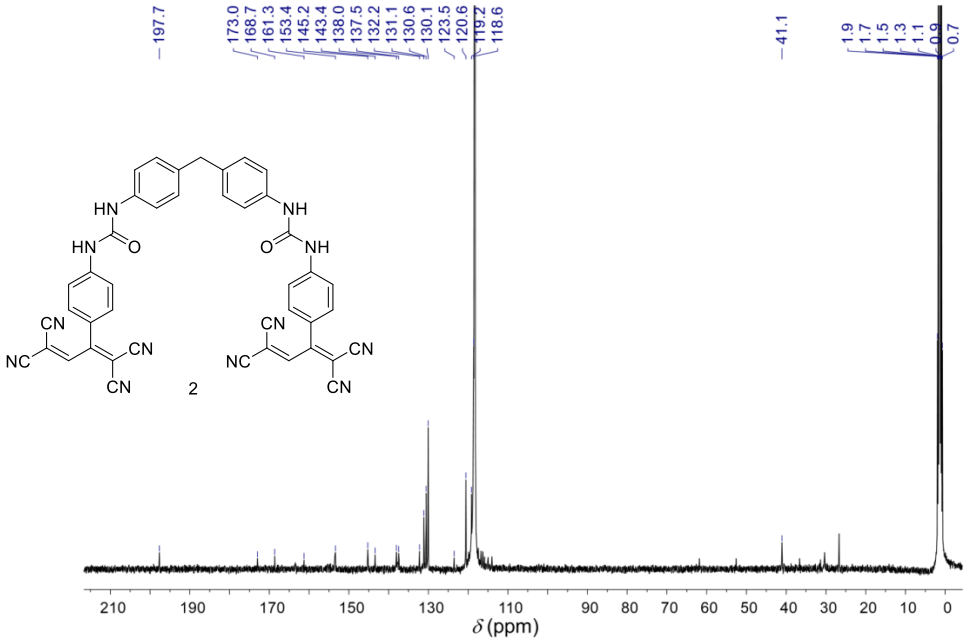

Figure 3.15. 100 MHz ^{13}C NMR spectrum of **2** recorded at 298 K in CD_3CN.

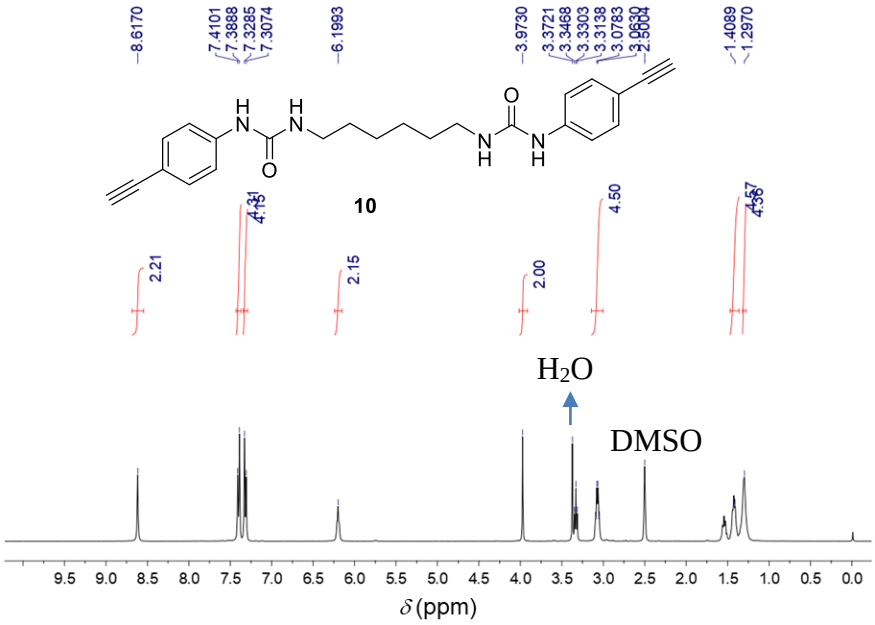

Figure 3.16. 400 MHz ^{1}H NMR spectrum of **10** recorded at 298 K in DMSO-d_6.

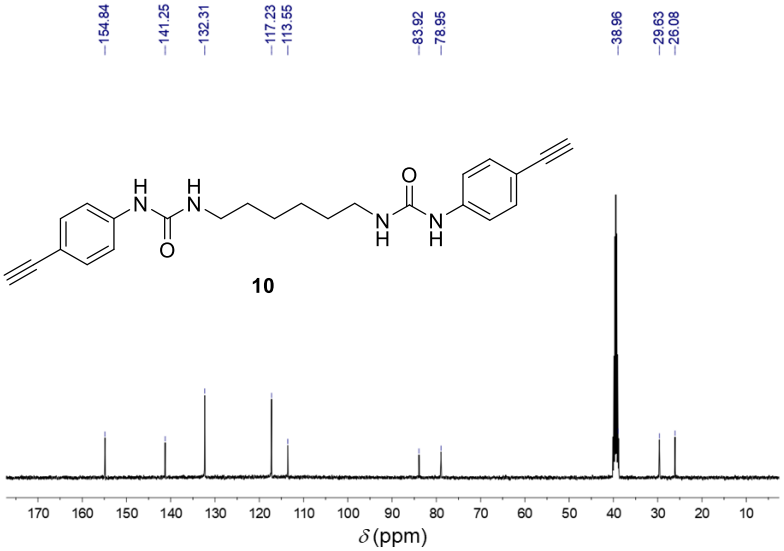

Figure 3.17. 100 MHz ^{13}C NMR spectrum of **10** recorded at 298 K in DMSO-d_6.

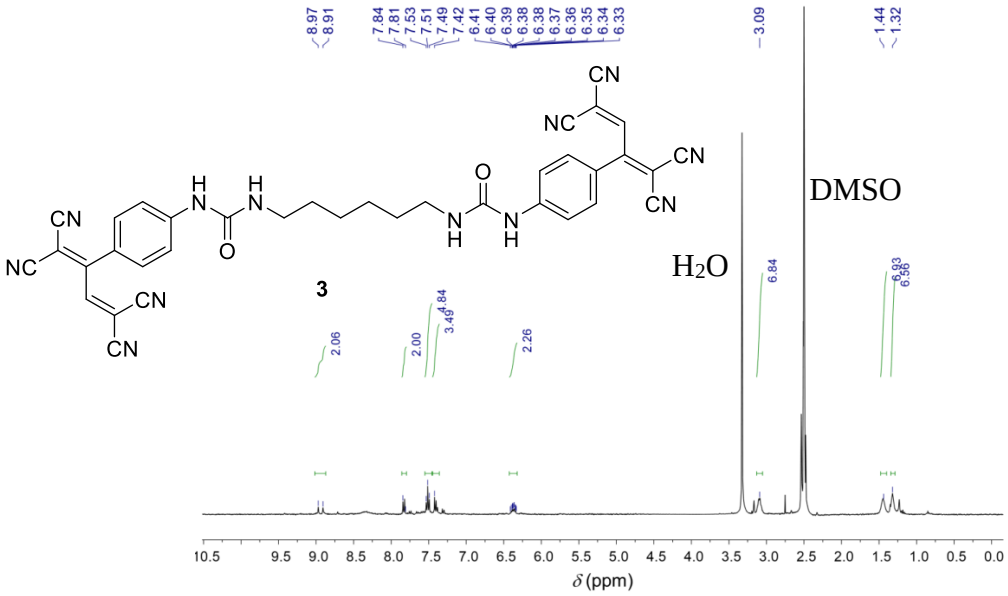

Figure 3.18. 400 MHz ^{1}H NMR spectrum of **3** recorded at 298 K in DMSO-d_6.

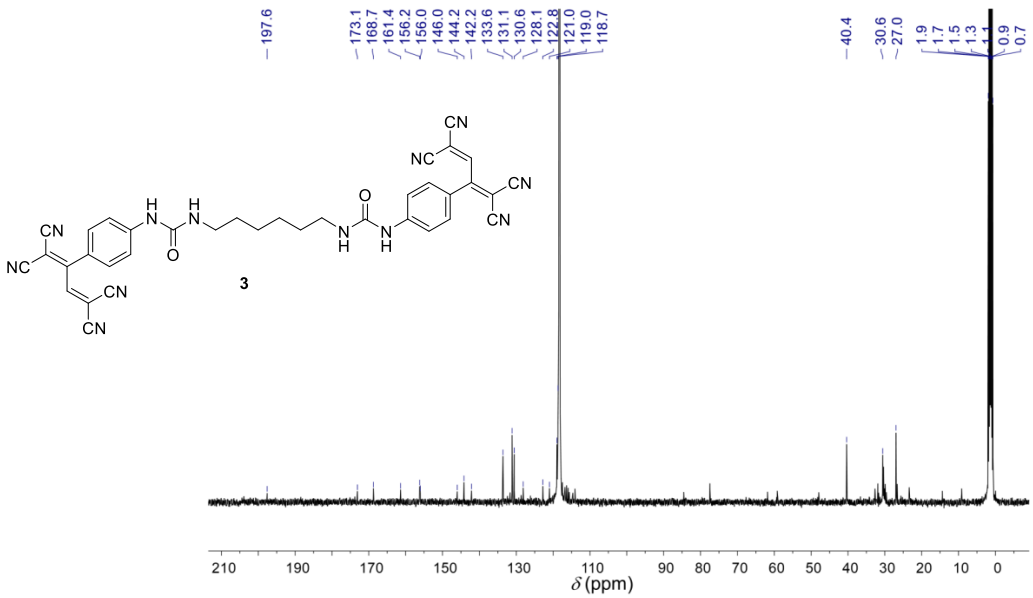

Figure 3.19. 100 MHz ^{13}C NMR spectrum of **3** recorded at 298 K in CD_3CN.

3.11. H-bonding: addition of D_2O effect:

Among the urea-based push−pull chromophores, the NMR spectrum of mono-TCBD **1** is quite simple and matches well with the structure (Figure 3.20). However, bis-TCBDs **2** and **3** both show additional peaks making the spectra look more complex. We infer that this is due to aggregated structures mediated by H-bonds between the bis-urea moieties. To verify this, D_2O was added to disrupt the H-bonding; thus, the NMR pattern gets changed as depicted (Figures 3.21, 3.22). Interestingly, mono-TCBD **1** did not show any significant change upon the addition of D_2O.

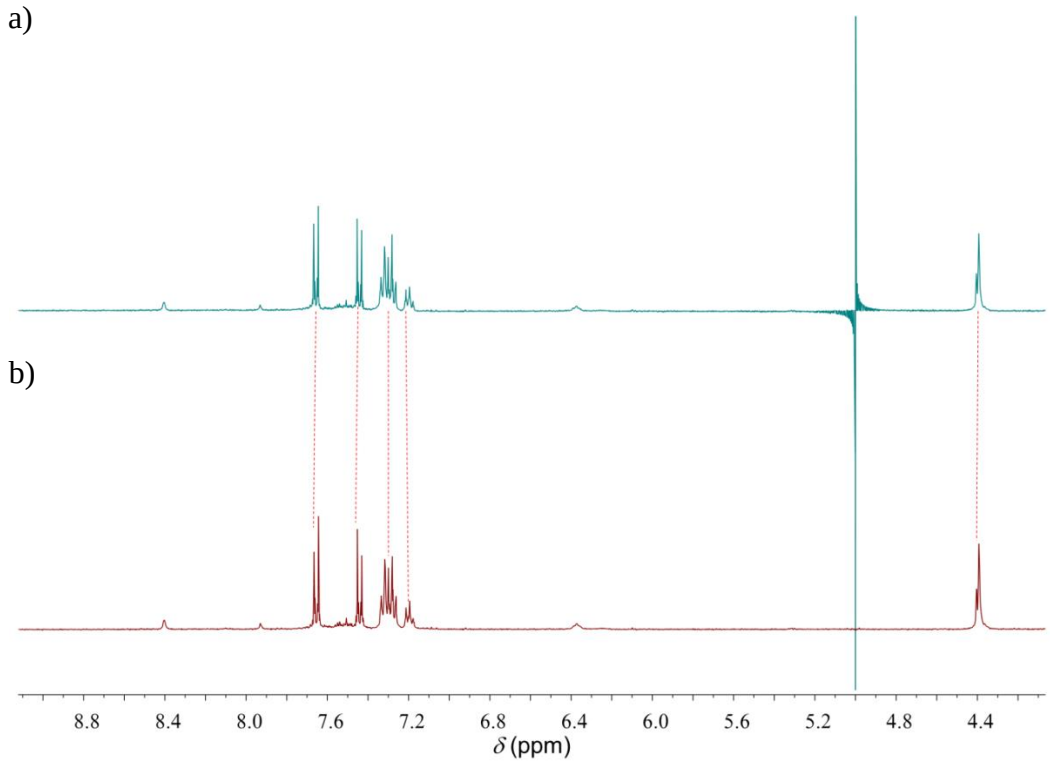

Figure 3.20. 400 MHz ^{1}H NMR spectra of **1** recorded at 298 K in a) CD_3COCD_3, b) after addition of D_2O (200 μL).

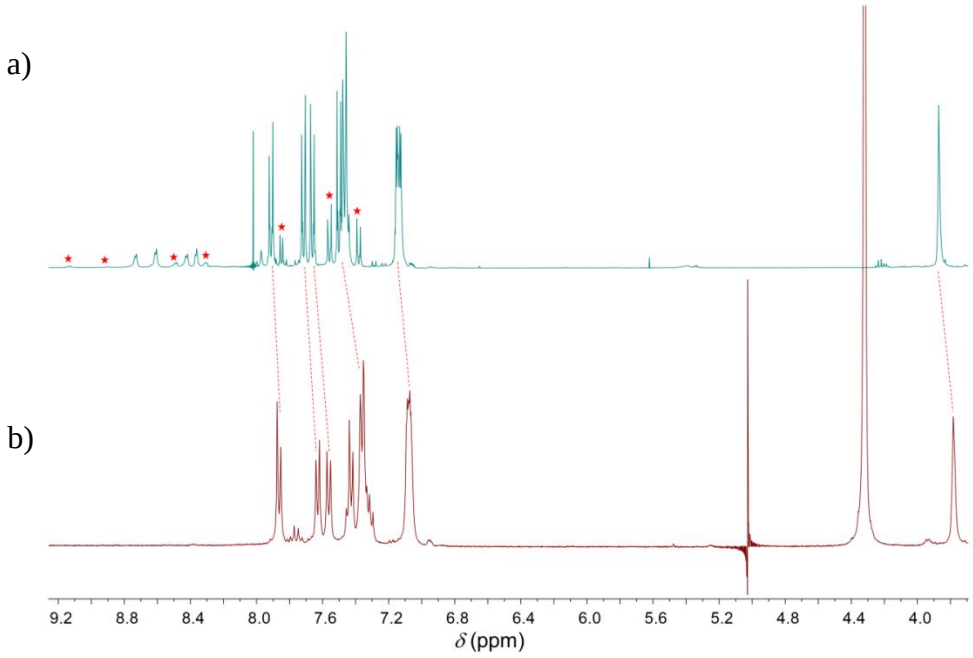

Figure 3.21. 400 MHz ^{1}H NMR spectra of **2** recorded at 298 K in a) CD_3COCD_3, b) after addition of D_2O (200 μL).

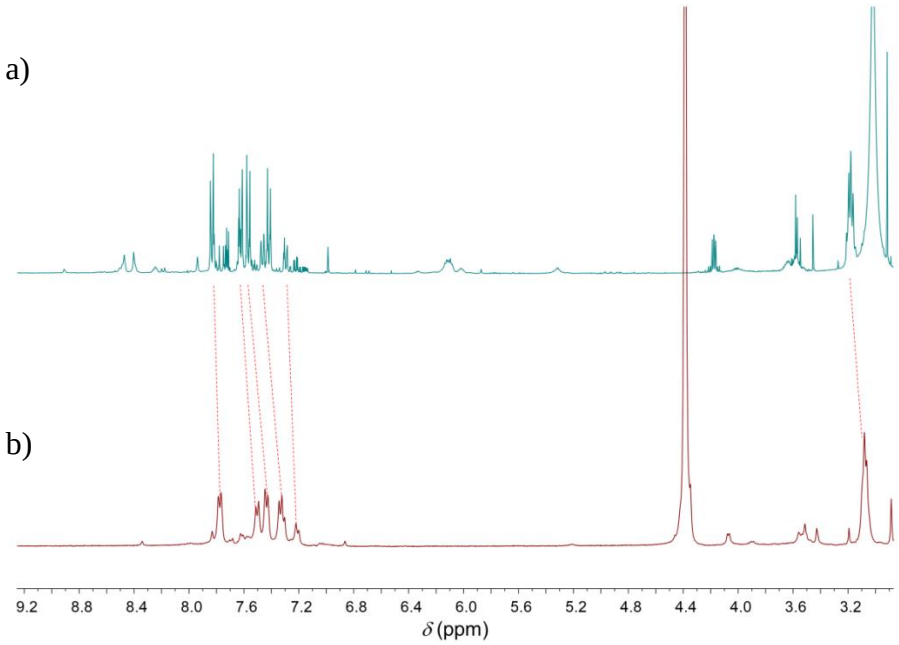

Figure 3.22. 400 MHz ^{1}H NMR spectra of **3** recorded at 298 K in a) CD_3COCD_3, b) after addition of D_2O (200 μL).

3.12. Conclusion:

Urea-based fluorescent push−pull chromophores have unfolded the limitations of previous TCBD based push−pull chromophores. We have designed versatile and effective CT chromophores encompassing the inherent properties, that is, PL and strong ICT bands, using formal [2 + 2] CA−RE between urea-substituted alkynes as new EDG and acceptor alkene at ambient conditions.[36] Interestingly, these chromophores exhibit white light emission when excited at λ_{ex} = 420 nm with relatively good quantum yield. For the first time, we show that the unusual PL of TCBD chromophore is due to the unique electron-donating ability of the urea donor through the field effect. Easy access to differently functionalized precursors[35] makes it promising to synthesize functionalized urea push−pull chromophores which, may open up the possibility of several avenues like hydrogen bond-mediated organocatalysis, as inhibitors, sensors, and above all, optoelectronic materials. We are currently exploring this approach's versatility to synthesize various TCBDs from mono- and bis-substituted urea-functionalized alkynes to tune their optoelectronic and photo-luminescent properties.

3.13. References:

1. Hales, J. M.; Barlow, S.; Kim, H.; Mukhopadhyay, S.; Brédas, J. -L.; Perry, J. W.; Marder, S. R. *Chem. Mater.* **2014**, *26*, 549–560.
2. Ostroverkhova, O. *Chem. Rev.* **2016**, *116*, 13279–13412.
3. Tlach, B. C.; Tomlinson, A. L.; Ryno, A. G.; Knoble, D. D.; Drochner, D. L.; Krager, K. J.; Jeffries-EL, M. *J. Org. Chem.* **2013**, *78*, 6570−6581.
4. Luan, X.; Liu, J.; Pei, Q.; Bazan, G. C.; Li, H. *ACS Appl. Mater. Interfaces* **2017**, *9*, 16750−16755.
5. Li, X.; Gao, X.; Shi, W.; Ma, H. *Chem. Rev.* **2014**, *114*, 590–659.
6. Campagnola, P. *Anal. Chem.* **2011**, *83*, 3224–3231.
7. Chen, L.; Wu, D.; Yoon, J. *ACS Sens.* **2018**, *3*, 27–43.
8. Malla, J. A.; Umesh, R. M.; Vijay, A.; Mukherjee, A.; Lahiri, M.; Talukdar, P. *Chem. Sci*. **2020**, *11*, 2420–2428.
9. Vikram, V.; Penumutchu, R. S.; Vankayala, R.; Thangudu, S.; Amperayani, K. R.; Parimi, U. *J. Chem. Sci.* **2020**, *132*, 126 (1)-126(8).
10. Kivala, M.; Diederich, F. *Acc. Chem. Res*. **2009**, *42*, 235–248.
11. Shoji, T.; Ito, S.; Toyota, K.; Iwamoto, T.; Yasunami, M.; Morita, N. *Eur. J. Org. Chem.* **2009**, 4316–4324.
12. Shoji, T.; Maruyama, M.; Maruyama, A.; Ito, S.; Okujima, T.; Toyota, K. *Chem. –Eur. J.* **2014**, *20*, 11903–11912.
13. Kivala, M.; Boudon, C.; Gisselbrecht, J.-P.; Seiler, P.; Gross, M.; Diederich, F. *Angew. Chem. Int. Ed*. **2007**, *46*, 6357–6360.
14. Jayamurugan, G.; Dumele, O.; Gisselbrecht, J.-P.; Boudon, C.; Schweizer, W. B.; Bernet, B.; Diederich, F. *J. Am. Chem. Soc*. **2013**, *135*, 3599–3606.
15. Michinobu, T.; May, J. C.; Lim, J. H.; Boudon, C.; Gisselbrecht, J.-P.; Seiler, P.; Gross, M.; Biaggio, I.; Diederich, F. *Chem. Commun*. **2005**, 737–739.
16. Michinobu, T.; Boudon, C.; Gisselbrecht, J.-P.; Seiler, P.; Frank, B.; Moonen, N. N. P.; Gross, M.; Diederich, F. *Chem. Eur. J.* **2006**, *12*, 1889–1905.
17. Michinobu, T.; Diederich, F. *Angew. Chem. Int. Ed*. **2018**, *57*, 3552–3577.
18. Michinobu, T.; Boudon, C.; Gisselbrecht, J. -P.; Seiler, P.; Frank, B.; Moonen, N. N. P.; Gross, M.; Diederich, F. *Chem. –Eur. J.* **2006**, *12*, 1889–1905.
19. Tang, X.; Liu, W.; Wu, J.; Lee, C. -S.; You, J.; Wang, P. *J. Org. Chem.* **2010**, *75*, 7273–7278.

20. Leliège, A.; Blanchard, P.; Rousseau, T.; Roncali, J. *Org. Lett.* **2011**, *13*, 3098–3101.
21. Misra, R.; Maragani, R.; Gautam, P.; Mobin, S. M. *Tetrahedron Lett.* **2014**, *55*, 7102–7105.
22. Rout, Y.; Gautam, P.; Misra, R. *J. Org. Chem.* **2017**, *82*, 6840–6845.
23. Reutenauer, P.; Kivala, M.; Jarowski, P. D.; Boudon, C.; Gisselbrecht, J. -P.; Gross, M.; Diederich, F. *Chem. Commun.* **2007**, 4898–4900.
24. Jayamurugan, G.; Gisselbrecht, J. -P.; Boudon, C.; Schoenebeck, F.; Schweizer, W. B.; Bernet, B.; Diederich, F. *Chem. Commun.* **2011**, *47*, 4520–4522.
25. Betou, M.; Kerisit, N.; Meledje, E.; Leroux, Y. R.; Katan, C.; Halet, J. -F.; Guillemin. J. -C.; Trolez, Y. *Chem. –Eur. J.* **2014**, *20*, 9553–9557.
26. Hansch, C.; Leo, A.; Taft, R. W. *Chem. Rev.* **1991**, *91*, 165–195.
27. Remya, G. S.; Suresh, C. H. *Phys. Chem. Chem. Phys*. **2016**, *18*, 20615−20626.
28. Asthana, D.; Pandey, R.; Mukhopadhyay, P. *Chem. Commun.* **2013**, *49*, 451–453.
29. Masunov, A.; Dannenberg, J. J. *J. Phys. Chem. B.* **2000**, *104*, 806–810.
30. Zhou, J.; Booker, C.; Li, R.; Zhou, X.; Sham, T. -K.; Sun, X.; Ding, Z. *J. Am. Chem. Soc.* **2007**, *129*, 744–745.
31. Jacquemin, D.; Wathelet, V.; Perpète, E. A.; Adamo, C. *J. Chem. Theory Comput.* **2009**, *5*, 2420–2435.
32. Janssen, M. J. *Spectrochim. Acta*. **1961**, *17*, 475–485.
33. Neese, F. *Comput. Mol. Sci.* **2012**, *2*, 73−78.
34. Yanai, T.; Tew, D. P.; Handy, N. C. *Chem. Phys. Lett.* **2004**, *393*, 51–57.
35. Nagaraju, N.; Kuriakose, G. *Green Chem.* **2002**, *4*, 269–271.
36. Dar, A. H.; Gowri, V.; Gopal, A.; Muthukrishnan, A.; Bajaj, A.; Sartaliya, S.; Selim, A.; Ali, Md. E.; Jayamurugan, G. *J. Org. Chem*. **2019**, *84*, 8941–8947.

Chapter 4

Nanotechnology Assisted White Light Emission (WLE) from Single Chromophoric Organic Molecule

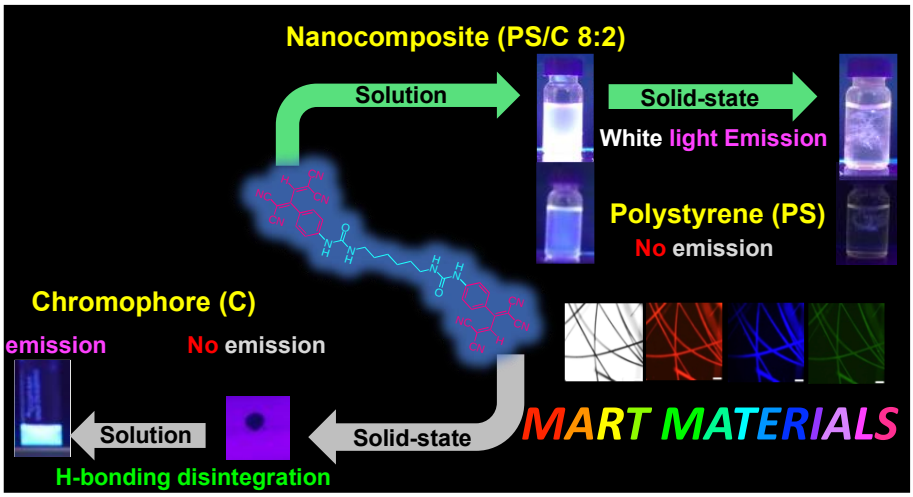

4.0. Introduction:

Organic molecules interacting with light have always been fascinating and gained a lot of interest among the scientific community for their exploitation in different material applications.[1–4] Organic molecules surpass the available inorganic or organic/inorganic hybrid counter molecules effectively in making themselves flexible and soft materials that exhibit other exciting and important properties like supramolecular self-assembly,[5-9] interactions with biological membranes, delivery systems, sensors[10,11] and bioimaging,[12,13,] *etc*. In particular, organic π-conjugated systems are being explored very much from the last many decades. They are continuously on blunt of exposure because of their tremendous application in future generation OLEDs[5] and already available functional and biological materials,[14] e.g., biological chromophores[15] like porphyrins and metalloenzymes and other critical organic molecules containing π–conjugated systems. The design of push–pull chromophores based on merocyanine dyes[16,17] and other twisted push–pull chromophores-based systems were explored mainly for their use in biological systems.[18,19] However, the design of non-planar push–pull chromophores (TCBDs) obtained through [2+2] CA–RE reactions for their use in biological systems has not been explored so far.[19] Since the development of TCBD type non-planar push–pull chromophores doesn't feature fluorescence and issues related to solubility (soluble only in organic solvents), this chapter's primary aim and inspiration of generation of these organic non-planar push–pull systems are to address these problems. Since the development of fluorescent TCBD type non-planar push–pull chromophores started with exploring H-bonding susceptible urea group acting as a donor to undergo facile [2+2] CA–RE with TCNE.[20,21] In the case of usual TCBD type non-fluorescent push–pull chromophores,[22–25] the properties and their solubility are usually static and are found only in organic solvents. So we infer that their properties related to the functional group modifications cannot be modulated easily. However, urea-based fluorescent TCBD type push–pull chromophores because of their susceptible H-bond mediated supramolecular self-assembly patterns,[20,26] their activities, properties, and fluorescence in different phases can be tuned by the summation of varying modification and functional group induction sites available in monomeric structures.

We wish to address the problem of fluorescence in solid-state and activity modulation in the same system. For such a design, nanotechnology caught our attention. Nanotechnology gives us desirable methods for self-assembly due to its specific

conformation and directional intermolecular hydrogen bonding ability. The urea in the **Hexyl-TCBD** moiety offers two hydrogen bond donors, which results in efficient self-assembly.[27] Our lab has recently reported that urea-based TCBDs are emissive chromophores.[20,21] As light-emitting organic materials enjoy broad attention because of their capacity to tune and adjust themselves in modern-day electronic devices[28–30] and biomaterials.[30] Therefore, these chromophores can be active ingredients in organo-electronic devices as future generation organic material. Based on it, multicolor photoluminescence, including white-light emission, can be finely tuned through various modes, including excitation wavelength and solvent polarity. White-light emission (WLE) generation commonly requires the simultaneous emission of three primary RGB (red, green, and blue) colors or at least two complementary colors.[3] In commercial white-light sources, one or more light-emitting diodes coated by one or more phosphors yield a combined emission that appears white.[4] However, combining emitters leads to changes in the emission color over time due to the unequal degradation rates of the emitters and efficiency losses due to the different components' overlapping absorption and emission energies. A single material that emits broadband WL (a continuous emission spanning 400−700 nm) would prevent these problems. Various approaches have been adopted to develop efficient white-light-emitting systems, including polymers,[30] metal-organic frameworks,[8,9] quantum dots,[30] nanoparticles,[31–33] self-assemblies,[9,34] and small molecules.[35] Most of the organic WL emitters reported in the literature rely on a combination of several components that emit different colors of light to cover the visible spectrum (400 to 700 nm).[35,36] Compared with multicomponent emitters, WL emission from a single molecule offers advantages[1–3] over the former, including improved stability, excellent reproducibility, and a simplified fabrication process. Nevertheless, only a few examples of WL emission from single-molecule systems have been reported to date. Herein, we explored a symmetric acceptor-π–donor-π–donor-π–acceptor (A–π–D-π–D-π–A) organic molecule containing urea as a functional backbone with a hexyl spacer (Figure 4.0).

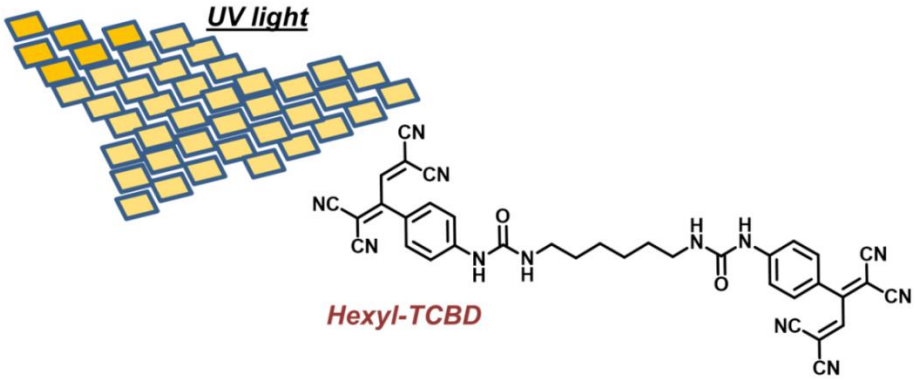

Figure 4.0. Structure of **Hexyl-TCBD under study**.

Then onwards, we tried to explore their new design strategies to facilitate its biocompatible nature. Surprisingly, the fluorescence retaining capacity in solid-state came into the limelight along with its biocompatible nature. The design of retaining fluorescence in the solid-state of push–pull chromophore demands perfection in maintaining its molecular form and its activity in respective phases. Furthermore, urea-based push–pull chromophore and their inherent ICT bands might possess excellent ICT state stabilization by space charge distribution through intensive H-bonding interactions.[37] A WL emitting fibers were also facilely prepared using electrospinning methodology and polystyrene as the matrix to segregate the chromophoric molecules. This innovative study helps to enrich the strategies to construct single-molecule organic white-light-emitting material, which can even be used in the aqueous medium.

Translation of WL emission from a solution to fiber form has been demonstrated here. Solvent-dependent WL emission with variable CIE values (values close to WL emission) (0.33, 0.33) were also validated by optical microscopic images and biocompatibility studies.

Overall, here in this work, we exploited **Hexyl-TCBD** as a potential candidate for WL emission and explored its photophysics and structural behavior in different polarity possessing solvents. We also studied its biocompatibility and fluorescence studies in nanofibers for potential applications in biology such as MTT assay.

4.1. Results and discussion:

Solution-Phase Photophysical Studies of Hexyl-TCBD:

The spacer hexyl chain present in **Hexyl-TCBD** (Figure 4.0) has been chosen for the photophysical study because of its enhanced electron-donating ability and susceptibility

to conformational changes, altering its effect self-assembly behavior in comparison with rigid spacer.[20] As reported, the photoluminescence nature of push-pull chromophore is greatly affected by the parameters (e.g., through space stabilization), which controls the stabilization nature of ICT and alters the speed of charge recombination and radiative emission.[37] Similarly, it was reported that unusual photoluminescence behavior of TCBDs with urea as an electron-donating group (EDG) was attributed due to its unique Field effect property of urea donor,[20] which enhances the charge distribution and retards their charge recombination process and ultimately expanding its emissive behavior along with ICT state stabilization.

We initially performed solvent-dependent absorption, steady-state, and time-resolved emission spectroscopies using UV/Vis and photoluminescence (PL) spectrophotometers to explore its photophysical properties. Figure 4.1a shows the light-absorbing property of **Hexyl-TCBD** in different solvents with the presence of ICT bands. More specifically, two bands were observed at λ_{max1} 507 nm and λ_{max2} 560 nm in relatively non-polar solvents (acetone, THF, and acetonitrile (CH_3CN)) between 440 640 nm. Further, it has been observed that the disappearance of the longer wavelength ICT band at λ_{max2} = 560 nm in polar solvents (DMF, DMSO, and MeOH) implying non-favorable H-bonding interaction, thus exhibiting the dis-integration of aggregated **Hexyl-TCBD** into its monomer state. We infer that the band at λ_{max1} 507 nm corresponds to the intrinsic ICT band from urea to dicyanovinyl (DCV). In contrast, the λ_{max2} 560 nm results from *J*-type aggregation formed by H-bonding mediated self-assembly.[38] The strong aggregation phenomenon in solution was observed previously by NMR studies.[20]

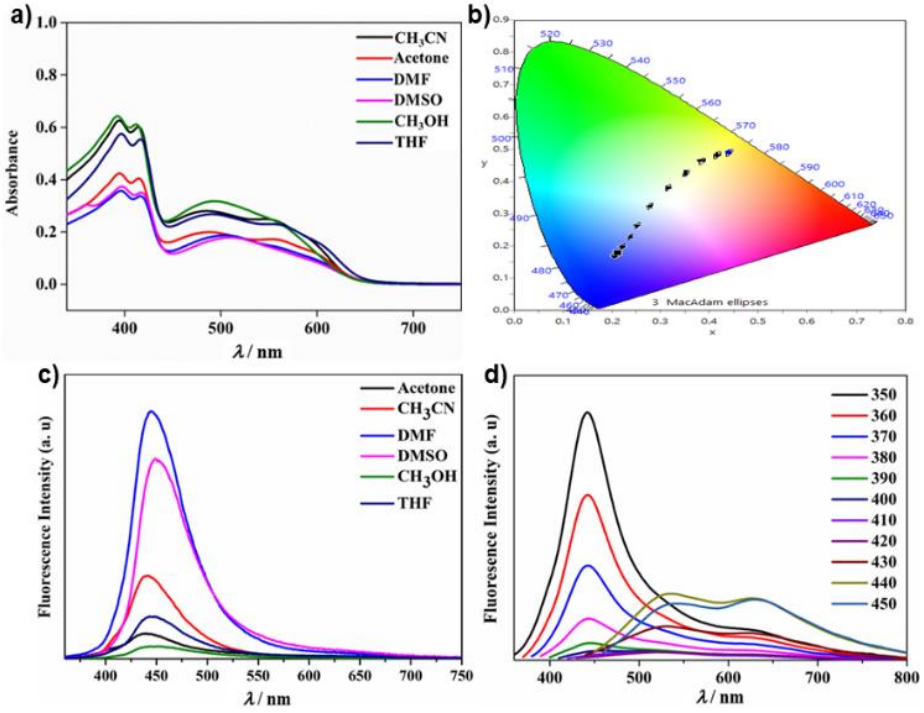

Figure 4.1. a) UV-Visible spectra of **Hexyl-TCBD** in different solvents. b) CIE plot of **Hexyl-TCBD** with varying excitation wavelengths in THF (6×10^{-5} M) λ_{ex} = 350 – 450 nm) c) Fluorescence spectra of **Hexyl**-TCBD upon excitation at 350 nm d) Fluorescence spectra of **Hexyl-TCBD** in THF excited at different wavelengths (6×10^{-5} M) (λ_{ex} = 350 – 450 nm).

The results obtained from the UV/Vis experiments were further corroborated with the emission experiments (Figures 4.1c,d). Initially, we excited the **Hexyl-TCBD** first at 350 nm in solvents of varying polarity (Figure 4.1bc). The disappearance of ICT band at λ_{max} = 560 nm in DMF and DMSO (UV/Vis) has resulted in increased emission intensity at λ_{em} = 450 nm of **Hexyl-TCBD**, probably due to stabilization of the first ICT-state. Whereas, in relatively less polar solvents, lower emission intensities have been observed. From the excitation spectra, for the PL peak at 446 nm, the excitation peak is located at 350 nm. The *J*-type aggregates leading to the destabilization of the second ICT state are the reason for the non-emission nature of the solid-state of this chromophore.

Different excitation wavelengths (λ_{ex} = 350 − 450 nm) were used to obtain emission spectra of **Hexyl-TCBD** in THF to identify the appropriate excitation wavelengths which can provide dual emission corresponding to nearest WLE (CIE values of 0.33, 0.33) and to demonstrate the tunability of the luminescence (Figure 4.1b). Figure 4.1b shows the CIE plot of **Hexyl-TCBD** with varying CIE values upon using different excitation wavelengths. The remaining studies were performed with this wavelength since the nearest CIE values of 0.31 and 0.38 was obtained at 420 nm in DMF.

It was also observed that single push–pull chromophoric unit, *i.e.*, TCBD moiety exhibiting dual emissions at λ_{max1} = 535 nm and λ_{max2} = 625 nm upon exciting in 400 − 450 nm, which may correspond to the ICT bands 1 and 2, respectively. The respective CT states may originate from the n–π* transition of the urea moiety. It is well known that strong quenching of emission for TCBD type push-pull molecules was observed because of excited state events such as energy or electron transfer.[39] The present work suggests that the appropriate modification on the EDG of the push-pull chromophore to modulate the electronic structure of the molecular system may allow achieving the multicolor luminescence emission through introducing additional CT. During the solvent-dependent optical study, the solution of **Hexyl TCBD** varies emissive colors and covers almost the entire visible region of the spectrum as validated by the CIE plot. It was found that **Hexyl TCBD** chromophore is robust to temperature, light, and sonication as no change in optical properties was observed even after 30 min of sonication (30 kHz) or on refluxing (75 °C) condition. The high tunability of emission properties may be ascribed due to a change in solvent-dependent polarization of a TCBD conjugated urea chromophore (**Hexyl-TCBD**) molecule, which affects intramolecular electronic conjugation. Figure 4.1d shows the CIE plot of **Hexyl-TCBD** with varying CIE values upon using different excitation wavelengths. Since nearest CIE values of 0.31, 0.38 were obtained at 420 nm in DMF, and the remaining studies were performed with this wavelength.

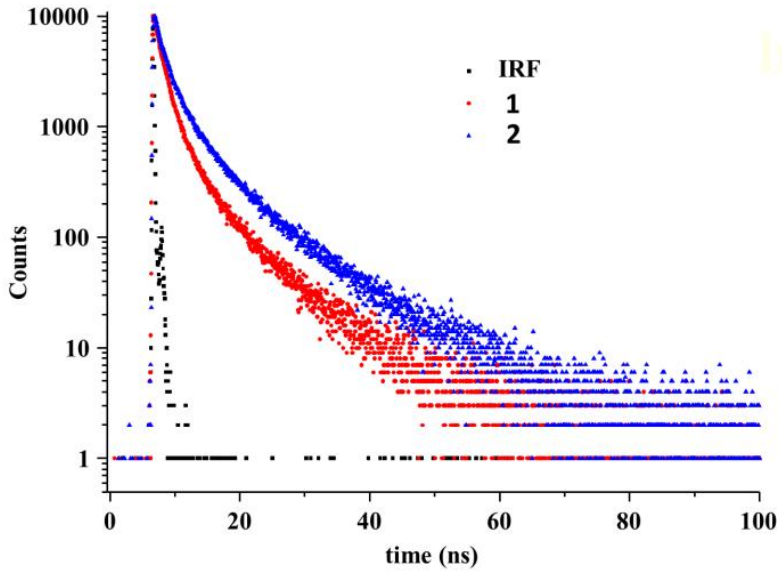

Figure 4.2. TCSPC decay profile of Hexyl-TCBD in CH_3CN (**1**) and THF (**2**).

Table 1. Measured emission lifetimes (τ) and fractionation intensities (α) of **Hexyl-TCBD**

Solvent	$\tau_1(\alpha_1)$	$\tau_2(\alpha_2)$	$\tau_3(\alpha_3)$
CH_3CN	2.23 (0.32)	0.87 (0.63)	7.77 (0.05)
THF	1.01 (0.60)	3.19 (0.33)	10.22 (0.07)

Lifetime measurements were carried out for the emission of **Hexyl-TCBD** using the time-correlated single-photon counting (TCSPC) study to further understand the steady-state fluorescence results. We have chosen THF and CH_3CN as they feature relatively non-polar and polar solvents, respectively.[1] The results are summarized in Table 1. The decay curves (Figure 4.2) of **Hexyl-TCBD** in THF and CH_3CN are successfully fit by the sum of three exponential components with different decay times of τ_1, τ_2, τ_3 corresponding to 1.01, 3.19 and 10.22 ns and 2.23, 0.87, and 7.77 ns, respectively.

Interestingly, the emission behavior of **Hexyl-TCBD** in CH_3CN and THF is markedly different (CIE of CH_3CN and THF are (0.34,0.39) and (0.31,0.36), respectively). In THF, the polarized transition state by solvation lowers its excited state energy, enhancing its fluorescence lifetime. For instance, in CH_3CN, a significantly faster component of 7.77 ns was observed than 10.22 ns in THF, implying the decay of the ICT state being favored in the polar environment. Thus the effect of multiple TCBDs with a non-conjugated spacer in fluorescence is understandable by the role of photochemical events such as prolonging the lifetime of charge-separated states *via* the electron exchange mechanism and.

We infer that the significant change in the lifetime of solvents (THF, CH_3CN) might be connected with the self-assembly nature of **Hexyl-TCBD**. We envisage that in THF, the "O" donor group may form a better hydrogen bonding network. Hence, it can stabilize the "enolic" form of "zwitterionic **Hexyl-TCBD** and in CH_3CN containing "N" atom as an electron donor participate in stabilizing "keto" form of the push-pull chromophore. To support this, ATR-FT-IR was performed for solutions of **Hexyl-TCBD** in CH_3CN and THF after evaporation, and the results are shown in Figure 4.3a,b.

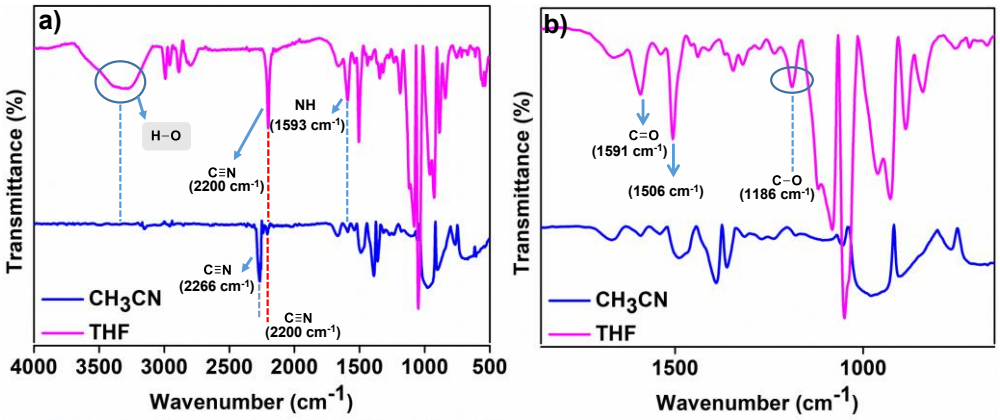

Figure 4.3. a) Full and b) partial FT-IR spectra **of Hexyl-TCBD** in CH_3CN and THF.

The FT-IR spectra of **Hexyl-TCBD** clearly show the distinct pattern for two different solvents of CH_3CN and THF. The urea-tautomer in acetonitrile shows a characteristic peak for carbonyl stretching frequency at 1670 cm^{-1} and for C≡N at 2266 cm^{-1}, whereas, in THF, the C=O stretching frequency got reduced and a new peak corresponding to of C—O peak of enol-tautomer at 1186 has appeared indicating in THF the enol form is present. Similarly, the nitrile peak at 2266 cm^{-1} has shifted to 2200 cm^{-1} for the enolic state. Further, O—H stretching frequency for enol form is also present in THF at 3196 cm^{-1}, absent in CH_3CN. Precautions were taken to avoid water content in THF by using a dry solvent. These characteristics signals corresponding to the possible keto-enol tautomerism are schematically represented in Figure 4.4.

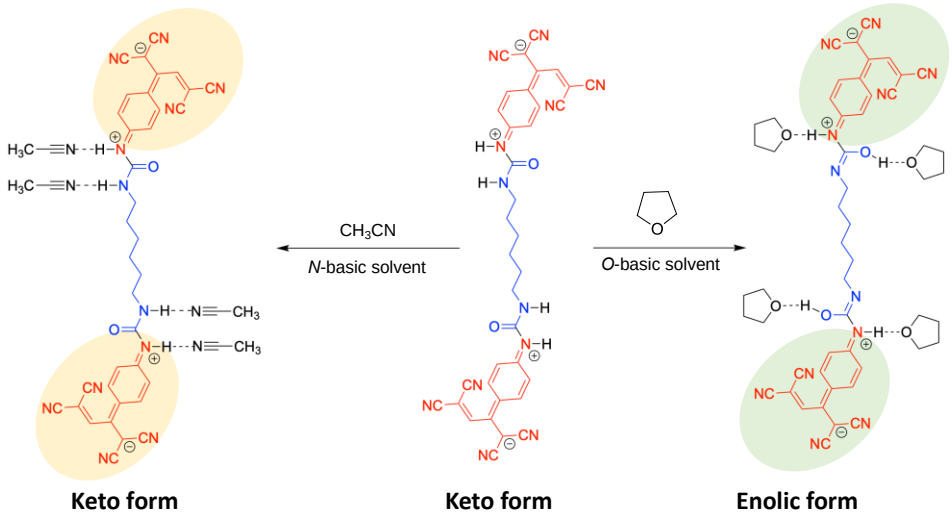

Figure 4.4. Schematic representation of Keto-enol tautomerism of **Hexyl-TCBD** stabilized by *N*- and *O*-basic solvents.

4.2. Solvent-Dependent Morphological Study by Scanning Electron Microscopy (SEM):

To better understand the aggregation process and emission from the **Hexyl-TCBD**, we have performed scanning electron microscopy (SEM) studies (Figure 4.5a-d). Specifically, **Hexyl-TCBD** was dissolved in solvents such as CH_3OH, CH_3CN, DMF, and THF, then allowed to evaporate slowly and observed under SEM. In all these solvents, the SEM images show well-pattered structures with variation in packing density, indicating different level self-assembly mediated mainly by H-bonding interactions between urea moieties. Unlike solvents like CH_3CN and CH_3OH, where it ends up with a random aggregation of urea moieties leading to flakelike structures, THF and DMF form very well patterned structures (Figures. 4.5a,b).

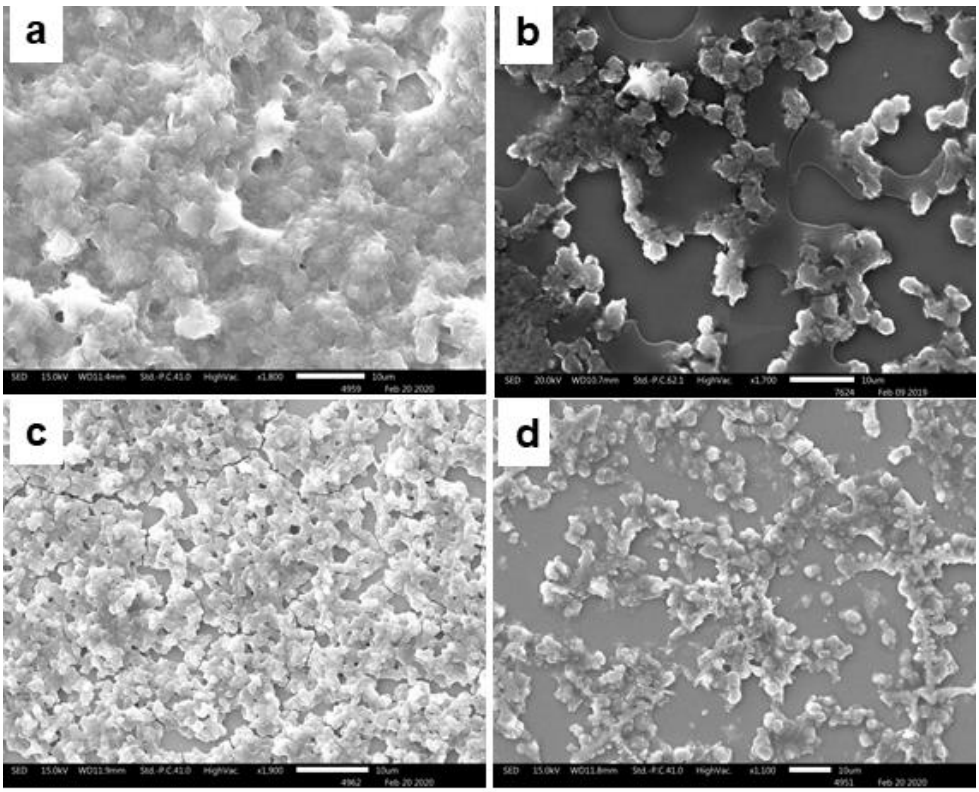

Figure 4.5. SEM images of **Hexyl-TCBD** in different solvents a) THF (inset: zoomed image showing fiber type structure) b) DMF c) CH_3CN d) CH_3OH (The scalebar is 10 μm).

In THF, it forms a thread-like fibrous type structure; the morphology shows that **Hexyl-TCBD** is assembled in a continuous fashion, which we further corroborated by AFM studies (Figure. 4.6). The fibrous ordered arrangement of **Hexyl-TCBD** in THF confirms its self-assembly by using predominantly *H*-bonding interactions between two urea units and slight π-π interactions between two phenyl rings and other non-covalent

interactions, which may also accelerate its self-assembly into fibers. The AFM images have given a clear insight into its fiber formation in THF solvent.

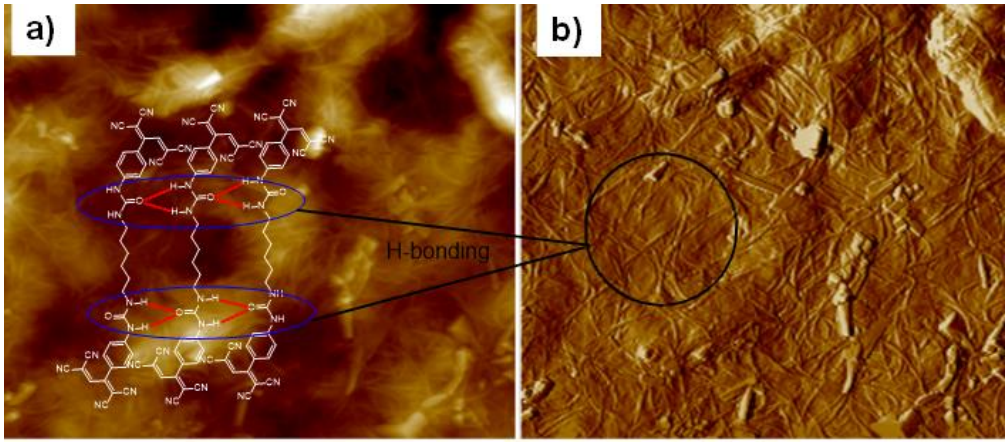

Figure 4.6. AFM images of **Hexyl-TCBD** a) Normal AFM image b) Vertically aligned image. Inset schematic representation of H-bonding mediated self-assembly.

We have also observed red, green, and blue (RGB) color emission while evaporating the THF from the nascent **Hexyl-TCBD** (Figure 4.7). After successfully testing the fluorescence (WL emission) versatility of **Hexyl-TCBD** in different solvents, we focused on solid-state emission studies.

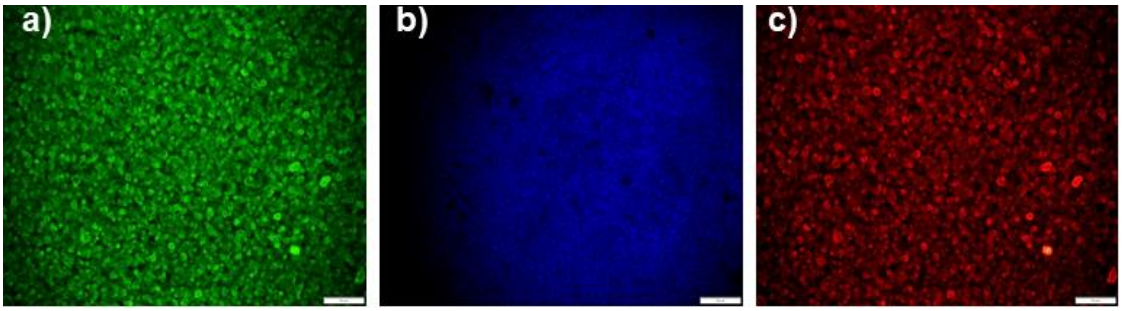

Figure 4.7. Optical Microscopic images of **Hexyl-TCBD** in THF Solvent. a) FITC b) DAPI c) TRITC.

4.3. Translation of WLE from solution to fibers:

Theπ stacking of the planar molecules may facilitate the formation of detrimental excimer species and lead to fluorescence quenching in the solid-state. The *J*-type aggregates leading to the destabilization of the second ICT state are the reason for the non-emissive nature of the solid-state of this chromophore, as suggested by the DFT calculations. Though the luminescence for **Hexyl-TCBD** was observed in solution only, it is desirable to achieve solid-state luminescence and an aqueous medium for real-time

applications. Hence, based on UV/Vis results (*vide supra*), we hypothesize that the disintegration of aggregated molecules may regenerate solid-state luminescence. On this account, we used the nanocomposite approach using polystyrene polymer as the matrix in significant excess (up to 80%) for maintaining the particular emissive molecular form of **Hexyl-TCBD** even in the solid-state. We adopted a nanotechnology-driven approach to preparing nanocomposite fibers using electrospinning technique and synthesized soft fibers of **Hexyl-TCBD** with polymer PS matrix and elucidated the solid-state luminescence of **Hexyl-TCBD.** The soft fibers of **Hexyl-TCBD** with polymer PS matrix were obtained With the help of a nanotechnology-driven approach for the synthesis of nanocomposite fibers using the electrospinning technique.

4.3.1. **Synthesis of nanofibers.** We choose DMF as a solvent to synthesize nanowires using electro-spun because of its high boiling point and self-assembly-friendly nature. We added 20 Wt/Vol (%) polymer polystyrene with **Hexyl-TCBD** in 2 mL of DMF and stirred for 3 h. Then, we get a slightly viscous reddish-colored solution. While carrying out electrospinning, we used a 2 mL syringe at 8.7 KeV to collect fibers on aluminum foil. We collected white-colored finely textured fibers and kept them in water for many days. These fibers were observed after 20 days, still showing collective RGB emissions under the optical microscope. These images corroborate their stable emissive behavior even while encapsulating **Hexyl-TCBD** in non-polar polystyrene polymer.

As-prepared nanofibers of PS-chromophore and PS were initially tested for their luminescence property in an aqueous medium upon shining UV light (UV lamp 35nm). The PS fiber was not emitting light under the UV lamp (handheld), while the nanocomposite has shown apparent light-emitting behavior (Figure 4.8). The fluorescent organic push–pull chromophores form a black-reddish powder in solid-state and dark-red solution while dissolving in polar solvents, as WL emission is perceived from their dilute solutions only (Figure 4.8f). After closely observing the fluorescence behavior of **Hexyl-TCBD** in different solvents using steady-state and time-resolved measurements. We also elucidated the white light emission from a single organic push–pull chromophore using an optical microscope. The optical microscope uses different energy filters for exciting a molecule, and for perfect WL emission, a molecule should emit all the colors *viz* RGB (red, green, and blue). The utilization of these materials in illuminating devices can benefit significantly if such WLE can be accomplished in a solid-state, particularly in the form of flexible fibers.

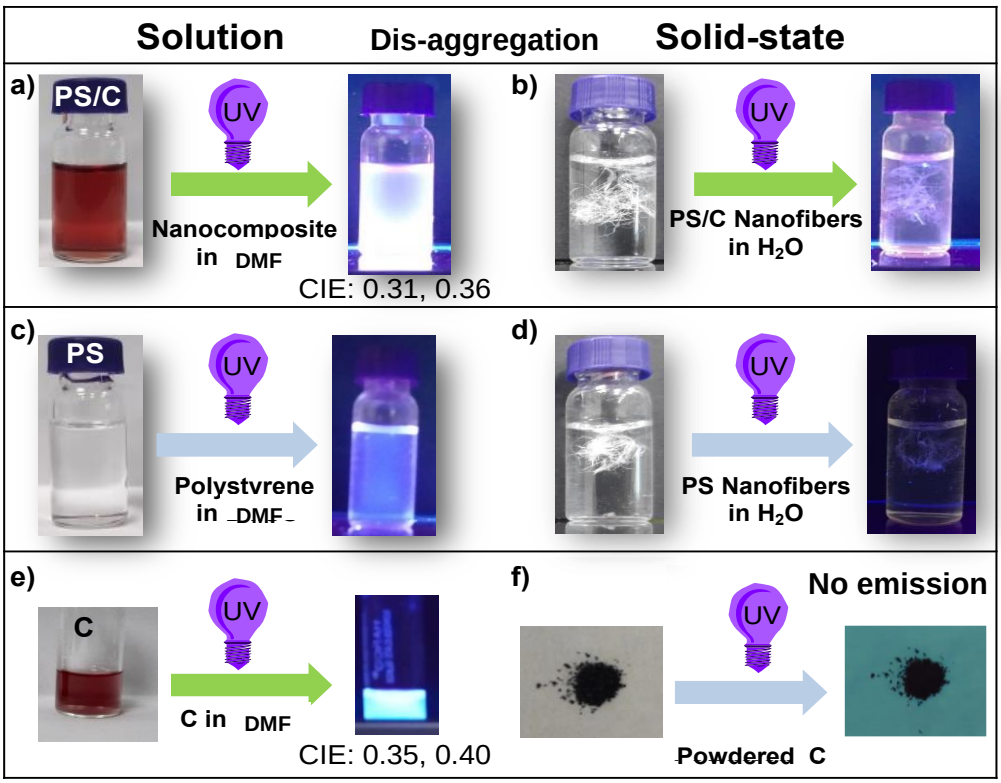

Figure 4.8. In DMF solution a) Polystyrene/Chromophore (PS/C) composite upon shining UV light. b) only PS with and without a UV lamp (hand-held UV lamp 365 nm). c) only C with and without a UV lamp. In Solid-state d) PS/C fibers with and without a UV lamp. e) PS-fibers with and without a UV lamp. F) powdered C with and without a UV lamp.

The solid-state luminescence from **Hexyl-TCBD** with the matrix of PS polymer was analyzed using an optical microscope. The representative images showing RGB colors are given in Figure 4.9. We infer that the **Hexyl-TCBD** arrested within the hydrophobic polymer exists as isolated spheres against the platy aggregates found in the bulk powder (which limits its fluorescence in solid-state). Inevitably, these long fibers facilitate the molecular individuality and retain its fluorescence in the polymer matrix, and eventually, fibers were found stable in water.

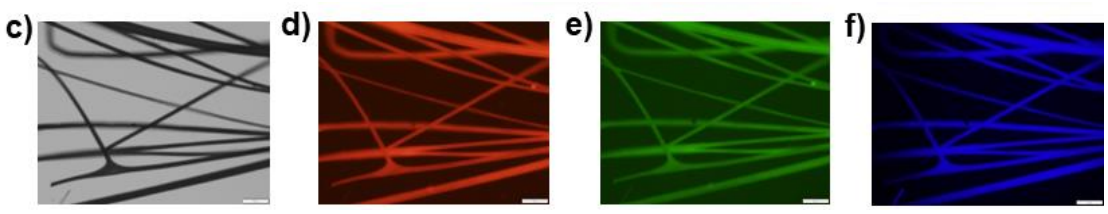

Figure 4.9. (a). TCSPC of **Hexyl-TCBD** in 1) CH_3CN 2) THF (b).UV-Visible spectra with the fraction of water (6×10^{-5}M) (c). Optical microscopic images of nanowires of **Hexyl-TCBD** after electrospinning with polystyrene polymer (c) (bright field) (d) TRITC (red emission) (e) FITC (green emission) (f) DAPI (blue emission).

4.4. Biocompatibility of Hexyl-TCBD on HTERT and HCT116 Cells:

In-vitro cytotoxicity of **Hexyl-TCBD** was determined using MTT assay to explore further its applications in biosystems such as bio-imaging probes (Figure 4.10). The anti-proliferative effects were assessed employing EZcount^{TM} MTT cell Assay Kit (HiMedia Laboratories Pvt. Ltd., India) by treating **Hexyl-TCBD** with different concentrations against normal (HTERT) and cancer (HCT116) cell lines. The cells carrying **Hexyl-TCBD** were incubated for 24 h. It was observed that more than 80% viability up to 25 µg/L concentration of **Hexyl-TCBD** (DMF) towards standard cell line, suggesting the low cytotoxicity of **Hexyl-TCBD** towards normal live cells. Whereas, significant toxicity, i.e., 58% viability up to 25 µg/L concentration, was observed against cancer (HCT116) cell lines indicating good use as photodynamic therapy.

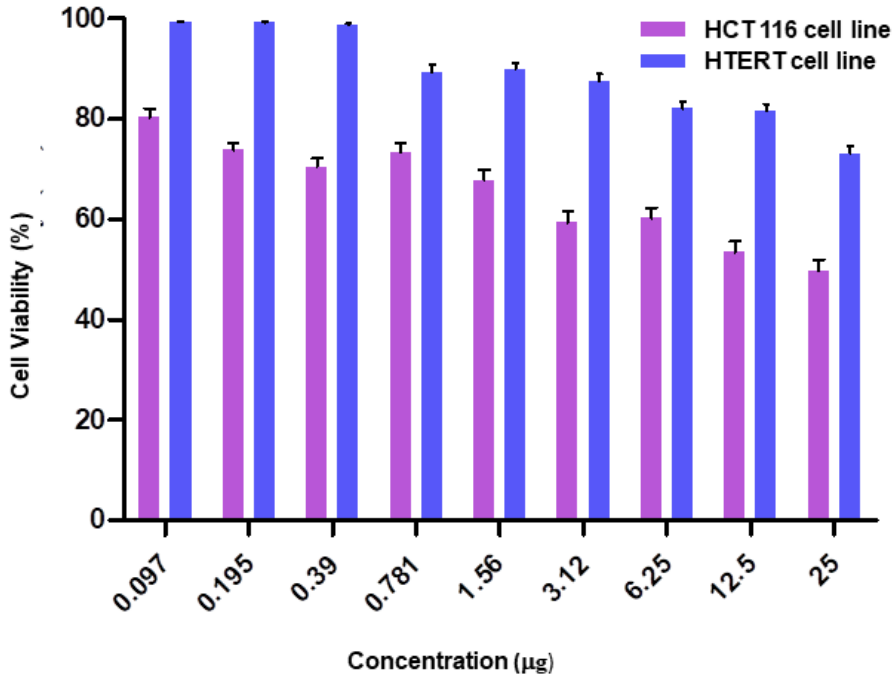

Figure 4.10. MTT assay of **Hexyl-TCBD** in two different cell lines (Cancer and standard cell line).

Cell Culture and Cytotoxicity Studies:

Human colon cancer cells (HCT116) cells were obtained from NCCS Pune and were cultured in McCoy's media supplemented with 10% fetal bovine serum (FBS) and 1% antibiotics (penicillin and streptomycin). These cultures were maintained at 37 °C, 5% CO_2, humidified incubator. The media was changed every 24 h and sub-cultured when the cells reached confluence. The MTT assay was performed in a 96-well plate with a

seeding density of 1.5×10^4 cells in each well to evaluate the cytotoxicity of **Hexyl-TCBD** on human colon cancer cells (HCT116). The cells were then treated with different concentrations of **Hexyl-TCBD** (25, 12.5, 6.25, 3.12, 1.56, 0.781, 0.390, 0.195, and 0.097 μg/mL) and were incubated for 24 h at 37 °C under 5% CO_2 atmosphere. After treatment, the media was removed, and 50 μL MTT reagent (1 mg/mL) was added to each well and incubated for 4 h in the dark at 37 °C in the incubator. Furthermore, the medium was removed, and 100 μL of DMSO was added to each well. The absorbance was measured at 570 nm after 15 min using a microplate reader (Molecular device).

4.5. Conclusion:

In the present work, we investigated a transition metal-free, non-hazardous, non-toxic single organic push–pull chromophore, i.e., **Hexyl-TCBD**, as a WL emitting fluorescent probe. We had studied the photostability of **Hexyl-TCBD** in various solvents (protic/aprotic) to unravel the role of morphology obtained differently by the strength of H-boning mediated self-assembly. Interestingly, The IR and other studies indicated that the enol-tautomer is stabilized in THF solvent, whereas the urea tautomer is retained in CH_3CN medium. Further, we had translated the fluorescence emission from the solution to solid-state using an electrospinning approach. The observed RGB emissions (WL) were successfully tested using microscopic studies. The nontoxicity nature of the **Hexyl-TCBD** fibers is promising to be used as an actively targeted bioimaging fiber for specific cell organelles imaging.

4.6. References:

1. Pal, K.; Sharma, V.; Koner, A. L.; *Chem. Commun*. **2017**, *53*, 7909–7912.
2. Zhu, C. N.; Bai, T.; Wang, H.; Bai, W.; Ling, J.; Sun, J. Z.; Huang, F.; Wu, Z. L.; Zheng, Q. *ACS Appl. Mater. Interfaces* **2018**, *10*, 39343–39352.
3. Li, D.; Hu, W.; Wang. J.; Zhang, Q.; Cao, X.-M.; Ma, X.; Tian, H. *Chem. Sci*. **2018**, *9*, 5709–5715.
4. Thomas, K. R. J.; Venkateswararao, A.; Joseph, V.; Kumar, S.; Jou, J.-H. *Organic Electronics*. **2019**, *64*, 266–273.
5. Würthner, F.; Saha-Möller, C. R.; Fimmel, B.; Ogi, S.; Leowanawat, P.; Schmidt, D. *Chem. Rev*. **2016**, *116*, 962–1052.

6. Huo, S.; Jiao, T.; Peng, Q.; Huo, S.; Duan, P.; Liu, M.;Liu, M. *Angew. Chem. Int. Ed*. **2017**, *56*, 12174–12178.
7. Shinde, S.; Asha, S. K. *Macromolecules* **2016**, *49*, 8134–8145.
8. Zhang, M.; Yin, S.; Zhang, J.; Zhou, Z.; Lal Saha, M.; Lu, C.; J. Stang, P. *Proc. Natl. Acad. Sci. U. S. A*. **2017**, *114*, 3044–3049.
9. Huynh, H. V.; He, X.; Baumgartner, T. *Chem. Commun*. **2013**, *49*, 4899–4901.
10. Li, M.; Wang, Y.-X.; Wang, J.; Chen, Y. J. *J. Mater. Chem. C*. **2017**, *5*, 3408–3414.
11. Pushina, M.; Farshbaf, S.; Shcherbakova, E. G.; Anzenbacher, P. *Chem. Commun*. **2019**, *55*, 4495–4498.
12. Griesbeck, S.; Michail, E.; Wang, C.; Ogasawara, H.; Lorenzen, S.; Gerstner, L.; Zang, T.; Nitsch, J.; Sato, Y.; Bertermann, R.; Taki, M.; Lambert, C.; Yamaguchi, S.; Marder, T. B. *Chem. Sci*. **2019**, *10*, 5405–5422.
13. Chen, S. Y.; Zhang, M. Z.; Zhu, C. Z.; Lu, H. X.; Zhao, M.; Tian, X. H.; Zhang, Q.; Souza, S. C. D.; Rong, F.; Zhou, H. P.; Wu, J. Y.; Tian, Y. P. *Dyes and Pigments*. **2018**, *148*, 429–436.
14. Petrizza, L.; Collot, M.; Richert, L.; Mely, Y.; Prodi, L.; Klymchenko, A. S. *RSC Adv*. **2016**, *6*, 104164–104172.
15. Koner, A. L.; Krndija, D.; Hou, Q.; Sherratt, D. J.; Howarth, M. *ACS Nano*. **2013**, *7*, 1137–1144.
16. Würthner, F. *Acc. Chem. Res*. **2016**, *49*, 868–876.
17. Würthner, F.; Yao, S.; Debaerdemaeker, T.; Wortmann, R. *J. Am. Chem. Soc*. **2002**, *124*, 32, 9431–9447.
18. Lou, A. J.-T.; Marks, T. J. *Acc. Chem. Res*. **2019**, *52*, 1428–1438.
19. Michinobu, T.; Diederich, F. *Angew. Chem. Int. Ed*. **2018**, *57*, 3552–3577.
20. Dar, A. H.; Gowri, V.; Gopal, A.; Muthukrishnan, A.; Bajaj, A.; Sartaliya, S.; Selim, A.; Ali, Md. E.; Jayamurugan, G. *J. Org. Chem*. **2019**, *84*, 8941–8947.
21. Gowri, V.; Jalwal, S.; Dar A. H.; Gopal, A.; Muthukrishnan, A.; Bajaj, A.; Ali, E, Md.; Jayamurugan G. *J. Photochem. Photobiol. A* **2021**, *410*, 113163.
22. Michinobu, T.; May, J. C.; Lim, J. H.; Boudon, C.; Gisselbrecht, J.-P.; Seiler, P.; Gross, M.; Biaggio, I.; Diederich, F. *Chem. Commun*. **2005**, *6*, 737–739.
23. Michinobu, T.; Boudon, C.; Gisselbrecht, J.-P.; Seiler, P.; Frank, B.; Moonen, N. N. P.; Gross, M.; Diederich, F. *Chem. Eur. J*. **2006**, *12*, 1889–1905.

24. Reutenauer, P.; Kivala, M.; Jarowski, P. D.; Boudon, C.; Gisselbrecht, J.-P.; Gross, M.; Diederich, F. *Chem. Commun*. **2007**, *46*, 4898–4900.
25. Kivala, M.; Boudon, C.; Gisselbrecht, J.-P.; Seiler, P.; Gross, M.; Diederich, F. *Angew. Chem. Int. Ed*. **2007**, *46*, 6357–6360
26. Asthana, D.; Pandey, R.; Mukhopadhyay, P. *Chem. Commun*. **2013**, *49*, 451−453.
27. Masunov, A.; Dannenberg, J. J. *J. Phys. Chem. B* **2000**, *104*, 806−810.
28. Xie, Z.; Chen, C.;Xu, S.; Li, J.; Zhang, Y.; Liu, S.;, Xu, J.; Chi, Z. *Angew. Chem. Int. Ed*. **2015**, *54*, 7181–7184.
29. Tu, D.; Leong, P.; Guo, S.; Yan, H.; Lu, C.; Zhao, Q. *Angew. Chem. Int. Ed*. **2017**, *56*, 11370–11374.
30. Wu, H.; Ying, L.; Yang, W.; Cao, Y. *Chem. Soc. Rev*. **2009**, *38*, 3391–3400
31. Huo, S.; Jiao, T.; Peng, Q.; Huo, S.; Duan, P.; Liu, M.;Liu, M. *Angew. Chem. Int. Ed.* **2017**, *56*, 12174–12178.
32. Malinge, J.; Allain, C.; Brosseau, A.; Audebert, P. *Angew. Chem. Int. Ed*. **2012**, *51*, 8534–8537.
33. Layek, A.; Stanish, P. C.; Chirmanov, V.; Radovanovic, P. V. *Chem. Mater*. **2015**, *27*, 1021–1030.
34. Molla, M. R.;Gehrig, D.; Roy, L.; Kamm, V.; Paul, A.; Laquai, F.; Ghosh, S. *Chem. Eur. J*. **2014**, *20*, 760–771.
35. Xie, Z.; Chen, C.;Xu, S.; Li, J.; Zhang, Y.; Liu, S.;, Xu, J.; Chi, Z. *Angew. Chem. Int. Ed*. **2015**, *54*, 7181–7184.
36. He, Z.; Zhao, W.; Lam, J. W. Y.; Peng, Q.; Ma, H.; Liang, G.; Shuai, Z.; Tang, B. Z. *Nat. Commun*. **2017**, *8*, 416.
37. Shen, P.; Zhuang, Z.; Jiang, X.; Li, J.; Yao, S.; Zhao, Z.; Tang, B. Z. *J. Phys. Chem. Lett*. **2019**, *10*, 2648−2656.
38. Xu, J.; Liu, X.; Lv, J.; Zhu, M.; Huang, C.; Zhou, W.; Yin, X.; Liu, H.; Li, Y.; Ye, J. *Langmuir* **2008**, *24*, 4231–4237.
39. Gautam, P.; Misra, R.; Thomas, M. B.; D'Souza, F. *Chem. Eur. J*.**2017**, *23*, 9192–9200.

Chapter 5

Push–pull Chromophore Encapsulated Nano-micelle as Active Nanoformulation for Bio-imaging and Photodynamic Therapy

- ✓ Nanoparticles with Dual emission
- ✓ PDT for Selective cancer cells
- ✓ Mitochondrial bio-imaging
- ✓ Functional Group fabrication
- ✓ Tunable optoelectronic property
- ✓ Photoluminiscent material

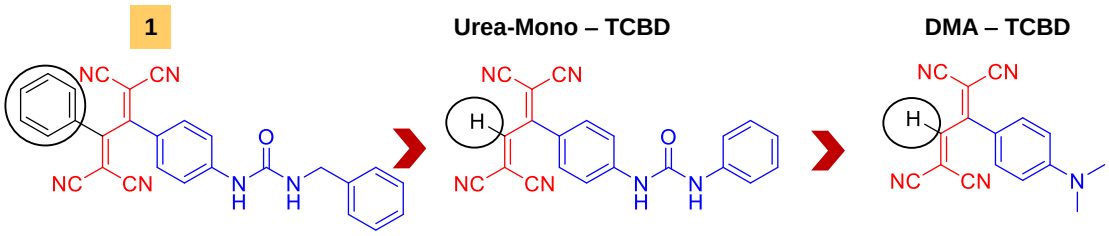

5.0. Introduction:

To further implement the fluorescent 1,1,4,4-tetracyanobuta-1,3-diene (TCBDs) as an efficient bio-imaging and therapeutic probes, the chromophore should retain the luminescence property and act as an efficient photosensitizer (PS) in cells.[1] Further, it should allow extending into the NIR region, making the chromophores even more attractive.[2] Photosensitizers have been found as active bio-probes.[3,4] Among the reported applications of bio-probes, photodynamic therapy (PDT) has been considered one of the effective clinical treatment strategies for malignant tumors.[5] In PDT, the photosensitizer gets activated (excited state of PS) under the light irradiation process then interacts with molecular oxygen to generate reactive oxygen species (ROS). This ROS is now able to oxidize biomolecules which eventually leads to cancer cell death.[6,7]

Theranostics has recently evolved and has been recognized as a promising technique to achieve the real-time and precise therapeutic effect of cancer drugs. It combines both diagnostic and therapeutic capabilities for monitoring the effect.[8] However, PDT and bio-imaging have attracted considerable attention because of their prominent advantages, such as high selectivity, non-toxic, and notably, fewer side effects.[9,10] Therefore, we envisage that the need to design and evaluate the novel PS that can produce both fluorescence and ROS is already in high demand. Also, as we are well aware that the particular photosensitizers can act as bio-imaging probes and can switch the cells to undergo apoptosis.[11–13] However, the system can't differentiate between healthy cells and cancer cells. Hence, the innocent, healthy cells must be sacrificed. Therefore, to overcome this problem, there is a need to develop responsive stimulus systems activatable by a suitable signal. Various studies have been reported in the literature to design such systems activated by specific stimuli.[14–17] For example, the cancer cells in tumor tissues utilize the acidic microenvironment for an external defense system against anticancer drugs, wherein acidification inhibits their permeation into the cells. Cancer cells have slightly decreased extracellular *p*H compared to healthy cells due to the anaerobic glucose metabolism.[14] Therefore, the acidic environment was used to activate the anticancer drug to overcome the limitation of healthy cells' innocent death and specifically target cancer cells.[18] There are many therapeutic systems available and explored for many years for studying the biological phenomenon either in terms of bio-imaging, measurement of membrane tension for determining the environment inside the

cells[19,20] or ion transporting systems as anticancer agents[21,22] or the use of organic molecules as photosensitizers and their respective use in PDT for cancer treatment.

The interaction of light with organic chromophores containing π-conjugation systems have been widely used to tune their optical and electronic properties.[23–25] The so-called push–pull chromophores are a subclass of conventional organic chromophores consisting of donor and acceptor parts available for varying their inherent properties, making them efficient fluorescent materials with characteristic features.[26–27] The fluorescent organic push–pull chromophores are beneficial for two-photon excited imaging in live samples due to minimal background fluorescence,[29] high spatial resolution, and deep tissue penetration because of their emission and absorption in high wavelength region due to the presence of strong donor and acceptor groups, further expanding the essence of organic push–pull chromophores in biological assays has been studied.

The traditional organic fluorescent molecules undergo aggregation-caused quenching (ACQ),[30–32] namely high emission in solution state but faint emission in the condensed form, due to the intrinsic intermolecular π–π stacking interaction, ACQ problem significantly limited their practical applications. Studies related to the utilization of aggregation-induced emission (AIE) properties in non–planer push–pull chromophores are limited[33,] and these molecules were primarily non-fluorescent. However, the push–pull chromophores with a non-rigidity in their structure endorses them to realize their numerous utilizations, especially in biological systems such as imaging due to controllable rotational motion.

As discussed in chapters **3** and **4**, that the mono-substituted tetracyanobuta-1,3-diene (TCBD) type push–pull chromophores with urea as an electron-donating group (EDG) have shown a remarkable fluorescence retaining capability even in solid-state (fibers made with polymer matrix). Further, the preliminary investigation on the good biocompatibility nature was ascertained for fluorescent TCBD type push–pull chromophore. Urea is susceptible to many investigative properties *viz.* functional group modification, H-bonding, and unique electron-donating ability have shown new photophysical properties. The fluorescence observed is remarkable compared to other EDG containing TCBDs (DMA-TCBDs, Urea-based mono-TCBDs),[33,34,36], and low fluorescence quantum yield levels (3-4%) is still a challenge to enhance their applications.

5.1. Result and discussion:

Synthesis and characterization of Phenyl-TCBD Nanoparticles:

To overcome the issues related to mono-TCBDs, such as difficulty in purification due to aggregation and limited emission properties, our group has designed and reported a new 2-benzylurea,3-phenyl,1,1,4,4-tetracyanobuta-1,3-diene (phenyl-TCBD (**1**)) and also observed its paper-strip based fluorine anion (F^-) sensing capabilities.[37] Based on the observed luminescence properties of Phenyl-TCBD 1, we envisage that its properties could be further tuned using the nanotechnology approach and hence arrive at better PS capability. With this objective, here in this chapter, we wanted to explore the modulation of photophysical property of **1** using nanomicelle upon encapsulation. For this purpose, we have synthesized nanoparticles of **1** encapsulated inside the nanomicelle suing PF-127 triblock copolymer (Scheme 5.0). Pluronic® block copolymers PF-127 is a proven biocompatible polymer studied extensively for various pharmaceutical applications, including drug and gene delivery systems.[38] PF-127 forms micelle-like structures in water with hydrophobic core moiety. We envisage that 1 in non-friendly medium (aqueous) would tend to aggregate inside the hydrophobic part of PF-127-micelle. Accordingly, we have adopted a nanoprecipitation method[39] using **1** (2 mg) in acetone solution and PF-127 (5 mg) in water. After evaporation of solvents and vacuum drying afforded **1** NPs@PF-127-micelle as powdery form, dissolved in water and used for further studies.

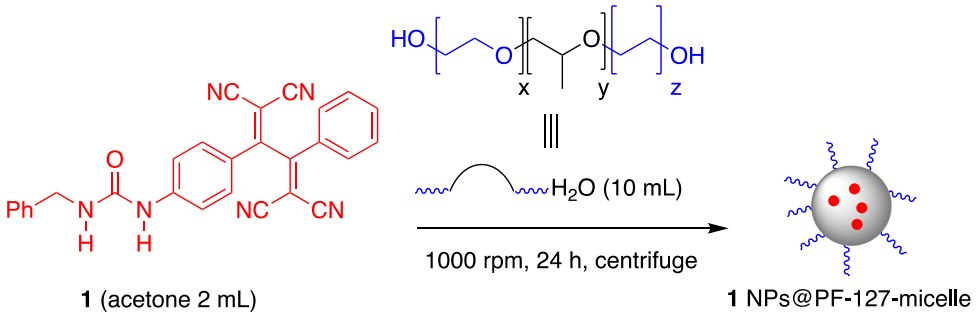

Scheme 5.0. Synthesis of **1 NPs@PF-127-micelle.**

After the successful synthesis, the characterization techniques such as the attenuated total reflection-Fourier transform infrared (ATR-FTIR), transmission electron microscopy (TEM), and atomic force microscopy (AFM) data were used to ascertain the formation of **1 NPs@PF-127-micelle**. FT-IR spectra of **1** and PF-127 have shown peaks at 2223 and 1100 cm^{-1} (Figure 5.0), respectively, which are not present in both of them. However,

both peaks are present in **1 NPs@PF-127-micelle,** indicating that compound **1** is encapsulated by micelles. Though **1** is not soluble in water, the **1 NPs@PF-127-micelle** is homogeneously soluble in water and further corroborates the previous statement. The TEM image shows the diameter of the average micelle of around ~80 nm (Figure 5.1a). This was further verified by the AFM image (Figure 5.1b).

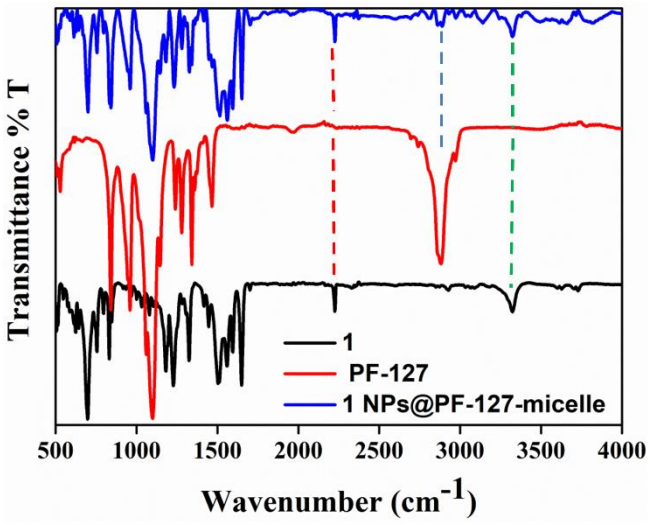

Figure 5.0. ATR-FTIR spectra of **1**, PF-127, and **1 NPs@PF-127-micelle.**

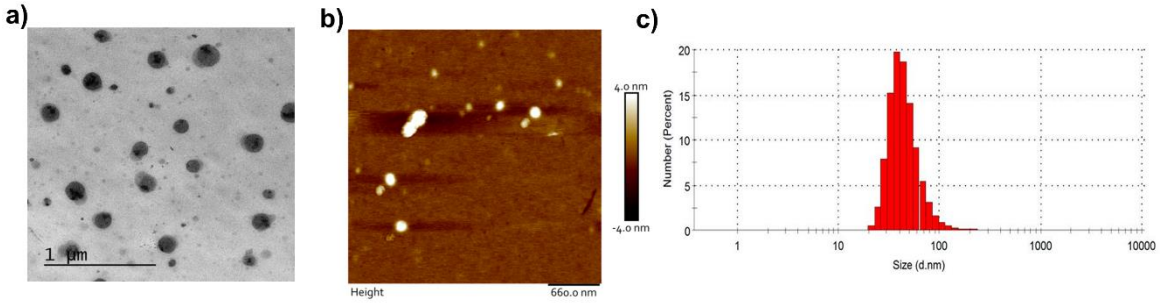

Figure 5.1. a) TEM image of **1 NPs@PF-127-micelle**. b) AFM image of **1 NPs@PF-127-micelle**. c) DLS of **1 NPs@PF-127-micelle**.

The measured average hydrodynamic diameter for **1 NPs@PF-127-micelle** was about 80 nm by TEM and DLS (Figure 5.1c). The morphology of nanoparticles has been studied not only by TEM and AFM (Figure 5.1b,c) and also optical microscopic study.

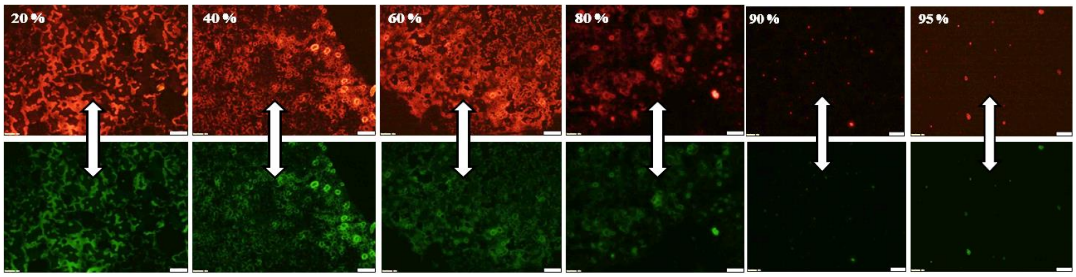

Figure 5.2. Optical microscopic images of **1** in THF with increasing H_2O (5×10^{-5} M) (Showing dual emission viz red and green.

The intense emission of nanoparticles inspired us to study the self-assembly property of these AIEgens due to their potential application in optical devices or probes. The self-assembled samples were prepared by the classical precipitation method in water and THF with varying amounts of water content. The resulted aggregates formed were examined using fluorescence optical microscopy (Figure 5.2). The push–pull chromophore 1 starts self-assembling with 20% (w/v) addition of water, resulting in red and green-emitting AIEgens with distinct floppy type morphology. The aggregation subsequently increases with the addition of water percentage from 20 – 95 %. The self-assembling at 95% of water results in the formation of nanoparticles, whereas lower water content did not show nanoparticles but rather showed floppy type morphology as already observed in TEM and AFM with 100% of water during the nanoprecipitation method for synthesizing **1 NPs@PF-127-micelle**. Surprisingly, during AIE with the increase in aggregation, fluorescence spectra show band broadening as shown in the above Figure, and also there occurs a change in morphology of molecule. The difference in morphology from aggregation at 20 % addition of water to 95 % i,e at nanoparticle formation is quite interesting, as evidenced by optical microscopic images. To validate the photostability of the synthesized NPs exhibit good photostability under continuous laser excitation (360 nm, 100 mW). We have performed the following experiments on whether the molecules of **1** remain within the NPs@PF-127-micelles or are released upon photoirradiation. We have performed the subsequent experiments. i) As molecule **1** in the solution phase is not significantly emissive, and the polymer PF-127 is not emissive at all while synthesizing NPs@PF-127-micelle, we observed a dramatic shift in luminescence which is quite different from that of molecules in solution or polymer PF-127 alone. ii) The respective solutions of **1** and NPs@PF-127-micelle were kept under the irradiation of xenon-lamp for 12 h. We observed that there is no significant change in the UV absorption and their luminescence property. iii) Furthermore, while performing the bioimaging studies, we

observed that the NPs@PF-127 does not undergo a decrease in luminescence intensity, indicating that the NPs do not come out of photoirradiation during photoirradiation of the micelle.

***Electronic Absorption and Photoluminescence Spectroscopic Studies*:**

The photophysical properties of synthesized push–pull chromophore 2-benzylurea3-phenyl 1,1,4,4-tetracyanobuta-1,3-diene (phenyl-TCBD (**1**)) and its nanoparticles were examined using absorption and emission spectra (Figure 5.3). Initially, the UV/Visible (UV/Vis) studies were carried out to understand the formation of nanoparticles and their changes in photophysical properties. The UV/Vis spectra of nascent compound **1** in acetonitrile exhibit absorption bands centered at ~255, 330, and 410 nm corresponding to π-π* and n-π* transitions. The longer wavelength absorption band at 410 nm is due to intramolecular charge transfer (ICT) transitions. The ICT was indicated by the acid-base titration experiment. The ICT band of the compound has diminished upon addition of trifluoroacetic acid (TFA) indicating the absence of ICT due to protonation on the urea moiety.[40] The protonated state showed a hypsochromically shifted band at 402 nm, in addition to the n-π* band at 330 and 410 nm. Interestingly, upon neutralization with Et_3N, it regained the ICT bands due to the comeback of its original state.

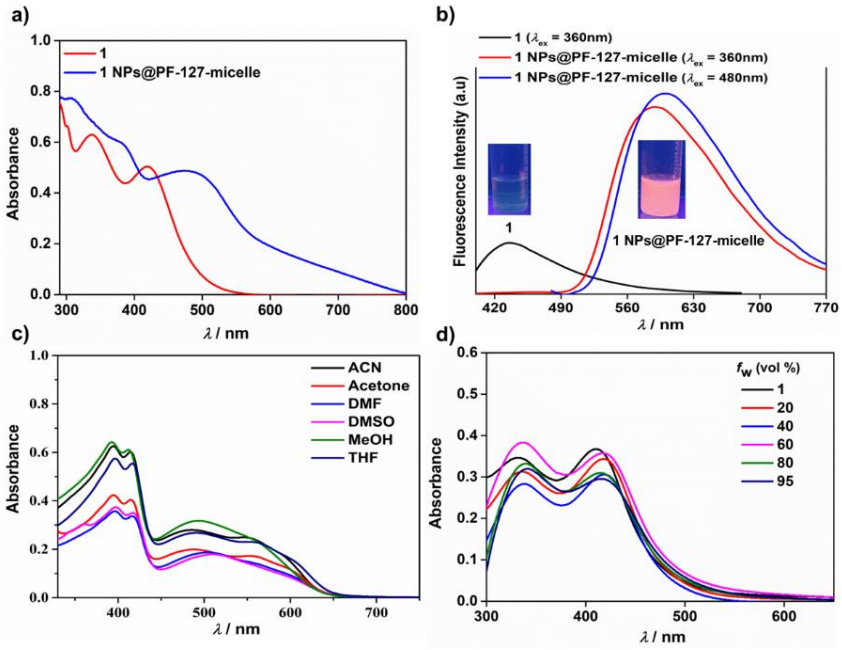

Figure 5.3. a) UV/Vis spectra of **1** and **1 NPs@PF-127-micelle** in CH_3CN and H_2O (5×10^{-5} M), respectively. b) Fluorescence spectra of **1** and **1 NPs@PF-127-micelle** in CH_3CN and H_2O (8×10^{-6} M), respectively. c) UV/Vis spectra of **1** in different solvents. d) UV/Vis spectra of **1** in CH_3CN (5×10^{-5} M) with varied water fractions.

Figure 5.3 shows the UV/Vis spectra of **1** and **1 NPs@PF-127-micelle** in CH_3CN and H_2O (5×10^{-5} M), respectively. Interestingly, upon nanoparticle formation, we observed a bathochromically shifted (53 nm) band along with the expansion of the ICT band compared to **1** in CH_3CN (Figure 5.3a). The bathochromic shift of the ICT band indicates the molecules are present in the aggregated state. Similarly, remarkable changes were observed for **1** in the emission spectra of **1** as neat, and nanoparticles form as shown in Figure 5.3b. It was observed that the neat form **1** had shown emission at λ_{em} of 422 nm, whereas the **1 NPs@PF-127-micelle** has shown emission at λ_{em} of 590 and 600 nm depending on the excitation wavelengths were kept at λ_{ex} at 360 and 480 nm, respectively. A massive Stokes shift of almost 240 may be attributed to the dipole moment of push-pull nature with restricted rotation motion caused by Aggregation induced emission. While compound **1** retained the charge-transfer property in different polar solvents(Figure 5.3c), to verify the possible AIE property of 1 in an unfriendly solvent environment, we have performed the addition of non-friendly solvent, i.e., varied water fraction as indicated in the UV/Vis and emission spectra in Figure. 5.3d and Figure 5.3a, respectively. The fluorescence spectra of the same nanoparticles show dual and distinct emission levels for the nanoparticles upon excitation at λ_{ex} at 360 nm (Figure 5.4a). The observed dual emission of push–pull chromophore may be ascribed due to aggregation-induced emission (AIE) property.

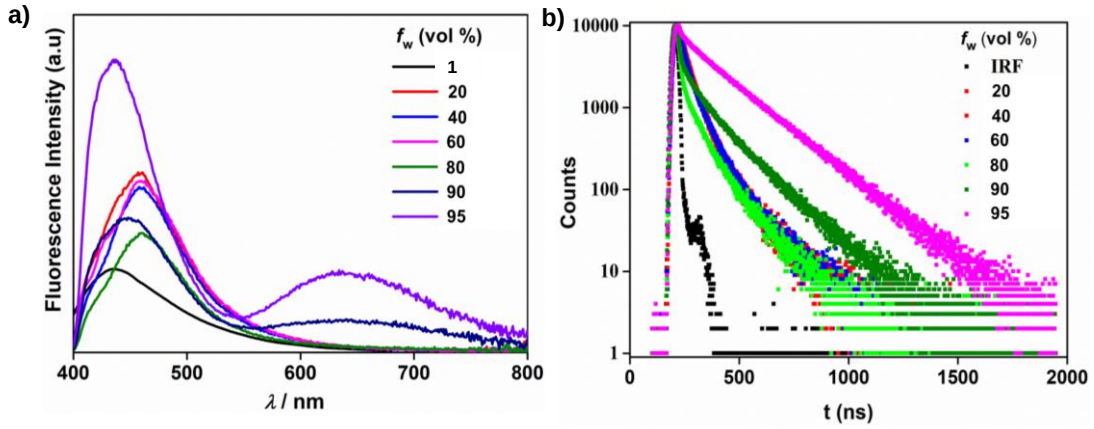

Figure 5.4. a). Fluorescence spectra of **1** in CH_3CN (5×10^{-5} M) with varied water fraction (λ_{ex} = 360 nm). b). TCSPC decay profile of **1** in CH_3CN increased H_2O (5×10^{-5} M) λ_{ex} = 450 nm, using a laser of 390 nm.

Table 1. TCSPS table of a lifetime with an increase in water fraction.

S. No	20%	40%	60%	80%	90%	95%
1	11.41 ns	11.93 ns	12.38 ns	11.10 ns	11.32	12.74

As we established in chapters 3 and 4, that the reason behind turn on fluorescence behavior for urea-substituted mono-TCBDs could be due to possible reduction in the photo-induced electron transfer (PET) quenching process, which we infer to be facilitated by the Field effect nature of the urea group and dis-favored H-bonding interactions. Whereas in the case of bis-substituted TCBDs, in addition to this, the restricted rotation motion aroused due to AIE has enhanced a three-fold increase in the quantum yield from 2.3% for a molecular form of **1** *vs.* 7.9% for the aggregated state of **1 NPs** as measured against quinine sulfate as standard.[41] This three-fold increase is quite remarkable as the fluorescence quantum yields of the reported urea-based chromophores were being found very low.[37] Further evidence for establishing the existence of nanoparticles of push–pull chromophore. The lifetime measurements were carried out using TCSPC (time-correlated single-photon counting system) (Table 1, Figure 5.4b). There are three lifetimes observed for compound **1** in CH_3CN. However, the longer lifetime, around 11.41 ns gets increases significantly from 11.41 to 12.74 ns for a 20% to 95% increase. This indicates at 95% the complete change in the morphology occurs from floppy type to nanoparticles.

5.2. Cellular uptake of nanoparticles (NPs):

After the careful observation of morphology and photophysics of **1 NPs@PF-127-micelle**, we tried to elucidate its biological aspects. To assess the cellular internalization capacity of **1 NPs@PF-127-micelle**, a cellular uptake study was performed in metabolically active HCT116 cells. Cells were incubated with **1 NPs@PF-127-micelle** and were observed to emit green and red luminescence showing the effective internalization of nanoparticles inside the cell cytoplasm (Fig. 5.5a,b). A 3-dimensional view of HCT116 cells indicates that the nanoparticles are located in the cytoplasm in close proximity to the DAPI stained blue nucleus (Figure 5.5c,d). Flow cytometry studies were carried out for cellular uptake of **1 NPs@PF-127-micelle** in HCT116 colorectal cancer cells (Figure 5.6).

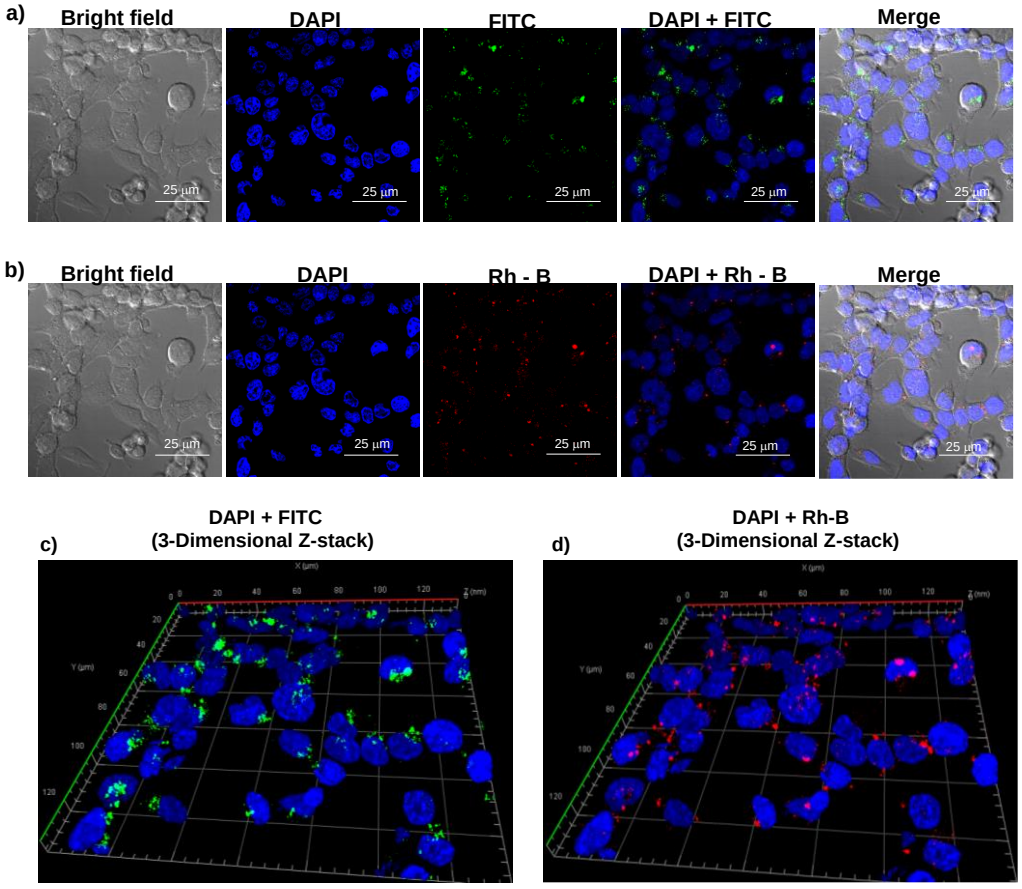

Figure 5.5. (a & b) Confocal microscopy images for **1 NPs@PF-127-micelle** uptaken in metabolically activeHCT116 colorectal cancer cells. (c & d) Corresponding Z-stack 3-dimensional analysis of HCT116 cells showing localization of **1 NPs@PF-127-micelle** in the cytoplasm in proximity to the DAPI stained blue nucleus.

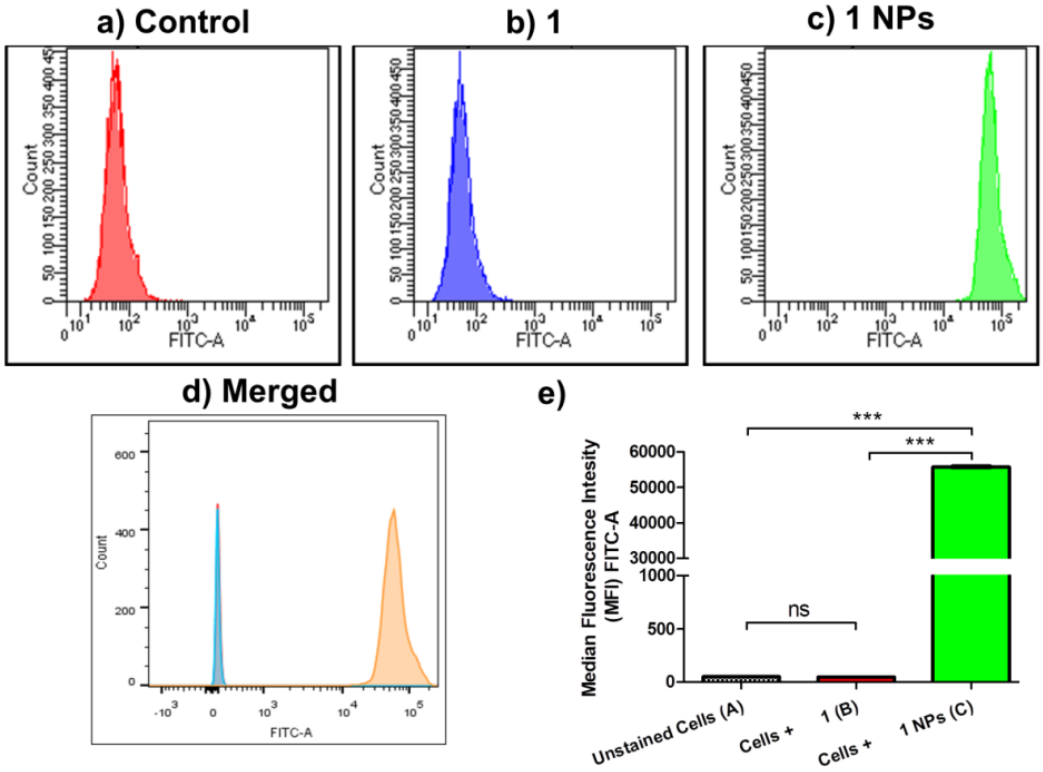

Figure 5.6. Flow cytometry analysis of cellular uptake of **1 NPs@PF-127-micelle** in HCT116 colorectal cancer cells: (a) control (unstained) cells, (b) cells treated with **1** compound form, (c) cells treated with **1 NPs@PF-127-micelle**; (d) merged graphs (e) Comparison of the median fluorescence intensity (MFI) exhibited by (a) unstained cells, (b) cells treated with **1** compound form, and (c) cells treated with **1 NPs@PF-127-micelle**. Experiments were performed in triplicate, and data are expressed as mean ± SEM of three independent sets of observations. **ns**: non-significant, ***P<0.001 **1 NPs@PF-127-micelle** compared to (a) unstained and (b) cells treated with **1** compound form.

5.3. Photodynamic therapy of HCT116 colorectal cancer cells:

The quenching of DHN has successfully demonstrated the photosensitizer capacity of 1 NPs@PF-127-micelle with time (Figure 5.7). The UV/Vis spectra of **1 NPs@PF-127-micelle** under xenon lamp have shown that the quantum yield efficacy of **1 NPs@PF-127-micelle** of up to 0.25 % for the generation of singlet oxygen.

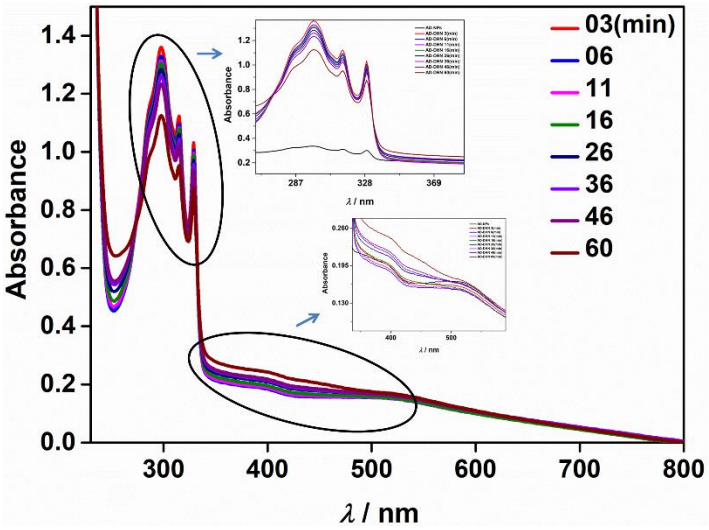

Figure 5.7. The UV/Vis absorption spectra wherein the absorption of **1 NPs@PF-127-micelle** with DHN was observed for singlet oxygen generation.

The cancer cell inhibiting property of compound **1** and **1 NPs@PF-127-micelle** was assessed both in the presence and absence of light at two different time points of 24 and 48 h in a dose-dependent manner. It was observed that the viability of HCT116 started getting reduced in the presence of light at the dose of 10 nM. Further, it was observed to be lesser than 10% at the highest doses of 10 µM. A more prominent decrement in cell viability was observed at higher doses of 0.5 – 10 µM when cells were treated for 48 h (Figure 5.8a,b). These effects were also corroborated with bright-field microscopic images of HCT116 cells in 96 well plates (Figure 5.8c,d).

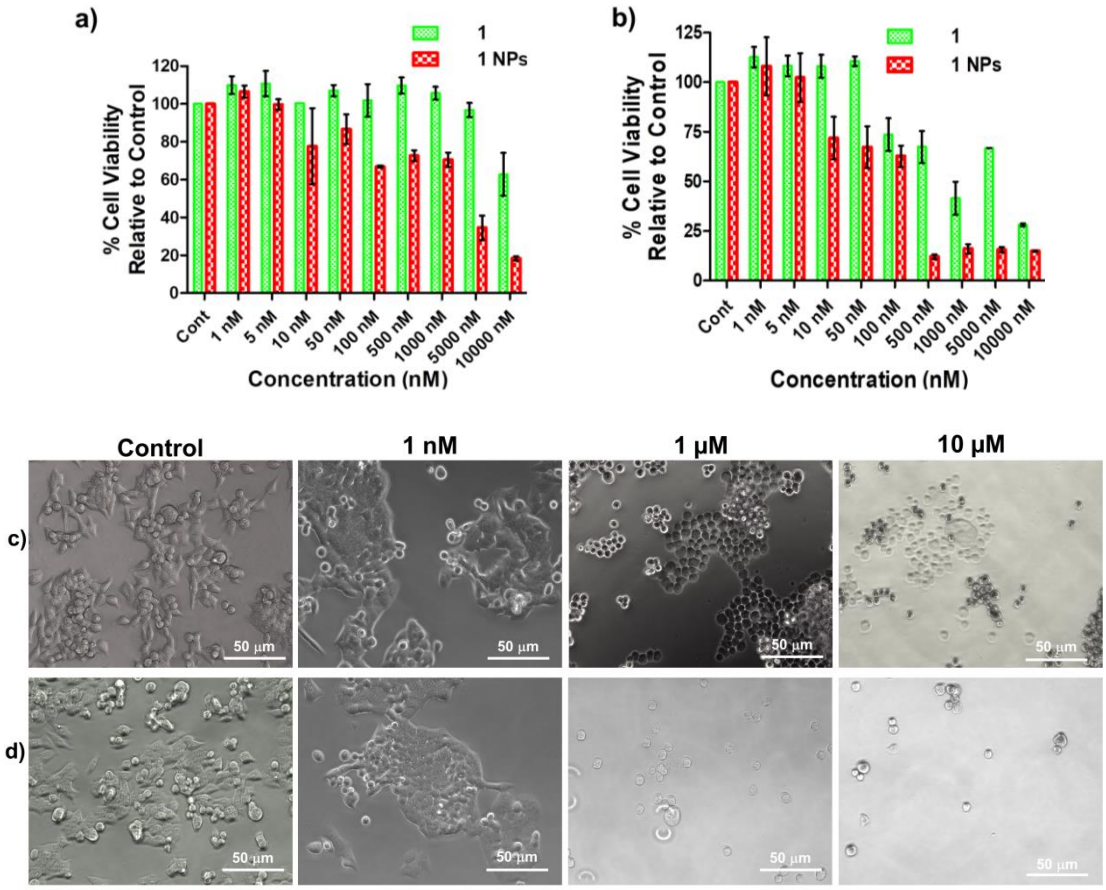

Figure 5.8. Cytotoxicity of HCT116 cells after photodynamic therapy of **1** and **1 NPs@PF-127-micelle** . (a) Cell viability relative to control after photodynamic therapy of **1** and **1 NPs@PF-127-micelle** for 24 hours. (b) Cell viability relative to control after photodynamic therapy of **1** and **1 NPs@PF-127-micelle** for 24 hours. (c) Bright filed optical micrographs of HCT116 confluency and morphology relative to control after photodynamic therapy of **1** and **1 NPs@PF-127-micelle** for 24 hours. (d) Bright filed optical micrographs of HCT116 confluency and morphology relative to control after photodynamic therapy of **1** and **1 NPs@PF-127-micelle** for 48 hours.

5.4. Cancer cell death mechanism (Annexin-FITC / PI assay):

After the inhibition of HCT116 colorectal cancer cell death by photodynamic therapy of **1 NPs@PF-127-micelle**, Annexin-FITC / PI assay was performed to assess the percentage of cells in different stages of apoptosis and necrosis. It was observed that the maximum percentage of cells (19.2%) were in late apoptosis when treated with **1 NPs@PF-127-micelle** in the presence of light as compared to the treatment of **1 NPs@PF-127-micelle** without light. Further, it was also observed that only compound form could not induce any significant apoptosis in HCT116 colorectal cancer cells either with or without light (Figure 5.10a-e). Comparative statistical analysis also revealed that nanoparticles in the

presence of light-induced significantly higher late apoptosis as compared to either only nanoparticles or native compound form in the presence of light (Figure 5.9f).

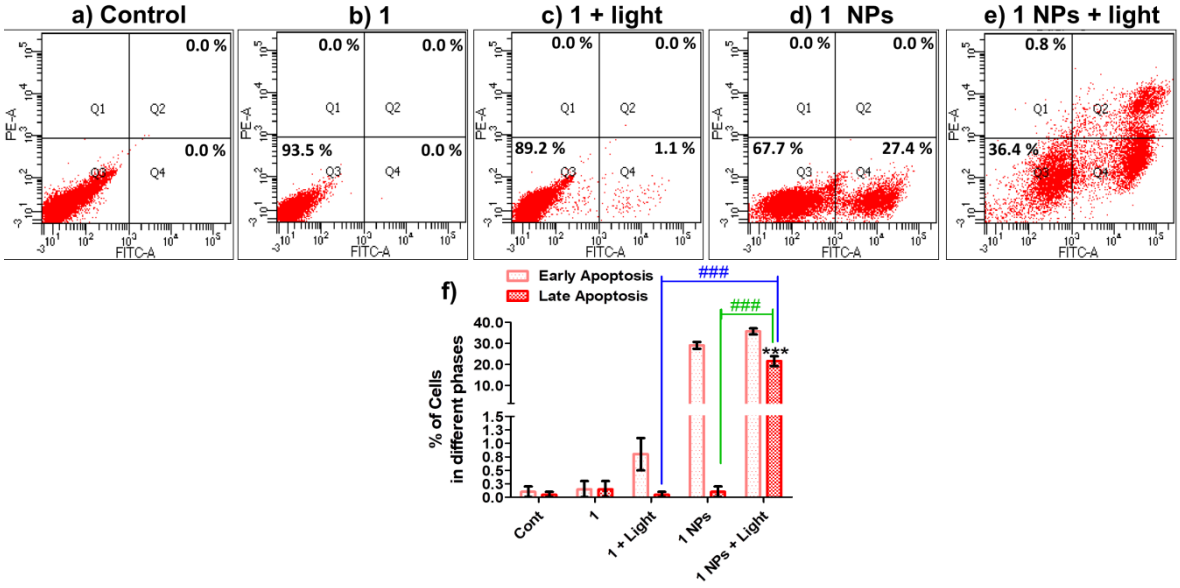

Figure 5.9. (a) Flow cytometry analysis of HCT116 cells following after 48 h of the different treatment regimen. (a) **Control:** Normal control HCT116 cells without any treatment. (b) **1:** HCT116 Cells treated with only **1** compound form. (c) **1 + light:** HCT116 cells treated with **1** compound in the presence of light. (d) **1 NPs@PF-127-micelle:** HCT116 cells treated with **1** nanoparticles. (e) **1 NPs@PF-127-micelle + light:** HCT116 cells treated with **1 NPs@PF-127-micelle** in the presence of light. (f) Quantitative analysis of the percentage of cells in different phases of cell death (early apoptosis, late apoptosis, and necrosis) after different treatment regimens. Experiments were performed in triplicates, and data are expressed as mean ± SEM of three independent sets of observations. ***P≤0.001 for late apoptosis in **1 NPs@PF-127-micelle** + light treated cells vs control while ###p≤0.01 for late apoptosis in **1 NPs@PF-127-micelle** + light treated cells vs **1** + light and **1 NPs@PF-127-micelle**

Bio-distribution studies: After assessing photodynamic therapy and cell death mechanism, the biodistribution of **1 NPs@PF-127-micelle** was studied in Swiss albino mice at different time points. Healthy mice were administered with 2 mg/kg of **1 NPs@PF-127-micelle** intravenously and were sacrificed at other time points. Vital organs like liver, kidney, spleen, heart, and lungs were excised, and 1 mm thick sections were cut and observed under a confocal laser scanning microscope. It was observed that the liver and kidney sections exhibited maximal intensity of fluorescence at 1 h. This fluorescence indicated that maximal accumulation could occur in these organs during the initial 1 h of intravenous administration of **1 NPs@PF-127-micelle. The** biotransformation and/or excretion of the **1 NPs@PF-127-micelle** occurs mainly through

the liver and kidneys. Besides the liver and kidneys, no significant fluorescence was observed in any of the other vital organs at the given time points (Figure 5.10).

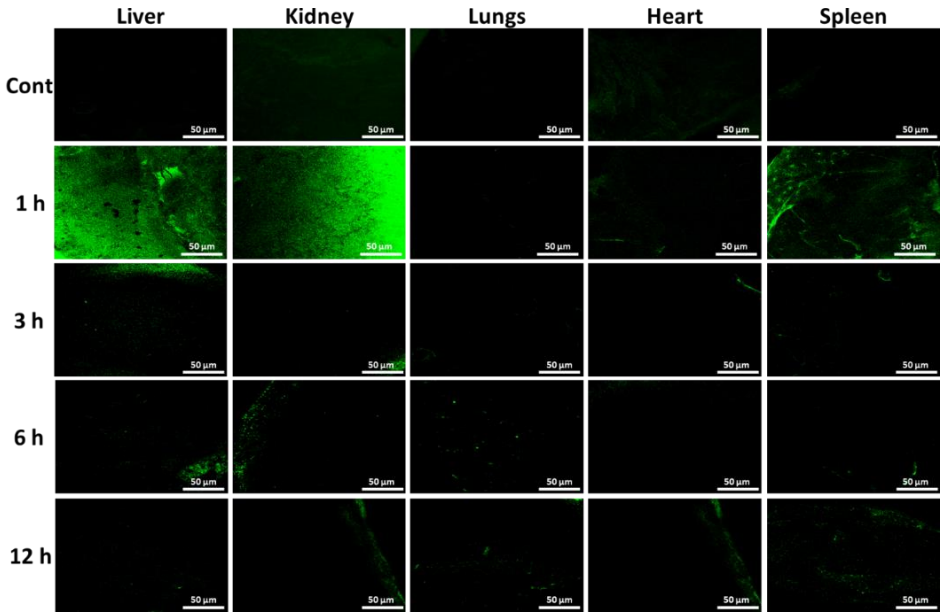

Figure 5.10. Confocal microscopic images of vital organ sections after treatment of mice with **1 NPs@PF-127-micelle** for various time points.

Toxicological Studies: Probable toxicological effects of customized nanomaterials and nanoparticles can arise in the course of due treatment of animal models. These are often a matter of grave concern for researchers working in nanomedicine areas. Therefore, to assess the safety of **1 NPs@PF-127-micelle** in-vivo different biomarkers for vital organ toxicity were analyzed in the mice. It was observed that there histopathological sections of the liver of **1 NPs@PF-127-micelle** treated animals indicated that histoarchitecture of the liver was entirely well preserved and kept to be quite normal as compared to control animals (Figure 5.11). After treatment with **1 NPs@PF-127-micelle** hepatocyte were regular in shape and size, with no abnormal distortion, absence of any vascular damage, and no inflammatory cell infiltration and accumulation. Both control and **1 NPs@PF-127-micelle** treated group did not show any cellular, cytoplasmic or nuclear degeneration with well-preserved micro and microvasculature. In kidney histopathological sections stained with H&E, normal glomeruli shape and size, morphologically healthy tubules and tubular epithelial cells were observed in both **1 NPs@PF-127-micelle** treated and control group. In **1 NPs@PF-127-micelle** treated group, normal renal cortex and glomerular tufts were observed with complete absence of any inflammatory cell infiltration. No edema and lack of any necrosis also established the absence of any

damage or toxicity. In **1 NPs@PF-127-micelle** treated group, spleen sections also exhibited entirely normal and healthy histoarchitecture as that of the control group, in terms of well-defined lymphoid follicles and sinuses and no infiltration of any inflammatory cells.

Similarly, heart sections of the **1 NPs@PF-127-micelle** treatment group demonstrated well-preserved integrity of the cardiac structure. Intact myofibrils were observed with no inflammatory cell infiltration, no cellular, cytoplasmic and nuclear degeneration was observed in heart sections. With the considerably high blood supply in the lungs and resultant possible higher accumulation of nanoparticles, lung toxicity of nanoparticles becomes of particular concern. Likewise, H&E stained sections of lungs were observed in the control and **1 NPs@PF-127-micelle** treated group. Completely healthy lung sections were observed in animals treated with **1 NPs@PF-127-micelle** with no sign of inflammatory or any other damage. No alveolar morphological alteration was seen with normal healthy bronchiolar epithelium and intact pulmonary alveolar shape with healthy goblet cells.

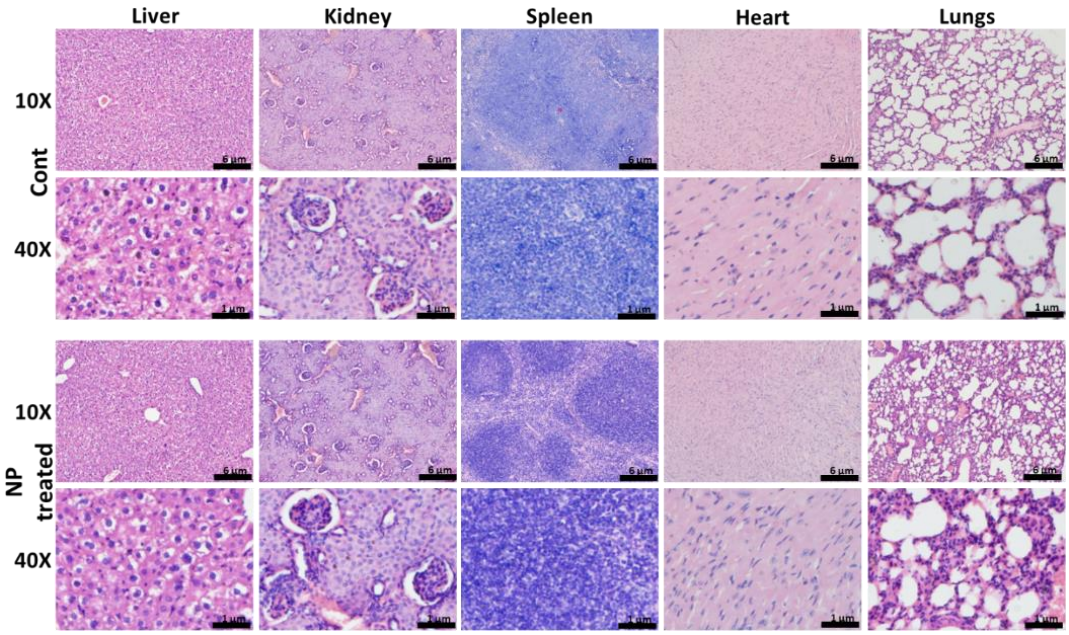

Figure 5.11. Representative photomicrographs showing H&E stained sections of mice liver, kidney, spleen, heart, and lungs in normal control (upper section) and **1 NPs@PF-127-micelle** (lower section) treated groups. Experiments were performed in triplicate sections (n=3). N = 6 i.e., number of animals taken in each group.

5.5. Experimental Section:

5.5.1. Synthesis and characterization of compound (1)

The first-time synthesis of 2,3-disubstituted non-planar push–pull chromophores **1** conjugated with urea receptor moiety has been reported by our group (Scheme 5.1) and has been synthesized using the reported procedure.[37] A simple two-step synthesis involving the preparation of urea-functionalized unsymmetrical alkyne **4**, followed by [2+2] cycloaddition-retroelectrocyclization (CA–RE) reactions with tetracyanoethene (TCNE) to provide the corresponding **1** as fluorescent chemosensor molecule. The alkyne precursors **4** was accomplished by the corresponding NH_2-functionalized unsymmetrical alkynes **3** reactions with benzylisocyanate **2**.

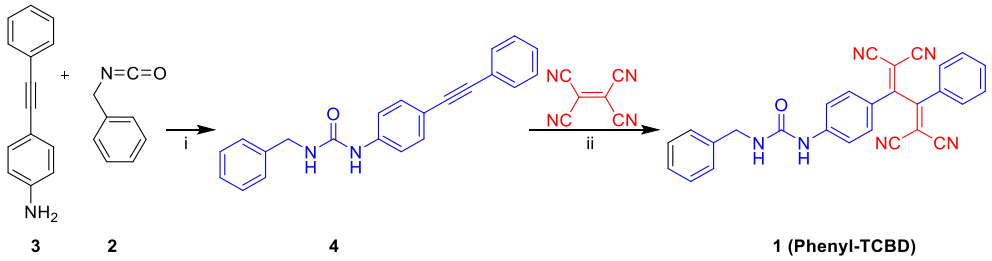

Scheme 5.1. Synthetic pathway for compound **1**: i) CH_2Cl_2, 25 °C, 24 h, 75% (**4**), ii) $ClCH_2CH_2Cl$, $LiClO_4$, 70 °C, 1 h, 83% (**1;** Phenyl-TCBD).

5.5.2. Synthesis and characterization of nanomicelles (1 NPs@PF-127-micelle):

The NPs of compound **1** was synthesized by a nanoprecipitation method.[39] A solution of **1** (2 mg) in acetone (5 mL) was added dropwise to the solution of P F-127 (Mw: 1000-1000, 5 mg) in distilled-deionized water (10 mL) for 15 min. Then the mixture was stirred overnight at room temperature to removed acetone. The **1 NPs@PF-127-micelle** were further purified through centrifugation and filtered through a 0.22 µm filter membrane. The **1 NPs@PF-127-micelle** dispersed in water or the freeze-dried solids were used for further characterization and application.

5.5.3. Cellular uptake of nanoparticles by confocal microscopy:

In vitro cellular uptake of nanoparticles was performed in metabolically active HCT116 cells as described earlier. 1×10^4 HCT116 cells were seeded on sterile poly-L lysine coated glass coverslips kept in each well of the 6 well plates. After overnight cell attachment over coverslips, media was aspirated; coverslips were washed with ice-cold PBS buffer (pH 7.4) and treated in triplicate with various concentrations of nanoparticles suspended in media. After a specified incubation period of 4 h at 37 ºC, cells were processed for confocal microscopy. Processing steps required washing cells with ice-cold PBS, fixing cells in 3.7% paraformaldehyde (PFA) solution, counterstaining with DAPI (10 µg/ml) for 5 minutes, and again a final wash using ice-cold PBS. Coverslips were examined under a confocal microscope (Zeiss, Model: LSM 880). Experiments were performed in triplicate to ensure reproducibility and consistency of results.

5.5.4. Cellular uptake of nanoparticles by flow cytometry:

Flow cytometry was performed as described earlier1 with some modifications. Briefly, 1×10^6 HCT116 cells/well were seeded in a 6-well culture plate. After 24 hour growth period, cells were treated with nanoparticles (10 µg/mL) for 6 h at 37 °C. Cells were then washed to remove excess nanoparticles, trypsinized and centrifuged. The cell pellets were resuspended in PBS, and fluorescence was measured by BD FACS Aria™ Fusion Flow cytometer (BD Biosciences). The experiments were performed in triplicate, and the fluorescence from 10,000 cells per sample was obtained. Data analysis was performed with Flowjo Software.

5.6. PDT of colorectal cancer cells:

In vitro cytotoxicity of nanoparticles at different time points, both in the presence and absence of light, was determined in metabolically active HCT116 cells using MTT assay. HCT116 cells (70-80% confluent) were seeded in 96-well plates at a density of 10,000 cells per well in triplicates for each group, grown for 24 h in a CO_2 incubator. Cells were treated with different concentrations of nanoparticles followed by treatment of light, and anti-proliferative effects of nanoparticles were assessed using EZcount^{TM} MTT cell Assay Kit (HiMedia Laboratories Pvt. Ltd., India) according to manufacturers' protocol. Absorbance was taken at 590 nm and 630 nm using an ELISA plate reader. Percentage cell viability was calculated using the following equation:

$$\% \text{ Cell Viabiility} = \frac{\text{Absorbance of MTT formazan produced by cells grown in the presence of NP treatments}}{\text{Absorbance of MTT formazan produced by cells grown on media alone}} \text{ X } 100$$

5.6.1. Evaluation of nanoparticles-induced apoptotic cell death (Annexin V-FITC / PI assay by flow cytometry):

To further assess the efficacy of nanoparticle-mediated apoptosis in HCT116 cells, propidium iodide (PI) assay was carried out using flow cytometry. After nanoparticle treatment, cells were washed with PBS to remove NPs, trypsinized, again washed, and transferred to CellPro™ flow cytometry tubes. Annexin V-FITC (5 µl) and PI (1 µl of 100 µg/mL) were added to the cell suspension, followed by incubation at room temperature in the dark for 30 min. After this step, 400 µl of binding buffer was added, and the samples were analyzed by a BD FACS Aria™ Fusion Flow cytometer (BD Biosciences). Results were then analyzed using CELLQuest 3.0 software. Dots in the lower left quadrant (LL), upper left quadrant (UL), upper right quadrant (UR), and lower right quadrant (LR) represents viable, healthy cells (Annexin V−, PI−), necrosis undergoing cells (Annexin V−, PI+), cells in late apoptosis (Annexin V+, PI+) and cells in early apoptosis (Annexin V+, PI−), respectively. The experiment was carried out in triplicate, and data are expressed as mean ± SEM. Quantification was performed using GraphPad Prism software Version 5.0.

5.7. In-vivo studies of nanoparticles:

5.7.1. Ethical statement for the use of experimental animals:

Animal experiments were performed as approved by Institutional Animal Ethical Committee and according to the guidelines of the Committee for the purpose of Control and Supervision of Experiments on Animals (CPCSEA, Government of India) and National Institutes of Health guide for the care and use of laboratory animals. Swiss albino mice were obtained from the animal house and maintained under standard laboratory conditions following guidelines. Mice were housed under an ambient temperature of 25 ± 1 °C with 12 hour light /dark cycles after initial acclimatization for about one week. They had free access to a standard rodent pellet diet and water ad libitum.

5.7.2. In-vivo biodistribution study:

To study biodistribution and accumulation of nanoparticles in vital organs after intravenous administration, 25 mice were randomly allocated to 5 groups of 5 mice each**.**

Group I (Control): Mice received basal diet and received 0.9% normal saline via tail vein.

Group II (1 h): Mice received 2 mg/kg **1 NPs@PF-127-micelle** dispersed in normal saline via tail vein and sacrificed after 1 hour of injection.

Group III (3 h): Mice received 2 mg/kg **1 NPs@PF-127-micelle** dispersed in normal saline via tail vein and sacrificed after 3 hour of injection.

Group IV (6 h): Mice received 2 mg/kg **1 NPs@PF-127-micelle** dispersed in normal saline via tail vein and sacrificed after 2 hour of injection.

Group V (12 h): Mice received 2 mg/kg **1 NPs@PF-127-micelle** dispersed in normal saline via tail vein and sacrificed after 12 h of injection.

All mice were anesthetized with mild anesthesia and sacrificed by cervical dislocation.

5.7.3 Safety assessment of nanoparticles by histological examinations (H&E staining) of vital organs:

After the sacrifice of mice, various organs were harvested, washed with normal saline, and fixed in 10% buffered formalin for at least 24 h. Organ specimens were dehydrated in ascending grades of ethanol, cleared in benzene, and embedded in paraffin wax. Blocks were made in paraffin wax, and 5 µm thick sections were cut from each respective vital organ viz. Liver, kidneys, spleen, heart, and lungs. Paraffin-embedded tissue sections were deparaffinized using xylene and ethanol. These sections were then stained with hematoxylin and eosin and were observed under a light microscope.

5.8. Conclusion:

Here in this work, we have demonstrated that it is possible to modulate photophysical properties remarkably. In particular, emission properties were significantly improved by adopting the AIE behavior of non-planar push-pull chromophores using water-soluble PF-127micelles. Interestingly, the aqueous insoluble chromophores were made soluble in water micelles with a promising 3-fold increase in luminescence, and dual emission

behavior has been observed. The generated nano-micelles using PF-127 as an encapsulating agent have shown a remarkable enhancement in their fluorescence lifetime along with quantum yield measurements. The activation of a luminescent photosensitizer (push–pull chromophore) in the presence of light inside cells leads to selective cancer cell death efficiently, switching the cells to apoptosis through the mitochondrial pathway. The novel concept exploiting nano-micelles of luminescent push–pull chromophores as active PDT and bio-imaging probes has been successfully demonstrated here.

5.9. References:

1. Karges, J.; Heinemann, F.; Jakubaszek, M.; Maschietto, F.; Subecz, Chloé.; Dotou, M.; Vinck, R.; Blacque, Olivier.; Tharaud, M.; Goud, B.; Zahínos, E.; V.; Spingler, B.; Ciofini, Ilaria.; Gasser, Gilles. *J. Am. Chem. Soc*. **2020**, *142*, 6578–6587.
2. Qian, G.; Wang, Z. Y. *Chem. Asian J*. **2010**, *5*, 1006–1029.
3. Nguyen, V-N.; Park, S. J.; Qi, S.; Ha, J.; Heo, S.; Yim, Y.; Baek, Gain.; Lim, C. Su.; Lee, D. J.; Kim, H. M.; Yoon, J.; *Chem. Commun*., **2020**, *56*, 11489–11492.
4. Kazantzis, K. T.; Koutsonikoli, K.; Mavroidi, B.; Zachariadis, M.; Alexiou, P.; Pelecanou, M.; Politopoulos, K.; Alexandratou, E.; Sagnou, M. *Photochem. Photobiol. Sci*. **2020**, *19*, 193–206.
5. Li, X.; Lee, S.; Yoon, J.; *Chem. Soc. Rev*. **2018**, *47*, 1174–1188.
6. Agostinis, P.; Berg, K.; Cengel, K. A.; Foster, T. H.; Girotti, A. W.; Gollnick, S. O.; Hahn, S. M.; Hamblin, M. R.; Juzeniene, A.; Kessel, D.; Korbelik, M.; Moan, J.; Mroz, P.; Nowis, D.; Piette, J.; Wilson, B. C.; Golab, J. *Ca-Cancer J. Clin*. **2011**, *61*, 250–281.
7. Dolmans, D. E. J. G. J.; Fukumura, D.; Jain, R. K. *Nat. Rev. Cancer* **2003**, *3*, 380–387.
8. Ko, C.-N.; Li, G.; Leung, C.-H.; Ma, D.-L. *Coord. Chem. Rev*. **2019**, *381*, 79–103.
9. Dai, J.; Li, Y.; Long, Z.; Jiang, R.; Zhuang,;Z.; Wang, Z.; Zhao, Z.; Lou, X.; Xia, F.; Tang, B. Z. *ACS Nano* **2020**, *14*, 854–6866.
10. Yuan, Y.; Zhang, C.-J.; Gao, M.; Zhang, R.; Tang B. Z.; Liu, B. *Angew. Chem. Int. Ed*. **2015**, *54*, 1780–1786.

11. Cai, Y.; Si, W.; Huang, W.; Chen, P.; Shao, J.; Dong, X. *Small* **2018**, *14*, 1704247.
12. Cheung, S.; Wu, D.; Daly, H. C.; Busschaert, N.; Morgunova, M.; Simpson, J. C.; Scholz, D.; Gale, P. A.; O'Shea, D. F. *Chem.* **2018**, *4*, 879.
13. Sessler, J. L.; Eller, L. R.; Cho, W.-S.; Nicolaou, S.; Aguilar, A.; Lee, J. T.; Lynch, V. M.; Magda, D. J. *Angew. Chem. Int. Ed*. **2005**, *44*, 5989.
14. Tannock, I. F.; Rotin, D. *Cancer Res.* **1989**, *49*, 4373.
15. Van Rossom, W.; Asby, D. J.; Tavassoli, A.; Gale, P. A. *Org. Biomol. Chem*. **2016**, *14*, 2645.
16. Ohkuma, S.; Sato, T.; Okamoto, M.; Matsukya, H.; Arai, K.; Kataoka, T.; Nagai, K.; Wasserman, H. H. *Biochem. J*. **1998**, *334*, 731.
17. Davis, J. T. In Topics in Heterocyclic Chemistry; Gale, P. A.; Dehaen, W., Eds.; Springer: New York, 2010; Vol. 145.
18. Li, X.; Gao, X.; Shi, W.; Ma, H. *Chem. Rev.* **2014**, *114*, 590.
19. Sordé, N.; Matile, S. *J. Supramol. Chem.* **2002**, *2*, 191.
20. Saha, T.; Hossain, M. S.; Saha, D.; Lahiri, M.; Talukdar, P. *J. Am. Chem. Soc.* **2016**, *138*, 7558.
21. Hernando, E.; Soto-Cerrato, V.; Cortés-Arroyo, S.; Pérez-Tomás, R.; Quesada, R. *Org. Biomol. Chem.* **2014**, *12*, 1771.
22. Ko, S.-K.; Kim, S. K.; Share, A.; Lynch, V. M.; Park, J.; Namkung, W.; Van Rossom, W.; Busschaert, N.; Gale, P. A.; Sessler, J. L.; Shin, I. *Nat. Chem.***2014**, *6*, 885.
22. Ko, S.-K.; Kim, S. K.; Share, A.; Lynch, V. M.; Park, J.; Namkung, W.; Van Rossom, W.; Busschaert, N.; Gale, P. A.; Sessler, J. L.; Shin, I. *Nat. Chem.***2014**, *6*, 885.
23. Vallaitis, T.; Bogatscher, S.; Alloatti, L.; Dumon, P.; Baets, R.; Scimeca, M. L.; Biaggio, I.; Diederich, F.; Koos, C.; Freude, W.; Leuthold, J. *Opt. Express* **2009**, *17*, 17357–17368.
24. Senanayak, S. P.; Sangwan, V. K.; McMorrow, J. J.; Everaerts, K.; Chen, Z.; Facchetti, A.; Hersam, M. C.; Marks, T. J.; Narayan, K. S. *ACS Appl. Mater. Interfaces* **2018**, *10*, 21492–21498.

25. Griesbeck, S.; Michail, E.; Wang, C.; Ogasawara, H.; Lorenzen, S.; Gerstner, L.; Zang, T.; Nitsch, J.; Sato, Y.; Bertermann, R.; Taki, M.; Lambert, C.; Yamaguchi, S.; B. Marder, T. *Chem. Sci.* **2019**, *10*, 5405–5422.
26. Tydlitát, J.; Achelle, S.; Rodríguez-López, J.; Pytela, O.; Mikýsek, T.; Cabon, N.; Robin le Guen, F.; Miklík, D.; Růžičková, Z.; Bureš, F. *Dyes Pigm.* **2017**, *146*, 467–478.
27. Jose, D. A.; Kumar, D. K.; Ganguly, B.; Das, *Org. Lett*. **2004**, *6*, 3445–3448.
28. Murfin, L. C.; Weber, M.; Jun, P. S.; Kim, W. T. Lopez-Alled C. M.; McMullin, C. L.; Pradaux-Caggiano, F.; Lyall, C. L.; Kociok-Köhn, G.; Wenk, J.; Bull, S. D.; Yoon, J.; Kim, H. M.; James, T; D.; Lewis, S. E. *J. Am. Chem. Soc.* **2019**, *141*, 19389–19396.
29. Niu, G.; Zheng, X.; Zhao, Z.; Zhang, H.; Wang, J.; He, X.; Chen, Y.; Shi, X.; Ma, C.; Kwok, T. K. R.; Lam, W. Y. J..; Sung, H. Y. H.; Williams, D. I.; Wong, S. K.; Wang, P.; Tang, Z. B. *J. Am. Chem. Soc*. **2019**, *141*, 15111−15120.
30. Hua, B.; Zhang, C.; Zhou, W.; Shao, Li.; Wang, Z.; Wang, L.; Zhu, H.; Huang, F. *J. Am. Chem. Soc*. **2020**, *142*, 16557–16561.
31. Pratihar, S.; Bhattacharyya, A.; Prasad, E. *J. Photochem. Photobiol. A* **2020**, *396*, 112458
32. Ma, X.; Sun, R.; Cheng, J.; Liu, J.; Gou, F.; Xiang, H.; Zhou, X. *J. Chem. Educ*. **2016**, *93*, 345–350.
33. Xu, J.; Liu, X.; Lv, J.; Zhu, M.; Huang, C.; Zhou, W.; Yin, X.; Liu, H.; Li, Y.; Ye, J. *Langmuir* **2008**, *24*, 4231–4237.
34. Michinobu, T.; May, J. C.; Lim, J. H.; Boudon, C.; Gisselbrecht, J.-P.; Seiler, P.; Gross, M.; Biaggio, I.; Diederich, F. *Chem. Commun*. **2005**, 737–739.
35. For a review, see: Michinobu, T.; Diederich, F. Angew. Chem. Int. Ed. **2018**, *5*, 3552–3577.
36. Dar, A. H.; Gowri, V.; Gopal, A.; Muthukrishnan, A.; Bajaj, A.; Sartaliya, S.; Selim, A.; Ali, Md. E.; Jayamurugan, G. *J. Org. Chem*. **2019**, *84*, 8941–8947.
37. Gowri, V.; Jalwal, S.; Dar A. H.; Gopal, A.; Muthukrishnan, A.; Bajaj, A.; Ali, E, Md.; Jayamurugan G. *J. Photochem. Photobiol. A* **2021**, *410*, 113163.
38. Kabanov, A. V.; Batrakova, E. V.; Alakhov, V. Y. *J. Control. Release* **2002**, *82*, 189–212.

39. Zhang, X.; Wang, K.; Liu, M.; Zhang, X.; Tao, Lei.; Chena, Y.; Wei, Y. *Nanoscale.* **2015**, *7*, 11486-11508

40. Janssen, M. J. *Spectrochim. Acta* **1961**, *17*, 475−485.

41. Eaton, D. F. *Pure Appl. Chem*. **1988**, *60*, 1107−1114.

❖ Overall Conclusion

To summarize this thesis work as shown in the below Figure, the overall aim of my doctoral research was to expand the chemical structure space for push–pull chromophores and introduce new strong donor and acceptor in the list of donor-acceptor systems undergoing [2+2] CA-RE reactions. The newly synthesized urea-based push–pull chromophores were found to exhibit remarkable luminescence properties and allow easy functionalization. Also, we tried to investigate the concepts of self-assembly behavior in push–pull chromophores which allowed us to obtain white-light emission *via* tunable luminescence properties. Notably, the introduction of luminescence and its translation from solution state to solid-state has been governed using nanotechnology approaches. Lastly, we have successfully demonstrated for the first time that non-planar push–pull chromophores can be encapsulated inside the micelle and, in turn, modulate their photophysical properties to achieve the photosensitizing capability to use for PDT and bio-imaging applications. Though the newly developed chromophores will be of use in optoelectronic applications, this study will open new windows to establish its use in sensing and bio-imaging applications, as demonstrated in this work.

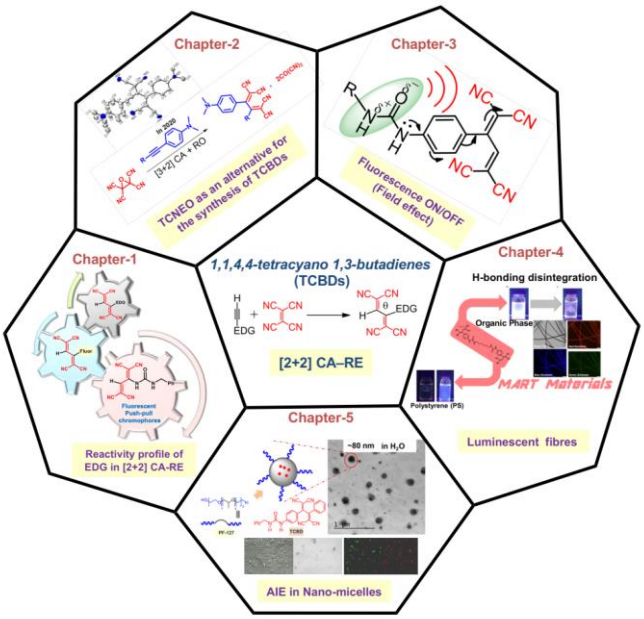

Figure: Synthetic methodology for the development of fluorescent push–pull chromophores using [2+2] CA–RE and nanotechnology assisted smart materials for applications in bio-imaging and photodynamic therapy

Synthesis of 1,1,4,4-Tetracyanobuta-1,3-Dienes using Tetracyanoethylene Oxide via [3 2]-Cycloaddition-Ring Opening Reaction

Author: Govindasamy Jayamurugan, K. M. Neethu, Vijayendran Gowri, et al

Publication: ChemistrySelect

Publisher: John Wiley and Sons

Date: Oct 23, 2020

Order Completed

Thank you for your order.

This Agreement between Mr. Arif Dar ("You") and John Wiley and Sons ("John Wiley and Sons") consists of your license details and the terms and conditions provided by John Wiley and Sons and Copyright Clearance Center.

Your confirmation email will contain your order number for future reference.

License Number	4990611410211
License date	Jan 16, 2021

Printable Details

Licensed Content

Licensed Content Publisher	John Wiley and Sons
Licensed Content Publication	ChemistrySelect
Licensed Content Title	Synthesis of 1,1,4,4-Tetracyanobuta-1,3-Dienes using Tetracyanoethylene Oxide via [3 2]-Cycloaddition-Ring Opening Reaction
Licensed Content Author	Govindasamy Jayamurugan, K. M. Neethu, Vijayendran Gowri, et al
Licensed Content Date	Oct 23, 2020
Licensed Content Volume	5
Licensed Content Issue	40
Licensed Content Pages	5

Order Details

Type of use	Dissertation/Thesis
Requestor type	Author of this Wiley article
Format	Print and electronic
Portion	Full article
Will you be translating?	No

About Your Work

Title	Design, Synthesis and Studies of Luminescent Organic Non-planar Push-pull Chromophores
Institution name	INST
Expected presentation date	Jan 2021

Additional Data

Requestor Location

Requestor Location	Mr. Arif Dar INST Mohali Sector 81 Mohali, Punjab 140306 India Attn: Mr. Arif Dar

Tax Details

Publisher Tax ID	EU826007151

Price

Total	0.00 USD

Would you like to purchase the full text of this article? If so, please continue on to the content ordering system located here: Purchase PDF
If you click on the buttons below or close this window, you will not be able to return to the content ordering system.

Total: 0.00 USD

CLOSE WINDOW ORDER MORE

Designing of Push–Pull Chromophores with Tunable Electronic and Luminescent Properties Using Urea as the Electron Donor

Author: Arif Hassan Dar, Vijayendran Gowri, Arya Gopal, et al

Publication: The Journal of Organic Chemistry

Publisher: American Chemical Society

Date: Jul 1, 2019

PERMISSION/LICENSE IS GRANTED FOR YOUR ORDER AT NO CHARGE

This type of permission/license, instead of the standard Terms & Conditions, is sent to you because no fee is being charged for your order. Please note the following:

- Permission is granted for your request in both print and electronic formats, and translations.
- If figures and/or tables were requested, they may be adapted or used in part.
- Please print this page for your records and send a copy of it to your publisher/graduate school.
- Appropriate credit for the requested material should be given as follows: "Reprinted (adapted) with permission from (COMPLETE REFERENCE CITATION). Copyright (YEAR) American Chemical Society." Insert appropriate information in place of the capitalized words.
- One-time permission is granted only for the use specified in your request. No additional uses are granted (such as derivative works or other editions). For any other uses, please submit a new request.

BACK CLOSE WINDOW

Arif Hassan Dar

Ph.D. Research Scholar
Institute of Nano Science and Technology (INST) &
Indian Institute of Science Education and Research (IISER) Mohali
Punjab, India

Arif Hassan Dar completed B.Sc. (H) and MSc Organic Chemistry in 2013 and 2015 from the Department of Chemistry, Aligarh Muslim University, UP, India. He joined the Institute of Nano Science and Technology (INST) in January 2016 and registered with the Indian Institute of Science Education and Research (IISER) Mohali for the Ph.D. program. His research interests include design, synthesis, and studies of luminescent organic non-planar push–pull chromophores and their applications. He authored several research articles in reputed international journals and coauthored a patent. He has presented his research work at several National and International conferences.